2020•2021

Faculteit Industriële Ingenieurswetenschappen

master in de industriële wetenschappen: bouwkunde

Masterthesis

Effects of Decelerated Moving Load of Automated Vehicles on the Pavement StressStrain Responses Using 3-D Finite Element Modelling

PROMOTOR :

Prof. dr. ir. Ali PIRDAVANI

BEGELEIDER :

De heer Ali YEGANEH

Domenic Daniels

Scriptie ingediend tot het behalen van de graad van master in de industriële wetenschappen: bouwkunde

Gezamenlijke opleiding UHasselt en KU Leuven

2020•2021

Faculteit Industriële Ingenieurswetenschappen

master in de industriële wetenschappen: bouwkunde

Masterthesis

Effects of Decelerated Moving Load of Automated Vehicles on the Pavement StressStrain Responses Using 3-D Finite Element Modelling

PROMOTOR :

Prof. dr. ir. Ali PIRDAVANI

BEGELEIDER :

De heer Ali YEGANEH

Domenic Daniels

Scriptie ingediend tot het behalen van de graad van master in de industriële wetenschappen: bouwkunde

UHASSELT KU LEUVEN

Foreword

During the final months of my third school year as an engineering student, I had to choose a subject for a master thesis. I was required to submit a shortlist with 3 possible research subjects. The subject "*Effects of decelerated moving load of automated vehicles on the pavement stress-strain responses using 3-D finite element modelling"* was assigned to me. I had chosen this subject as one of three possible subjects due to my interest in infrastructure and road construction.

Upon first being assigned this subject I was very motivated, but this project proved to be more difficult than I had expected. At the time when I made my decision regarding the thesis subject, I did not fully understand the difficulties that would come with researching anything about artificial intelligence, and my expectations about what this study would entail were totally different from what it ultimately became. Defining "Automated vehicle deceleration" behaviour proved to be the greatest difficulty, as a correct definition of this behaviour would make or break this project. The ABAQUS-program (the software in which the finite element calculations were done) also proved rather tricky to come to grips with, although I did manage to get the hang of it in the end. Finally, there was the experience of balancing the work for this thesis with all the other projects from school and my internship in the first semester.

During this project, I learned a lot of valuable lessons. Most were about properly conducting academic research and setting up a thesis, but I also had some experiences which might help me later in my professional career. For example the importance of time management and planning became very clear during this project.

Lastly, there are two persons whom I would like to thank for their contributions to this project. First, there is Prof. dr. ir. Ali Pirdavani who was my main thesis supervisor. His constructive criticism of my work was very valuable, and allowed me to improve parts of this project to create a better master's thesis as a whole. Furthermore, I would like to thank Mr. Yeganeh, who supervised my activities and helped me throughout this project with any questions and issues. You being almost always and quickly available to assist me was of great value to me. Finally, I would like to thank both Prof. dr. ir. Pirdavani and Mr Yeganeh for their continued patience. The progression of this project was far from smooth, but your continued support has been much appreciated.

Table of contents

Foreword 1
Table of contents 3
List of Figures 5
List of Tables 7
Abstract (English) 9
Abstract (Nederlands) 11
Glossary 13
1 Introduction 15
2 Literature study 17
2.1 HMA Pavement Stress-strain response 17
2.2 Pavement structure and Material Characteristics 20
2.2.1 Pavement Structure 20
2.2.2 Material characteristics 20
2.3 Automated vehicle deceleration Behaviour 21
2.3.1 Emergency deceleration behaviour 21
2.3.2 Comfort during deceleration 23
2.3.3 Non-AVs' normal deceleration behaviour 24
2.3.4 AVs' normal deceleration behaviour 26
3 Methodology 29
3.1 Geometry 29
3.1.1 Pavement Layers 29
3.1.2 Tyre imprint area 30
3.2 Material properties 31
3.3 Steps 34
3.4 Layer Interaction 35
3.5 Boundary conditions 35
3.6 Model Meshing 36
3.7 Modelling the Load 37
3.7.1 Load distribution 37
3.7.2 Characterization of moving Wheel Load amplitude 39
3.8 Infinite element 41
4 Model Validation 43
4.1 Model Validation steps 43
4.1.1 Vertical stress validation 43

4.1.2 Longitudinal strain validation 45
4.2 Model inaccuracies 47
4.2.1 Current inaccuracies 47
4.3 Model validation conclusion 48
5 Simulation setup 51
5.1 Deceleration behaviour 51
5.2 Step time period calculation 52
5.2.1 Determining of the speed and distance formulas 53
5.2.2 Determining the integration constants 53
5.2.3 Calculation of the step time 54
6 Simulation results 57
6.1 Vertical Stress 57
6.2 Longitudinal Stress 60
6.3 Vertical Strain 64
6.4 Longitudinal Strain 67
7 Discussion of results 73
8 Conclusion 79
Bibliography 81
Appendix 83
8.1 Numerical results of the simulations 83

List of Figures

Figure 1: contact stress distributions along tyre contact length for (a) vertical contact stress, (b) transverse contact stress, and (c) longitudinal contact stress (tyre moving from left to right) [4] 18
Figure 2: Illustration of torques and frictional forces due to (a) braking and (b) acceleration where: w is angular speed of tyre; v is vehicle speed; M is torque on tyre; Fz is vertical force on pavement; and Fx is frictional force on pavement [4] 19
Figure 3:Braking distance schematic [8] 21
Figure 4: Slip versus friction coefficient [9] 22
Figure 5:Typical acceleration and jerk criteria for public transportation and typical criteria of normal, aggressive and extremely aggressive drivers [9] 24
Figure 6: (a) different functions for deceleration profiles and (b) reference functions for deceleration profiles [10]. 25
Figure 7: idealized plots of deceleration-speed [11] 25
Figure 8: functions for AV and non-AV deceleration behaviour [10] 27
Figure 9: Pavement layer thickness [13] 29
Figure 10: ABAQUS Pavement model Geometry 30
Figure 11: actual wide base tyre footprint (a) and tread geometry in ABAQUS (b) 31
Figure 12: ABAQUS material property input window for damping characteristic 32
Figure 13: progressive contact pressure shifting on one set of ribs 34
Figure 14: schematic illustration of tire moving along pavement surface.[6] 35
Figure 15: Boundary conditions 36
Figure 16: Tyre imprint meshing [13] 36
Figure 17: Pavement model meshing 37
Figure 18: Tyre foot print[13] 38
Figure 19: tyre load imprint in ABAQUS 39
Figure 20: Definition of the trapezoidal loading amplitude 40
Figure 21: Continuous loading amplitude for (a) the entrance part of the tyre imprint elements and (b) the exit part of the tyre imprint elements [13] 41
Figure 22: Finished model in ABAQUS 42
Figure 23:Vertical stress results for outer tyre rib (a) and centre tyre rib (b) at the bottom of the wearing surface (AC1: 0.58m) – speed: 72 km/h 44
Figure 24: Vertical stress at the bottom of the wearing surface (AC1: 0.58m) at a speed of 72 km/h and 38 kN wheel load at 25°C [13] 44
Figure 25: Longitudinal strain results for the outer rib (a) and centre rib (b) at the bottom of the BM-25.0 layer (AC2 layer – 0.43m) - speed: 8 km/h 45
Figure 26: longitudinal strain at the bottom of the BM-25.0 layer (AC2 layer - 0.43 m) at a speed of 8 km/h and 38 kN wheel load at 25°C - wide base tyre [13] 46
Figure 27: Functions for AV and non-AV deceleration behaviour [10] 52
Figure 28: Change in step time due to deceleration in function of distance travelled 55
Figure 29: Non-AVs' Vertical stress Situation (a), AVs' vertical stress situation (b) 57
Figure 30: Non-AV vertical stress for outer tyre rib 58
Figure 31: AV vertical stress for outer tyre rib 58
Figure 32: non-AV vertical stress for centre tyre rib 59
Figure 33: AV vertical stress for centre tyre rib 60
Figure 34: Non-AV longitudinal stress situation (a), AV Longitudinal Stress situation (b) 61
Figure 35: Non-AV longitudinal stress for outer tyre rib 61

Figure 36: AV longitudinal stress for outer tyre rib 62
Figure 37:Non-AV longitudinal stress for centre tyre rib 63
Figure 38: AV longitudinal stress for centre tyre rib 63
Figure 39: Non-AV Vertical strain situation (a), AV Vertical strain (b) 64
Figure 40: non-AV vertical strain for outer tyre rib 65
Figure 41: AV vertical strain for outer tyre rib 65
Figure 42: non-AV vertical strain for centre tyre rib 66
Figure 43: AV vertical strain for centre tyre rib 67
Figure 44: non-AV longitudinal strain situation (a), AV longitudinal strain situation (b) 68
Figure 45: non-AV Longitudinal strain for outer tyre rib 68
Figure 46: AV longitudinal strain for outer tyre rib 69
Figure 47: non-AV longitudinal strain for centre tyre rib 70
Figure 48: AV longitudinal strain for centre tyre rib 70
Figure 49: Evolution of the speed of AV and non-AV load caused by their different deceleration behaviours 76
Figure 50: Closeup of tyre imprint and load position (a), model with the loads visible (b) 76
Figure 51: Step time (loading time) increase for both deceleration models 77

List of Tables

Table 1: Tread pressure and dimensions at a nominal pressure of 720 kPa and wheel load of 38 kN [13] 30
Table 2: Virginia smart road section input parameters [7] 31
Table 3: Prony coefficients for AC1 layer (left) and AC2 Layer (right) [7] 33
Table 4: Normalized Prony Coefficients for the AC1 Layer 33
Table 5: Normalized Prony Coefficients for the AC2 Layer 34
Table 6: Tread pressure and dimensions at a nominal tire pressure of 720 kPa and a wheel load of 38 kN [13] 38
Table 7: Tabulated data for the trapezoidal loading amplitude [13] 40
Table 8; Step time of Non-Automated Vehicles (Non-AVs) 54
Table 9: Step time of Automated Vehicles (AVs) 55
Table 10: table with the maximum values, the mean values of vertical stress for the centre rib (rib 9) 59
Table 11: table with the maximum and mean values of vertical stress for the centre rib (rib 9)..... 60
Table 12: table with the maximum and mean values of longitudinal stress for the outer tyre rib (rib 9) 62
Table 13: table with the maximum and mean values of longitudinal stress for the centre tyre rib (rib 5)..... 64
Table 14: the maximum and mean values of vertical strain for the outer tyre rib (rib 9) 66
Table 15: maximum and mean values of vertical strain for the centre tyre rib (rib 5)..... 67
Table 16: maximum and mean values of vertical strain for the outer tyre rib (rib 9) 69
Table 17: maximum and mean values of longitudinal strain for the centre tyre rib (rib 5)..... 71
Table 18: Vertical stresses – summary 73
Table 19: longitudinal Stresses – summary 74
Table 20: Vertical strains – summary 74
Table 21: Longitudinal strains – summary..... 75

Abstract (English)

Automated vehicles (AVs) are set to become more prevalent in the future, and their deployment has raised several questions about how these new types of “driverless” cars will affect road systems and pavements worldwide. One of the significant potential differences between AVs and non-AVs is the decelerating moving loads of the vehicles, influencing pavement performance. This paper aims to examine the effects of the decelerated moving load of AVs on pavement stress-strain responses using 3-D finite element modelling.

For this purpose, first, the difference in deceleration behaviour between AVs and non-AVs was examined. A linear deceleration model was proposed for AVs, while non-AVs were assumed to follow a parabolic deceleration model. Afterwards, a 3D pavement model was developed through the ABAQUS software, and the effects of decelerating moving loads on pavement stress-strain responses were determined using 3D finite element modelling. The transient dynamic tyre loading was simulated using a trapezoidal moving load and an implicit dynamic analysis. After validating the finite element model, the longitudinal and vertical stresses and strains induced by the AVs and non-AVs deceleration models and calculated by ABAQUS were compared.

The results of these comparisons, against expectations, show that there was hardly any difference in maximum values. Some possible explanations for this lack of difference were given: a lack of difference in speed and loading time of the pavement elements between the two proposed deceleration models, a lack of possibilities to simulate multiple vehicle passes, and a limited representation of the effects of braking in the 3D model.

Abstract (Nederlands)

Geautomatiseerde voertuigen (AVs) zullen, door de ontwikkeling van de technologie, in de toekomst meer en meer voorkomen. Er rijzen hierdoor echter vragen op over hoe deze nieuwe types van “onbemande” voertuigen invloed zullen hebben op het wegennetwerk en de wegverharding in de wereld. Een van de significante verschillen tussen AVs en gewone voertuigen is het deceleratie-gedrag van de AVs wat invloed kan hebben op de wegverharding. Deze studie heeft als doel om de effecten van decelererende bewegende lasten van AVs op de spanning-rek respons van wegverhardingen te onderzoeken met behulp van 3D eindige elementen modelleringen.

Om dit doel te kunnen bereiken moest eerst het verschil in deceleratie-gedrag tussen de AVs en gewone voertuigen gedefinieerd worden. Een lineair deceleratie-model werd voorgesteld voor de AVs, en voor gewone voertuigen werd uitgegaan van een parabolisch deceleratie-model. Hierna werd een 3D model gemaakt van een stuk wegverharding met behulp van de ABAQUS-software, en de effecten van de decelererende bewegende lasten op de spanning-rek respons van de wegverharding werden berekend met behulp van de eindige elementen modellering. De dynamische wiel-belasting werd gesimuleerd door een trapezoïde bewegende belasting en een impliciete dynamische belasting. Na validatie van het eindige elementen- model van de wegverharding werden de resultaten van de simulaties met elkaar vergeleken. De verticale en longitudinale spanning en rekken veroorzaakt door het deceleratie-gedrag van de AVs en gewone voertuigen werden met elkaar vergeleken.

De resultaten van deze vergelijking toonden, tegen de verwachtingen in, aan dat er nauwelijks verschil was in maximumwaarden. Hiervoor werden enkele mogelijke verklaringen gegeven; Een gebrek aan verschil in snelheid en belastings-tijd tussen beide voorgestelede deceleratie-modellen, een gebrek aan mogelijkheden om meerdere voertuigpassages te simuleren, en een beperkte voorstelling van de effecten van het remmen in het 3D model.

Glossary

- AV:
  Automated vehicle. A vehicle that is driven by artificial intelligence, a self-driving car.

- Non-AV:
  Non-Automated Vehicle. The opposite of an AV. A conventional car driven by a human driver.

- HMA:
  Hot mix asphalt.

- FEM / FE model
  Finite element modelling / Finite element model.

- Project Model:
  The model designed and produced for this thesis.

1 Introduction

The concept of autonomous vehicles (AVs) has been around for a long time. Ever since the 1920's vehicles that could pilot themselves have been a fascination for many, but in the end, it had always remained some futuristic fantasy. In recent years, however, that seems to be changing. Companies like Tesla and Volkswagen are propelling development forward, and it seems more and more likely that AVs no longer belong to sci-fi imagination but are becoming part of the near future.

The reason that AVs have always been so interesting is due to the fact that they can have a significant effect on many different parts of the world around them. They also have several important advantages over manually driven cars. The most important of these is eliminating human error in AVs, which will increase road safety. Another benefit would be greater independence for seniors and disabled people. Then there are also environmental gains to consider, as AVs could reduce fuel use and carbon emissions. Lastly, workers' productivity could also be increased, as it could allow them to recapture time due to faster travelling speeds and the ability to do other things during commuting now that they do not have to drive the vehicle anymore.

The extensive market introduction of autonomous vehicles could also have an impact on the traditional transportation systems. The boundaries between private and public transport systems could begin to blur. Due to the possibility of autonomous relocation of cars, car-sharing could become much more relevant, impacting the bus and cab sector. Private car ownership might even become redundant [1]. Also, transporting goods via trucks might be seriously impacted, as drivers might no longer be needed. The possibility of reduced congestion might also help cut the costs of transport of goods.

Autonomous vehicles might also impact road infrastructure and pavement performance since AVs can drive with reduced headways and in narrower lanes. This will result in more cars on the same road area, meaning that bridges, or even the pavement itself, will have to be redesigned to cope with the higher loads of more cars. Moreover, traffic junctions might be fundamentally changed, as traffic lights are no longer necessary and right of way rules change. Traffic flows might not even cross anymore, giving rise to the need for new viaducts and other designs to keep traffic flows from needing to cross each other. Lower parking demands are also a possibility freeing up space for other use.

Apart from increased load due to more cars on the road, there are also other ways that AVs will influence the pavement. Specifically, the stress exercised on the pavement is an important factor that will need to be taken into account. Due to the difference in behaviour between AVs and manually driven vehicles, some problems or benefits might arise. One example of this is the lateral wandering of cars. Since AVs have much less lateral wandering due to them not being subject to human inaccuracy, AVs will wander less over the width of the traffic lane. While the manually driven cars will "spread out" over the pavement, constantly oscillating between driving left or right off centre of the lane, AV will always drive in the centre of the road. This means that two small strips of pavement will be much more in contact with the car, which will have to resist much more stress than the rest of the pavement. This will result in drastically more rutting. Therefore, it will probably be necessary to program AVs to have some lateral wandering so as not to damage the pavement too much.

However, the focus of this study will not be on the lateral wandering behaviour of AVs but on their deceleration behaviour. Pavement rutting and fatigue cracking are caused by stresses applied on said pavement, and deceleration is one of the causes of these stresses. The higher the deceleration, the higher the stresses in the pavement will be. The possibility of AVs having different deceleration

behaviour from manually driven cars could change the way pavements will be designed. If AVs were to be smoother in deceleration, it would positively affect the pavement damage, which could reduce the thickness required, a reduction in costs, and even a change in material used for pavements. This paper will focus on researching the possible effects of AV deceleration on pavement stress-strain response.

2 Literature study

2.1 HMA Pavement Stress-strain response

The primary function of a “Hot-Mix Asphalt” (HMA) pavement is to make a resistant and convenient surface. A vehicle traveling over the pavement exerts a force on the pavement through its area of contact with the pavement, resulting in stresses on the pavement. The pavement is supposed to resist these stresses in order to remain a hard, convenient surface. The lifecycle of a pavement depends on how long it can function properly. If it fails to resist the resulting stresses, the damage will follow, and the pavement will no longer function properly.

The two most important types of damage that occur in HMA asphalt pavements are rutting and fatigue cracking. Rutting is the permanent displacement of pavement material that results in longitudinal depressions on the pavement in the wheel paths. This deformation results in low ride quality, and if the depressions are deep enough, rain water pooling in the rutted areas can even cause hydroplaning [2]. Fatigue is the cracking of the surface because of failure due to repeated traffic loading. Eventually, these cracks can lead to the disintegration of the surface, and finally, potholes [3].

The abovementioned pavement deterioration modes are caused by tensile and shear stresses resulting from tyre pavement interactions. Generally, tyre-pavement contact stresses have three components: Vertical, transverse, and longitudinal. The responses of flexible pavements, like pavements with HMA layers, to the 3D contact stresses caused by traffic loading can be determined by means of a 3D finite element model. This will be elaborated on later in the methodology chapter. The HMA is characterised as a linear viscoelastic material, and the dynamic tyre loading is simulated using continuous moving load and dynamic analysis [4].

There are two distinct situations concerning tyre-pavement responses. Wang and Al-Qadi illustrated these in their study about surface-related pavement damage due to tyre braking [4].

The first situation is tyre-pavement contact at free-rolling, where the vehicle is not accelerating nor decelerating, and thus no torque is applied to the wheel.

Their study demonstrates an example of normalized 3-D contact stress measurements along a tyre contact length under a free-rolling condition on a flat pavement surface, as shown in Figure 1. This figure illustrates the distribution of the 3D contact stresses [4].

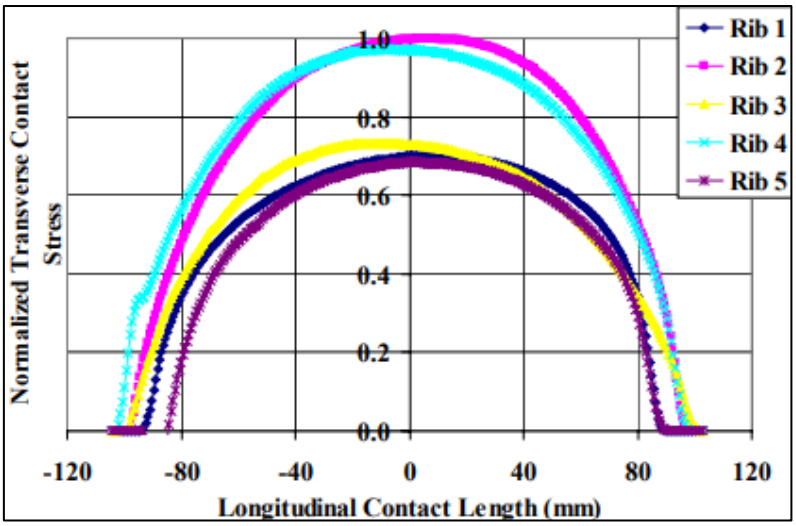

(a)

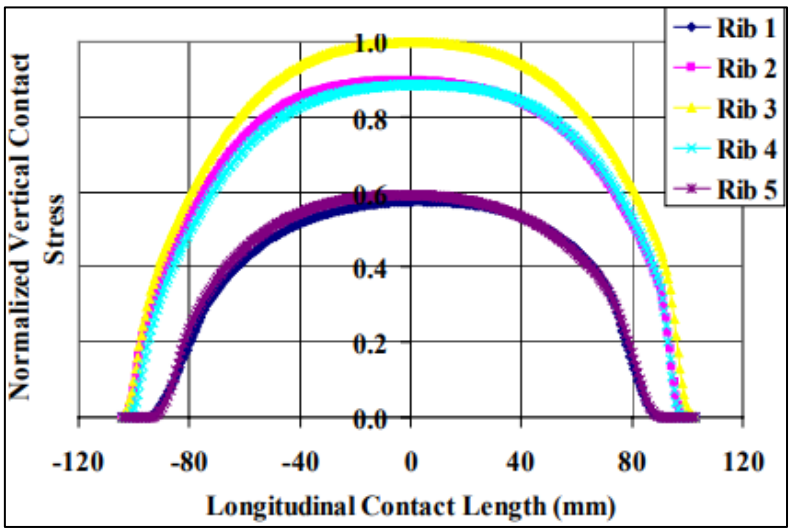

(b)

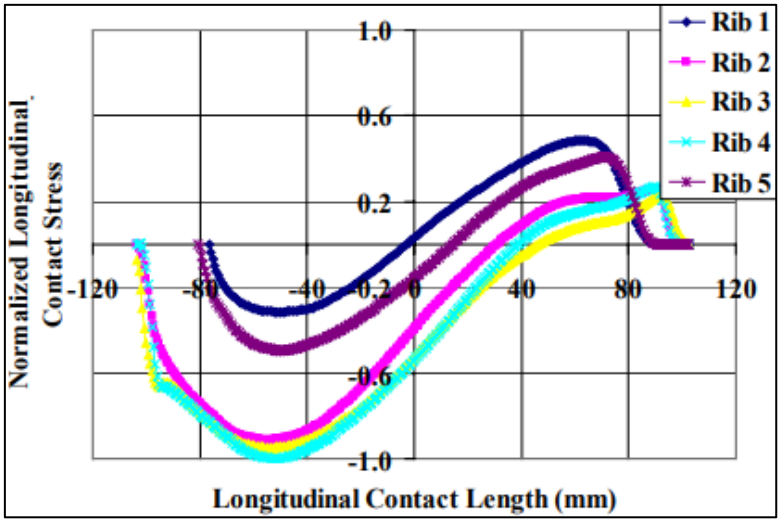

(c)

Figure 1: contact stress distributions along tyre contact length for (a) vertical contact stress, (b) transverse contact stress, and (c) longitudinal contact stress (tyre moving from left to right) [4]

The tyres in the study by Wang and Al Qadi [4] were modelled as rectangular shapes consisting of five ribs. It is important to note that the middle ribs (2,3 and 4) have longer contact lengths than the edge ribs and that the longitudinal tangential stresses "vary between the entrance and exit parts of the tyre imprint, with backward stresses in the front, and forward stresses in the rear half [4]. This causes the net total longitudinal stresses to be not significant when compared to the vertical contact stresses. It can thus be stated that the longitudinal contact stresses are negligible during the free-rolling of the tyre.

In this study, however, the tyres will probably be modelled as simple rectangular shapes to limit the complexity of the simulation. It is expected that this will not influence the results significantly. The design of the contact area between the tyre and the pavement will be elaborated on in another chapter

The second situation is tyre -pavement contact stress during braking or accelerating, where the longitudinal, transverse stresses have become much more significant. Because the vertical contact stresses are not constant in the tyre imprint area, the longitudinal contact stresses vary from one point to another. It is noted that the longitudinal stresses on pavement surface are forward stresses at braking and backward stresses at acceleration, which are opposite to the stresses on the tyre [4]. The schematic frictional forces on the pavement at braking and acceleration are illustrated in Figure 2.

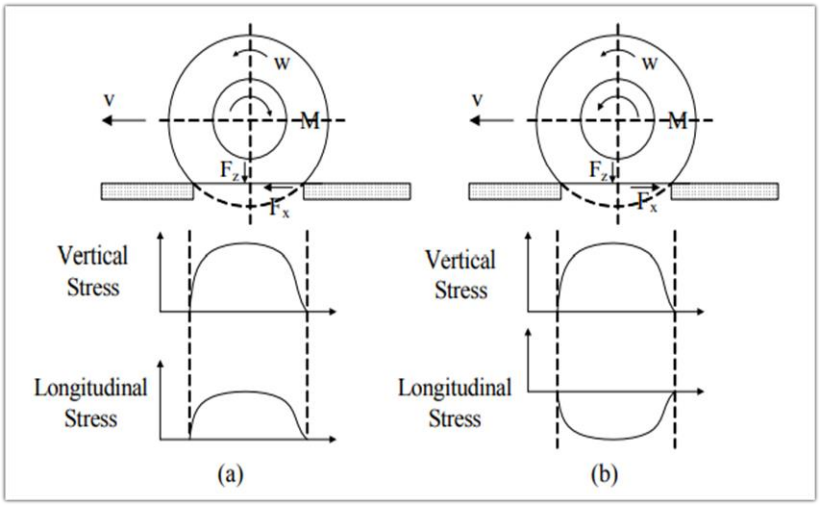

Figure 2: Illustration of torques and frictional forces due to (a) braking and (b) acceleration where: w is angular speed of tyre; v is vehicle speed; M is torque on tyre; Fz is vertical force on pavement; and Fx is frictional force on pavement [4].

Al-Qadi and Wang [4] concluded that low-speed vehicle loading induced more significant surface-related pavement damage than normal high-speed vehicle loading and that this was due to the increased loading time and the viscoelastic nature of HMA. Furthermore, they also concluded that tyre braking also caused additional longitudinal contact stresses on the pavement surface.

These findings showed that tyre-braking has 8 to 32 times the pavement surface cracking potential and 2.0 to 2.6 times the rutting potential compared to typical high-speed vehicle loading. This means that tyre-braking is clearly the most destructive of the two situations concerning tyre-pavement responses.

A good understanding of the tyre-pavement response of Non-automated vehicles will help us in the future when analysing the same tyre-pavement interactions for non-automated vehicles.

Finally, there are also other factors that influence the cracking and rutting potentials. These are, for example, temperature increases of the pavement, interface bonding condition, or tyre configuration. These will not be focused on in this project [5], [6].

2.2 Pavement structure and Material Characteristics

2.2.1 Pavement Structure

A hot mix asphalt (HMA) pavement is a flexible pavement comprising three distinct main layers. These are the HMA surface, the aggregate base layer, and the subgrade, with their own characteristics [7].

A flexible pavement is considered to react as flexible under an applied load. That means it is supposed to flex (bend) under a load of a tyre. Excessive flexing, however, should be avoided. Otherwise, this will result in over-stressing the layer, which will ultimately cause the layer to fail. In flexible pavements, the load distribution changes from one layer to another. This is due to the strength of the layers being different from each other. The strongest materials (least flexible) are in the top layer, and the weakest are in the lowest layer. This is because the wheel load is applied to a very small surface area at the top of the pavement, which causes high-stress levels. Deeper down in the pavement, the surface area to which the load is applied is larger, allowing the use of weaker materials [3].

2.2.2 Material characteristics

Hot mix asphalt is considered to be viscoelastic. The stress in such viscoelastic materials depends not only on the current state of strain but also on the history of strain development. Elastic theory cannot be used because it does not take this into account. The temperature will also influence the characteristics of HMA.

This time- and temperature-dependant behaviour will be modelled in the ABAQUS software by employing the viscoelastic models. This will, however, be elaborated on in the methodology.

An integral equation model for the deviatoric and bulk stresses is used in linear viscoelastic theory, as shown in Equations 1 and 2 [4]. "In these equations, the relaxation modulus of HMA can be modelled as a generalized Maxwell solid model in terms of a Prony series, equations 3 and 4 [4].

$$s = \int_{-\infty}^{t} 2G(t-\tau)\frac{de}{d\tau}d\tau \tag{1}$$

$$p = \int_{-\infty}^{t} K(t-\tau)\frac{d(tr[\varepsilon])}{d\tau}d\tau \tag{2}$$

$$G(t) = G_0\left(1-\sum_{i=1}^{n} G_i\left(1-e^{-\frac{t}{\tau_i}}\right)\right) \tag{3}$$

$$K(t) = K_0\left(1-\sum_{i=1}^{n} K_i\left(1-e^{-\frac{t}{\tau_i}}\right)\right) \tag{4}$$

where s is deviatoric stress
e is deviatoric strain
p is volumetric stress
$tr[\varepsilon]$ is trace of volumetric strain

G is shear modulus
K is bulk modulus
t is reduced relaxation time

G_0 and $K_0$are instantaneous shear and volumetric elastic modulus;
G_i , K_i , and τ_i are Prony series parameters.

2.3 Automated vehicle deceleration Behaviour

The main objective of this paper is to examine the effect of Automated vehicles on pavement stress-strain responses during braking. In order to be able to do this, first, a specific deceleration behaviour for Automated vehicles must be defined. This behaviour will be compared to the non-automated vehicles' behaviour to illustrate the effects that Non-AVs could possibly have on the pavement.

Defining the behaviour of an AV, however, is not an easy task. To make things simpler, the AV behaviour will be split into two parts. One part will consider emergency braking, a situation where the vehicle must suddenly decelerate quickly not to hit something. The Maximum possible braking force must be applied to stop the car as fast as possible. In this case, the vehicle's deceleration is mainly determined by the pavement friction and the distance to the object.

The second part of AV deceleration behaviour will centre around normal braking. This is braking under normal circumstances, where no harsh manoeuvres are required. There is enough distance between vehicle and object for which it has to decelerate. Here comfort will be a deciding factor in determining the deceleration of the vehicles.

2.3.1 Emergency deceleration behaviour

When an unexpected object, such as an animal or another vehicle, appears in front of a car, it is paramount that the car decelerates as fast as possible. The minimum stopping distance of the car will determine whether or not the car will hit the unexpected object. For AVs the following formula is given in the study by Binshuang et al. [8] to calculate the stopping distance:

$$S_T = S_{1+}S_2 = \frac{v * t}{3.6} + \frac{v^2}{254(\varphi + \psi)} \quad (5)$$

Where S_T is the total stopping distance of the AV in m, $S_1$is the vehicle reaction distance in m, S_2 is the vehicle braking distance in m, v is the vehicle speed in km/h, t is the braking time from hazard detected to vehicle automatic stop, φ is the adhesion coefficient between the road surface and the tyre, and ψ is the road drag coefficient.

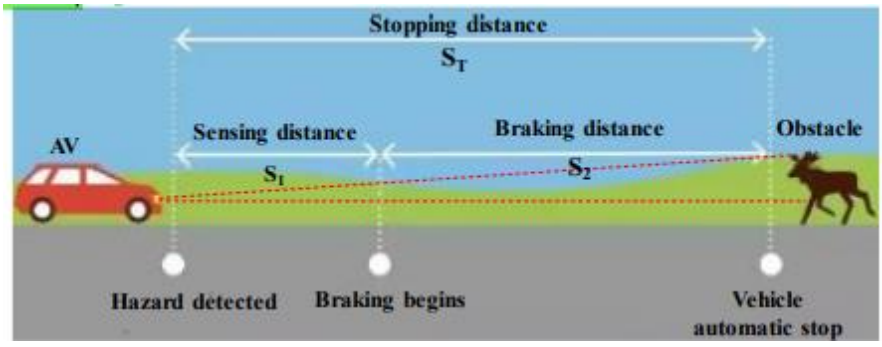

Figure 3:Braking distance schematic [8]

From equation 5, we can conclude that there are two factors, apart from the vehicle speed, that influence the stopping distance of an AV. These are the road frictional properties, represented by φ, and the sensing reaction time (SRT), the time needed for the AV system to recognize a hazard on the road and react. This SRT, however, can be reduced to milliseconds or even eliminated, thus leaving road frictional properties as the sole influence on stopping distance.

During tyre deceleration or acceleration, there are significant longitudinal frictional forces between tyre and pavement. The following equation from the study by Wang and Al-Qadi [4] can estimate these.

$$F_x(x, y) = F_y(x, y) * \varphi_p \tag{6}$$

Where $F_x(x, y)$ is longitudinal contact stress at the contact point, $F_y(x, y)$, is the normal contact stress at the contact point (x, y); and φ_p is the peak adhesion coefficient, or alternatively, the surface friction coefficient (SFC).

The surface friction coefficient at the tyre-pavement interface is not constant during the braking process, and it changes with vehicle speed and the slip ratio of the tyre. This friction coefficient usually achieves its peak value at a slip ratio of about 10% to 20%, depending on vehicle speed and surface texture condition, and decreases with the increase of slip until full slip (see Figure 4). The following formula characterises the slip ratio:

$$Slip\ ratio\ \% = \left(\frac{\omega * R_c}{v} - 1\right) * 100\ \% \tag{7}$$

Where ω is the angular velocity of the wheel, R_c is the effective radius of the corresponding free-rolling tire, and *v* is the forward velocity of the vehicle.

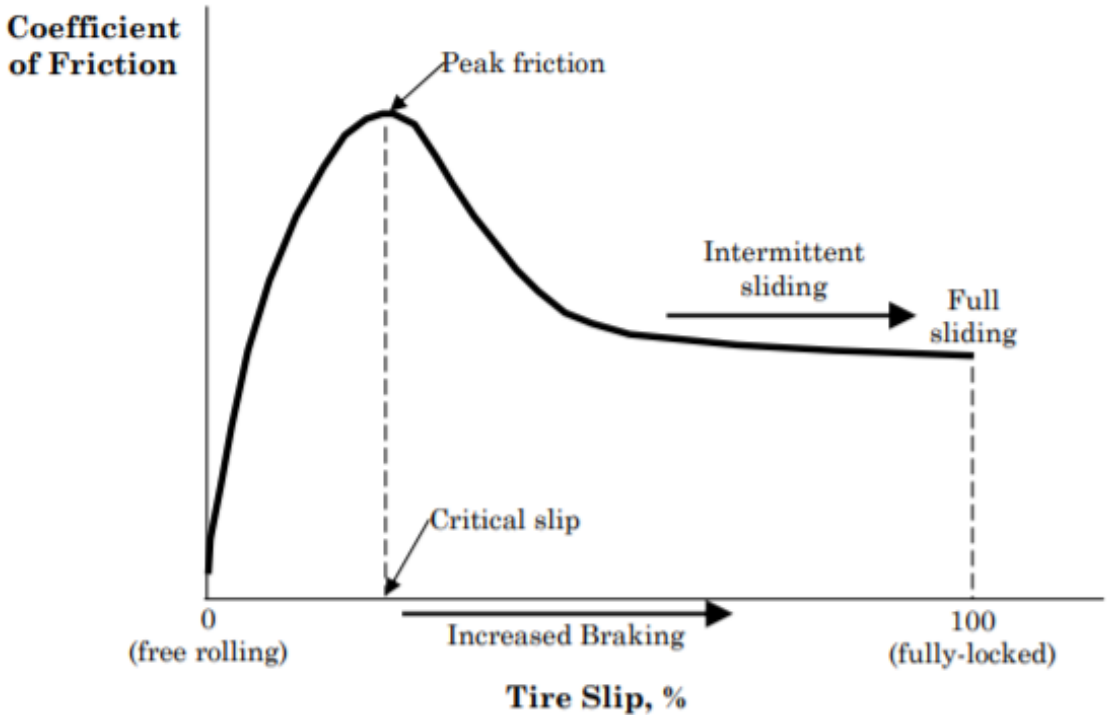

Figure 4: Slip versus friction coefficient [9]

For dry flexible HMA pavements, the peak friction coefficient φ_p lies between 0.7 and 0.8. In this study, the value 0.7 will be used, as it is used by Wang and Al-Qadi [4] as well. This also results in a maximum possible deceleration that the pavement can provide. The following formula gives this from the study by Bishuang et al. [8]:

$$a_{bmax} = g * \varphi_p \tag{8}$$

With g is the vehicle acceleration due to gravity in m/s² (taken as 9.8 m/s²).

Thus, in the situation that an AV will have to do an emergency braking manoeuvre, it is expected that it will use the maximum available deceleration, in this case using the peak friction coefficient φ_p that is achieved when the slip ratio is between 10% and 20%.

This is where AV behaviour will differ from non-AV behaviour. Human error and inaccuracy will prevent drivers from attaining constant maximum deceleration as they will not be able to keep the slip ratio of the wheels between 10-20%. Therefore φ will not reach the maximum value of 0,7, and the maximum average deceleration that non-AVs can achieve will be less than that of AVs.

Consequently, the longitudinal frictional forces (formula 6) exercised by non-AVs in these emergency situations will be less than that of AVs, which means that AVs can also cause greater pavement damage than non-AVs in these emergency situations.

2.3.2 Comfort during deceleration

Emergency braking only forms a very small part of the total picture of the deceleration behaviour of vehicles. Most of the time, vehicles decelerate at very low rates, primarily due to comfort. High rates of acceleration and deceleration are not comfortable to drivers and passengers and must therefore be limited to certain values. High rates of change in acceleration and deceleration are also not comfortable, and these must also be limited. These variables are called acceleration (m/s²) and jerk (m/s³). Figure 5 shows the limits of comfortable acceleration and jerk in the longitudinal and lateral directions.

The following ranges were given to acceleration and jerk [9]. Within these ranges, comfort is assured.

- Acceleration/deceleration:*-2.0-1.47 m/s²*
- Jerk: *-0.9 – 0.9 m/s³*

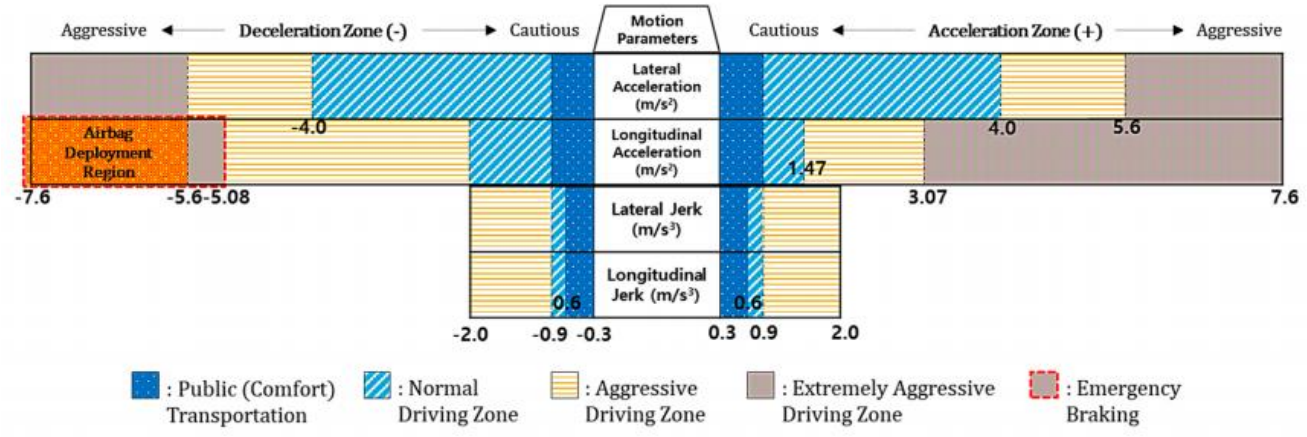

Figure 5:Typical acceleration and jerk criteria for public transportation and typical criteria of normal, aggressive and extremely aggressive drivers [9]

2.3.3 Non-AVs' normal deceleration behaviour

Three typical braking patterns can represent the normal deceleration behaviour of non-AVs according to the study of Deligianni et al. [10], in which research was conducted to examine drivers' braking behaviours by exploiting naturalistic driving data from the Pan-European TeleFOT (Field Operational Tests of Aftermarket and Nomadic Devices in Vehicles) project.

The first one of these determined models is the simplest one and is a linear relationship (see Figure 6) between the deceleration value (d) and elapsed deceleration time (t). In real traffic, this reflects the driver braking gradually. The function is:

$$d = a_1 * t \tag{9}$$

The second function represents, in real traffic, a situation in which the driver brakes firmly at the beginning of the event due to a sudden obstacle appearing. This is followed by gradually smoother braking since there is plenty of space to stop. The function in question (parabola 1) is as follows:

$$d^2 = 2 * a_2 * t \tag{10}$$

Finally, the last function depicts a situation where the driver makes an error of judgement and begins with smooth braking because he considers there is enough space to stop. A hard brake follows this due to lack of space and time. This function (parabola 2) is as follows:

$$t^2 = 2 * a_3 * d \tag{11}$$

Finally, reference functions were created using the average of the coefficients for each event for the best-fitted functions. The factors a_1, a_2 and a_3 are:

- $a_1 = -0.71$
- $a_2 = 2.96$
- $a_3 = -12.14$

Ultimately, the study determined that most of the braking events studied fit equation (10) best, which means that the majority of normal braking events are hard at the beginning and then gradually become smoother.

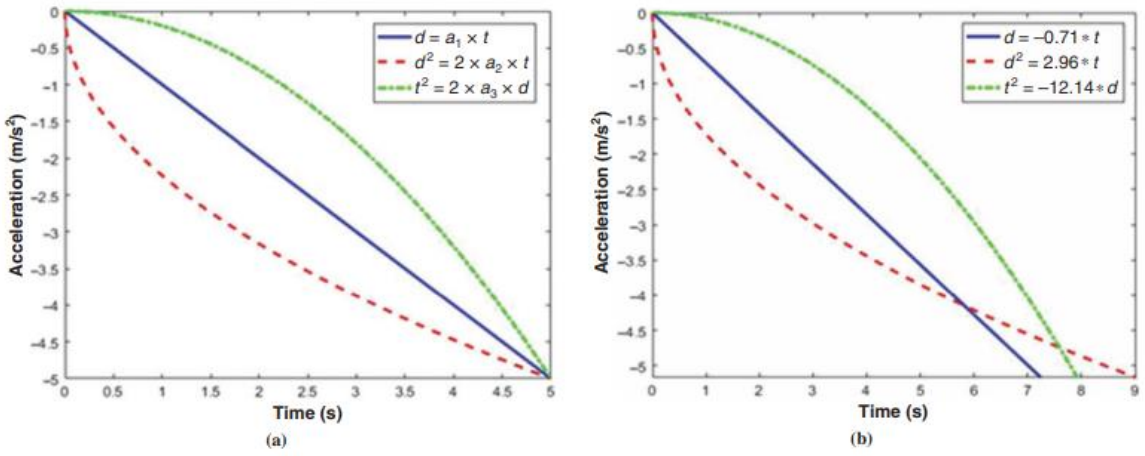

Figure 6: (a) different functions for deceleration profiles and (b) reference functions for deceleration profiles [10].

This is also confirmed in another study conducted by Bokare and Maurya [11]. It can clearly be seen in Figure 7 that first, the deceleration value rises to a peak, and then afterwards becomes lower again; in this study, different types of vehicles were also examined.

It is also observed from Figure 7 that critical speed (speed where deceleration is maximum) depends on vehicle type. The critical speed is highest for petrol cars and lowest for motorized three-wheelers, which has the lowest deceleration capability compared to other vehicle types.

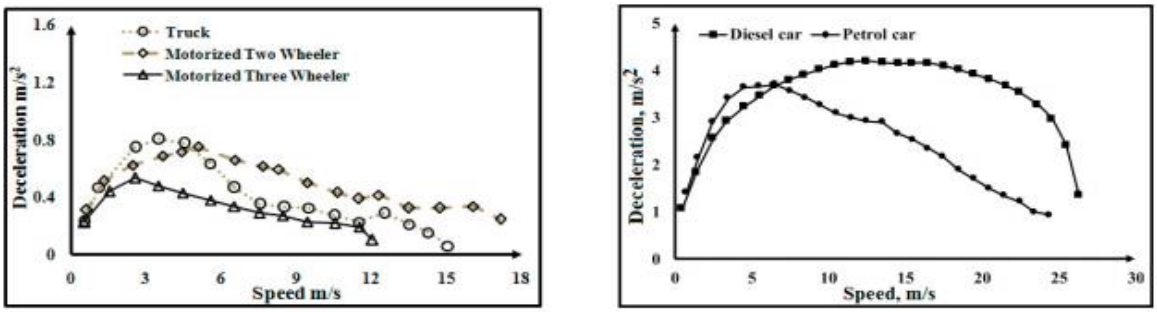

Figure 7: idealized plots of deceleration-speed [11]

The conclusion from the previously mentioned study by Deligianni et al. [10], that most deceleration events can be characterised by formula 10, can lead to certain hypotheses concerning the normal deceleration behaviour of AVs compared to non-AVs. The early sharp increase in deceleration in the behaviour of non-AVs can be explained by human error and inaccuracy. This peak, however, will probably have a negative effect on the pavement stress-strain response. In this case, the AV will have a positive advantage over non-AVs as its deceleration behaviour can be modelled more akin to formula 9. The linear, smoother deceleration will probably be less damaging to the pavement.

2.3.4 AVs' normal deceleration behaviour

Finally, the normal deceleration behaviour of an AV must be determined. There are many possible ways of doing this, but in this study, the deceleration behaviour of the AVs will be based on the model proposed in the study by Matute et al. [12] and on the three deceleration models proposed in the study by Deligianni et al. [10].

In the study by Matute et al. [12], a simple model predictive control (MPC) for longitudinal manoeuvres considering a bare speed planner is used. A maximum value constrains the speed profiles in this model at a specific time so that the total acceleration/deceleration is lower than the specified comfortable limits. These comfortable limits were already mentioned in chapter 2.3.2.

The speed planner uses Bezier curves to generate a smooth path along a proposed route with straights curves and even a lane change and uses the curvature of each road segment's curves (k) as parametric curves.

The objective of the proposed approach is to assure passenger comfort during autonomous driving. The comfort parameter is obtained through a combination of longitudinal (a_x), lateral (a_y) and vertical (a_z) accelerations, considering certain weights (n = n_x = n_y = 1.4)

$$a_w = \sqrt{n_x * \ a_x^2 + n_y * \ a_y^2 + a_z^2} \tag{12}$$

$$V_{max} = \sqrt{\frac{a_w}{n * k}} \tag{13}$$

a_w could be limited not to exceed the comfortable maximum deceleration value. The ABAQUS model that will be used in this study will only have a one-dimensional trajectory. The simulated load will move on one line.

In the study by Deligianni et al. [10] three models of deceleration behaviour were proposed for non-AVs. It was concluded that most drivers adhere to a rather conservative parabolic deceleration model (see Figure 6), where they brake firmly in the beginning in order to create some margin space and not run into the object in front of them. A typical driver cannot precisely calculate its distance to an object, and therefore it is usually best to decelerate a little extra at the beginning of the manoeuvre, and have a little extra room to play with instead of trying to measure the distance precisely and try to stop ideally in front of the object.

This braking behaviour will result in a rather abrupt change in deceleration initially, possibly putting higher strain on the asphalt surface and doing more damage in the long run. It is also not the most

efficient braking behaviour. This is where AV braking behaviour will differentiate itself from non-AV braking behaviour. Figure 8 accentuates this difference in deceleration behaviour.

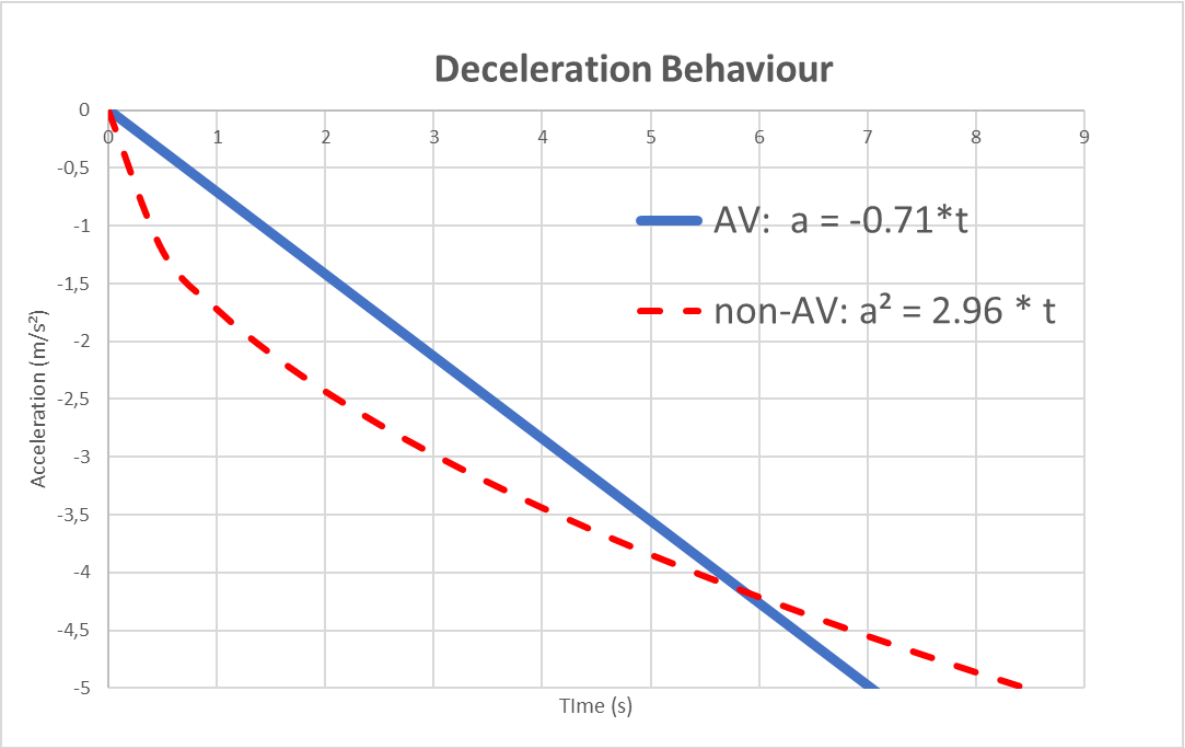

Figure 8: functions for AV and non-AV deceleration behaviour [10]

There is little information available about the exact deceleration behaviour of AVs, apart from the comfort thresholds mentioned before. Therefore in this study, a hypothetical deceleration behaviour will be proposed based on the three deceleration models determined by Deligianni et al. [10]. Due to being equipped with hi-tech sensors and computers which can calculate distances and speeds in split seconds, AVs will be much more accurate in calculating a required deceleration manoeuvre. This means that a less conservative approach can be used. There is now no more need for braking harder in the beginning to create some margin. Therefore, a more efficient deceleration model can be used.

The most efficient out of the three proposed deceleration models is the linear model. This model has a linear increase in deceleration with no sharp increases and dips in deceleration. This will also hypothetically have a positive influence on the stress applied on the pavement. The parabolic non-AV deceleration is expected to produce higher peak stress due to the sharp increase in deceleration in the beginning. This means that the AV impact on the pavement will be positive due to the reduced peak strain and stress.

Accordingly, the formula typifying AV deceleration behaviour will be:

$$d = -0.71 * t \tag{14}$$

And the formula for non-AV deceleration behaviour will be:

$$d^2 = 2.96 * t \tag{15}$$

Finally, the comfort factor has to be considered. This factor is of importance for AV behaviour but not for non-AV behaviour. The maximum allowed deceleration and jerk parameters are determined to be:

- Acceleration/deceleration:-2.0-1.47 m/s^2
- Jerk: -0.9 – 0.9 m/s^3

For jerk, this will not be a problem. The maximum the deceleration may change per second is 0,9 m/s^3. This value cannot be reached since the linear model can only change -0.71 m/s^2 per second.

The deceleration rate should be limited. The deceleration reaches the maximum allowed value of -2.00 m/s^2 after 2.8169 seconds. After 2.8169 seconds, the deceleration should no longer increase but remain at -2.00 m/s.

In this project, however, the time spans in the ABAQUS simulations will be so minuscule that the passed total time during the timing of the actual test will never come close to 2 seconds, never mind 2.8169 seconds. This means that it is safe to use these two equations as the comfortability threshold will never be crossed.

3 Methodology

In this chapter, the different steps of making the pavement model will be discussed in detail. The model geometry used in this project is based on the study by Yoo and Al-Qadi [13]. The pavement characteristics are taken from the "Virginia Smart Road – section B" at a temperature of 25°C and given in the study by Al-Qadi et al. [7]. The model parameters were taken at a temperature of 25°C, a tyre load of 38 kN, and a nominal tyre pressure of 720 kPa.

3.1 Geometry

First, the general geometry of the pavement block has to be modelled. Pavement is divided into different layers of different materials and has a general cuboid shape.

3.1.1 Pavement Layers

The exact measurements of the pavement block are 1900 x 1130 x 618 mm. The pavement is divided into different layers, of which each thickness is given in Figure 9. Below the lowest layer of Figure 9, the subbase layer, another layer is included, the subgrade layer, with a thickness of 30 mm. This layer will be the infinite layer, but this will be explained further in a different chapter. In total, there are 6 layers. Figures 9 and 10 show the composition of the pavement model.

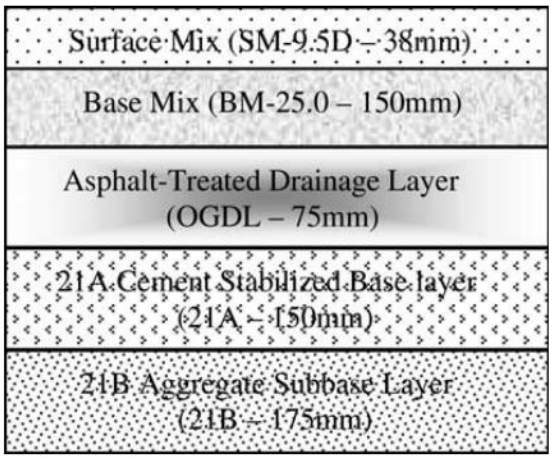

Figure 9: Pavement layer thickness [13]

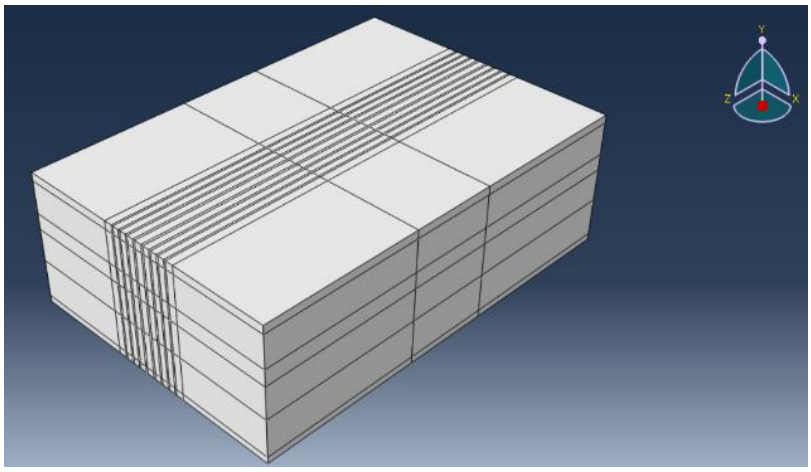

Figure 10: ABAQUS Pavement model Geometry

3.1.2 Tyre imprint area

In this thesis, a wide base tyre type (455/55R22.5) was used for the model. This tyre consists of 9 ribs in total, each with varying thickness, and has a nominal pressure of 720 kPa and a wheel load of 38 kN.

In order to be able to simulate a tyre with our model later on, with different loads on each rib and different sizes of each rib, the tyre geometry and imprint area must be included in the general geometry. The widths of each tyre rib and the corresponding tyre grooves are given in Table 1. These grooves and treads are then drawn over the complete length of the surface of the pavement block and continue on the sides. Only the bottom of the pavement block is left out, as this will become an infinite element.

Table 1: Tread pressure and dimensions at a nominal pressure of 720 kPa and wheel load of 38 kN [13]

Wide Base tyre	R1*	G1*	R2	G2	R3	G3	R4	G4	R5
Vertical Pressure (kPa)	502	-	832	-	883	-	936	-	956
Length (mm)	144	-	154	-	156	-	172	-	174
Width (mm)	38	9.6	31	9.6	31	10.3	31	11.4	35

*R: Tyre Rib *G: Tyre Groove
The wide-base tyre has nine treads and is symmetric with respect to the fifth tread

The total width of the tyre imprint area will be 378,8 mm. Next, the length of the tyre imprint area or loading area must also be defined. The length will be 400 mm. Why this distance has been chosen will be explained in chapter . These lines also run from top to the sides of the pavement block, but not on the underside of the pavement block. Figure 10 and Figure 11b show these tread lines. Figure 11a shows the actual wide bas tyre imprint.

The tyre imprint area will be 378,8 x 400 mm in total, and can be seen in Figure 10b.

Important to note for the rest of this thesis is that the wide base tyre has 9 treads and that for the rest of the paper, the centre tyre rib will be referenced as tyre rib 5, and the outer tyre ribs will be referenced as tyre ribs 1 and 9.

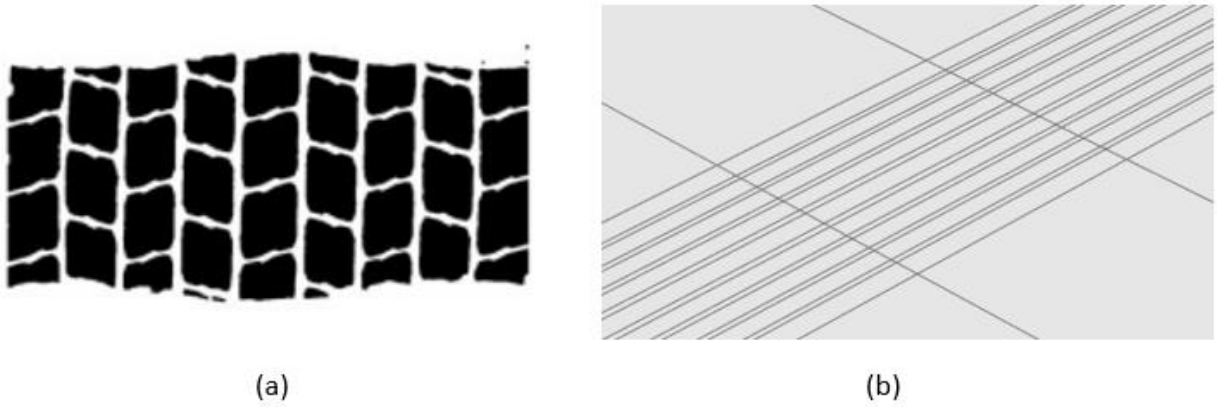

Figure 11: actual wide base tyre footprint (a) and tread geometry in ABAQUS (b)

3.2 Material properties

The next part in developing the ABAQUS finite element modelling is giving the different pavement layers defined in chapter 3.1.1. their material characteristics. These are given in the study by Gungor et al. [7]. The values of the characteristics of each pavement layer are listed in Table 2.

Table 2: Virginia smart road section input parameters [7]

Layer	Thickness (mm)	Instantaneous/Linear Modulus (Mpa)	Poisson's ratio	Density (x10^-6)	Rayleigh damping Parameters (α)	Rayleigh damping Parameters (β)
AC1	38	4230.9	0.35	2.30	N/A	N/A
AC2	150	4750.49	0.4	2.30	3.1416	0.000795
OGDL	75	2415	0.4	2.30	3.1416	0.000795
CTB	150	10342.14	0.4	2.30	3.1416	0.000795
Subbase	175	310.26	0.4	1.5	3.1416	0.000795
Subgrade	-	262.00	0.4	1.5	3.1416	0.000795

OGDL: Open-graded drainage layer,
CTB: Cement-treated base

The material properties of the pavement layers can be subdivided into four groups: Density, Elastic, Damping, and Viscoelastic. The density parameters for the layers are given in ton/m³ and must be transposed to kg/m³ for ABAQUS. This was determined by looking at another paper by Wang [6] concerning the same pavement. The elastic parameters consist of Poisson's ratio and Young's modulus. Lastly, for the damping, there are the Rayleigh damping parameters α and β. Figure 12 shows the input window for the material properties in ABAQUS.

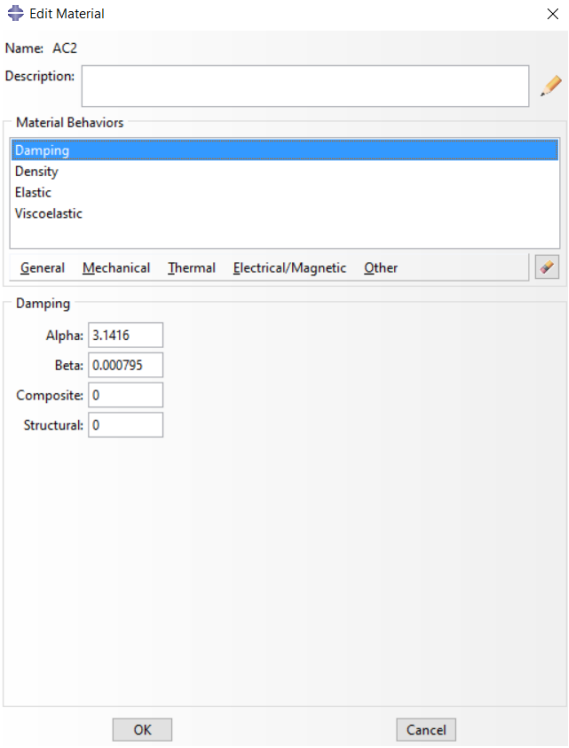

Figure 12: ABAQUS material property input window for damping characteristic

Finally, the Prony Coefficients symbolise the viscoelastic nature of the asphalt layers and can be found in Table 3. The values in Table 3 must be transposed first, however, in order to fit into the ABAQUS model. The values in Table 3 need to be normalized first before they can be put into ABAQUS. This is done with the following formula:

$$\frac{G_i}{G_1} = g_i \tag{16}$$

Where G_i is the Prony coefficient, which should be normalized, G_1 is the first coefficient of the Prony series, and g_i is the normalized value of the Prony Coefficient, which should be inserted into ABAQUS. This formula must then be used to normalize all the values for ABAQUS. There is one limitation, however. No normalized value can be greater than 1, and also, the sum of all the normalized coefficients of a Prony series must be smaller than 1.

$$0 < g_i < 1 \tag{17}$$

$$0 < \sum_{i=1}^{n} g_i < 1 \tag{18}$$

Due to these limitations, the first coefficient of each Prony series was left out, since G_1/G_1 will always be 1. This, however, does not cause an issue since it is only one term of the Prony series. The more terms in a Prony series, the more accurate the series describes the viscoelastic behaviour. This means that a smaller number of coefficients is a less accurate description of viscoelastic behaviour. The removal of one coefficient, however, does not impact the accuracy. The normalized values of the Prony series of AC1 and AC2 can be found in Table S 4 and 5.

Table 3: Prony coefficients for AC1 layer (left) and AC2 Layer (right) [7]

	AC1			AC2		
i	Gi (MPa)	Ki (Mpa)	τi	Gi (MPa)	Ki (Mpa)	τi
1	3277.4667	3277.4667	1.00 X 10^-2	3085.7378	3085.7378	1.00 X 10^-2
2	698.01388	698.01388	1.00 X 10^-1	1069.5918	1069.5918	1.00 X 10^-1
3	168.3602	168.3602	1.00	405.53936	405.53936	1.00
4	58.509116	58.509116	1.00 X 10^1	117.09055	117.09055	1.00 X 10^1
5	11.577435	11.577435	1.00 X 10^2	50.973233	50.973233	1.00 X 10^2
6	7.2373775	7.2373775	1.00 X 10^3	7.0927191	7.0927191	1.00 X 10^3
7	8,6331515	8,6331515	1.00 X 10^4	3.4551549	3.4551549	1.00 X 10^4
8	0,0699114	0,0699114	1.00 X 10^5	-	-	-
9	0,0288996	0,0288996	1.00 X 10^6	-	-	-

Table 4: Normalized Prony Coefficients for the AC1 Layer

AC1 Layer			
	gi	ki	τi
1	x	x	0.01
2	0,216272992	0,216272992	0.1
3	0,052059034	0,052059034	1
4	0,018128496	0,018128496	10
5	0,003587159	0,003587159	100
6	0,002242432	0,002242432	1000
7	0,0026749	0,0026749	10000
8	2,16614E-05	2,16614E-05	100000
9	8,95427E-06	8,95427E-06	1000000

Table 5: Normalized Prony Coefficients for the AC2 Layer

AC2 Layer			
	gi	ki	τi
1	x	x	0.01
2	0,346624331	0,346624331	0.1
3	0,131423791	0,131423791	1
4	0,037945722	0,037945722	10
5	0,016518977	0,016518977	100
6	0,002298549	0,002298549	1000
7	0,001119718	0,001119718	10000

3.3 Steps

The step times symbolize the loading time of a part of the pavement and are thus very important in symbolizing the movement of a load. They also signify the type of analysis. Following the study by Gungor et al. [7], the implicit dynamic analysis type was chosen for a pavement analysis to capture the inertial/damping effect and frequency-dependant material properties.

Each step will represent a sort of snapshot of a situation in time. The steps will follow each other, one after the other, and each step will show a different situation of the tyre position and the load applied by the tyre on the asphalt. Figures 13 and 14 will illustrate this concept more clearly.

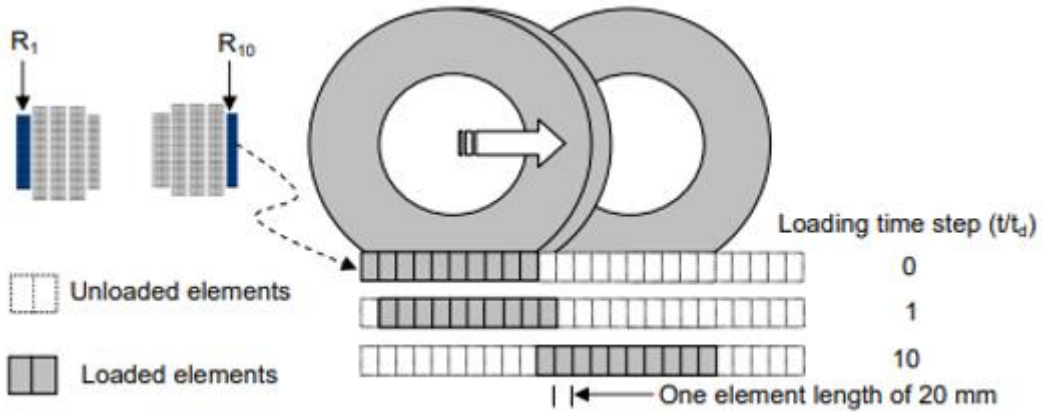

Figure 13: progressive contact pressure shifting on one set of ribs

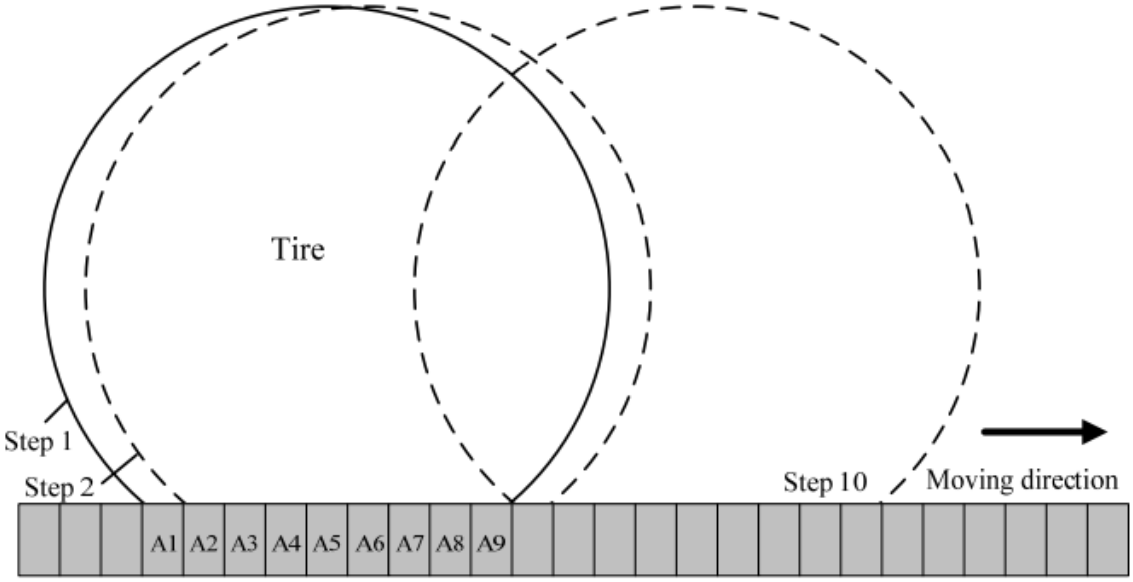

Figure 14: schematic illustration of tire moving along pavement surface.[6]

Further calculation of the step times and the number of steps required are explained in chapter 5.

3.4 Layer Interaction

The different pavement layers are supposed to be in interaction with each other. To model this, two methods were proposed in the studies by Gungor et al. [7] and Yoo and Al-Qadi [13]; a simple friction model (Coulomb model) and the elastic stick model. The simple friction model corresponded the best to reality in the case of a wide base tyre. Since this is rather difficult to model in ABAQUS, and since it is also not the focus of this study, it was chosen to keep all layers fully bonded. This will simplify the ABAQUS model but will probably cause some inaccuracies at the same time.

3.5 Boundary conditions

Next, the boundary conditions of the pavement block need to be defined. The pavement block is supposed to be part of a larger piece of pavement, and the effects of the material surrounding the pavement block need to modelled. There are three different boundary conditions. Figure 15 shows the ABAQUS model with the boundary conditions applied.

The first is related to the bottom of the pavement block. For this part of the pavement, the boundary conditions should be that the selected surface is fixed. This is performed by using “ENCASTRE (U1=U2=U3=UR1=UR2=UR3=0)” in ABAQUS, which signifies a fixed situation with movement restricted in x, y, and z directions.

Next, the long sides of the pavement block need to have the possibility of deflection in the y-direction but not in the z-direction. This is done by using “ZSYMM (U3=UR1=UR2=0)” in ABAQUS.

Finally, the short sides of the pavement block are supposed to have no deflection in the x-direction. This is done by using “XSYMM(U1=UR2=UR= 0)” in ABAQUS.

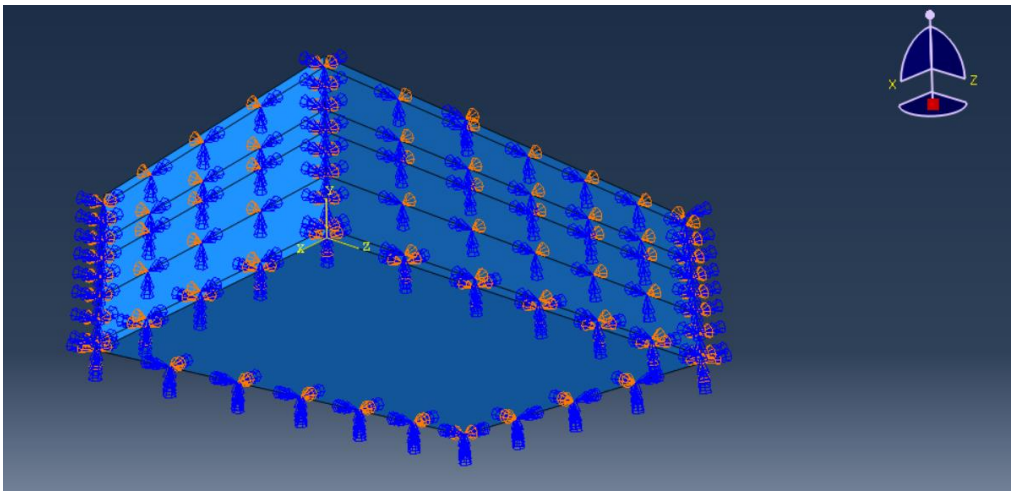

Figure 15: Boundary conditions

3.6 Model Meshing

Defining the meshing of the model is the next. The meshing used in this project is based on the meshing used in studies by Yoo and Al-Qadi [13], Yoo and Al-Qadi [14], Wang et al.[4], and Wang [6].

First, there is the meshing of the tyre loading area. Each tread is divided into two mesh blocks laterally (perpendicular on the traffic direction), while each rib remains one mesh element thick. The complete loading area is meshed like this, and these lines extend to the sides of the pavement block. In the traffic direction, the treads and grooves were divided into blocks of 20 mm. A simple square meshing type was used, and the element types are 8-node linear brick elements with reduced integration and hourglass control. Figure 16 shows the tyre imprint meshing, and Figure 17 shows the ABAQUS model fully meshed.

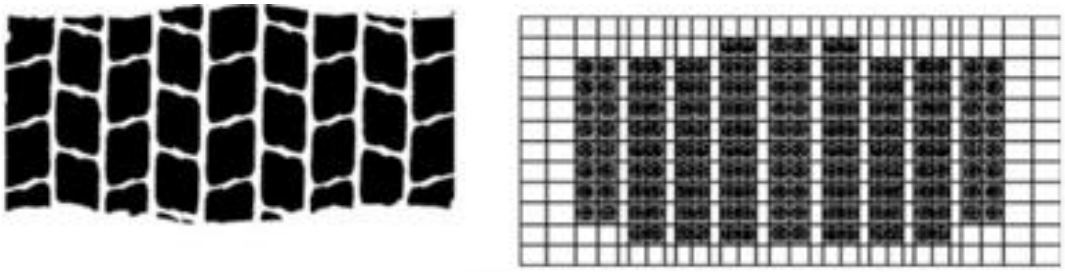

Figure 16: Tyre imprint meshing [13]

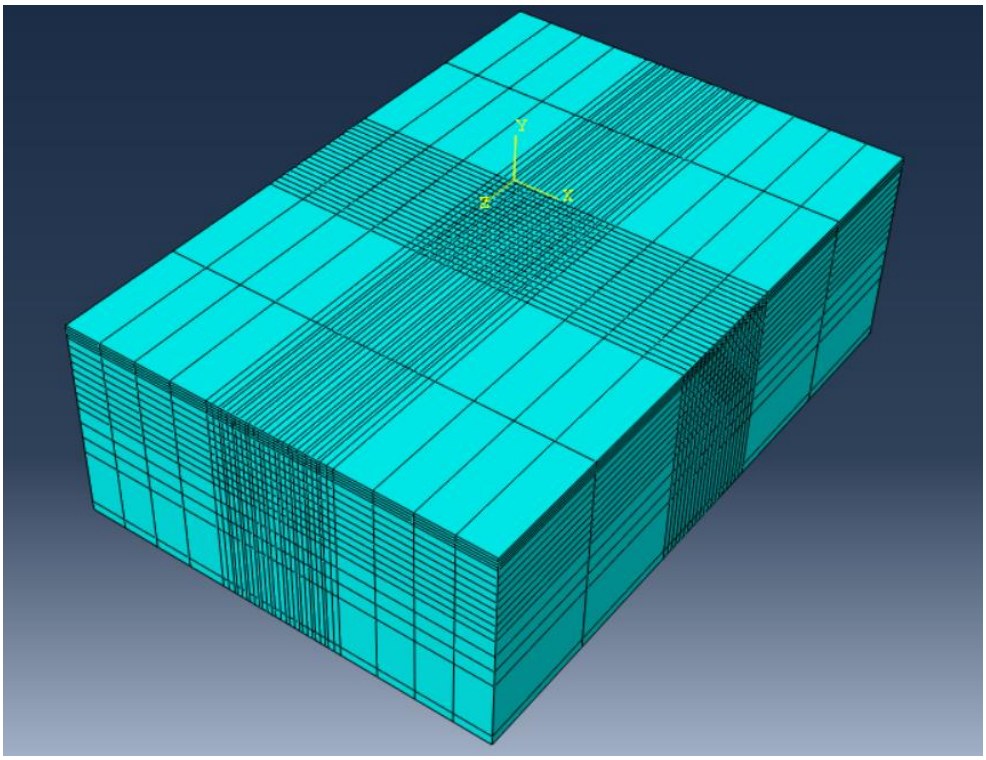

Figure 17: Pavement model meshing

The rest of the top surface of the model is divided into 2 in traffic direction and 4 laterally. This is done arbitrarily. Finally, the different layers are each divided horizontally and each in a different manner. The upper AC layer (AC1) is divided into slices of 9.5 mm.

The AC2, OGDL, and CTB layers are divided into 25, 35, and 45 mm horizontal slices, respectively. According to the study by Wang et al. [4], the subbase layer should be divided into slices of 200 to 500 mm thick, but since this layer is only 175 mm thick in total, the layer will be kept as one piece in the mesh. The subgrade layer is not divided but kept as one piece in the mesh. This is because it is a layer with infinite depth.

3.7 Modelling the Load

Finally, the load can be applied to the model. There are two critical parts to this process. First, there is the distribution of the load, and then there is the loading amplitude.

3.7.1 Load distribution

The load is not evenly distributed over the surface of the tyre footprint. Instead, it varies from rib to rib. Table 6 shows which load is applied to which tyre rib.

Table 6: Tread pressure and dimensions at a nominal tire pressure of 720 kPa and a wheel load of 38 kN [13]

Wide Base tyre	R1*	G1*	R2	G2	R3	G3	R4	G4	R5
Vertical Pressure (kPa)	502	-	832	-	883	-	936	-	956
Length (mm)	144	-	154	-	156	-	172	-	174
Width (mm)	38	9.6	31	9.6	31	10.3	31	11.4	35

*R: Tyre Rib *G: Tyre Groove
The wide-base tyre has nine treads and is symmetric with respect to the fifth tread

Table 6 shows the pressure/load on each individual rib. There is, of course, no load on the tyre grooves, as they are not touching the ground. In this project, a wide-base tyre setup was used.

These loads can then be applied to their respective ribs. However, it is important to note that the load will only be applied within the tyre imprint area, which finds itself in the loading area. This tyre imprint will then shift forward during the successive steps symbolising the movement of the tyre. The load must, of course, follow the tyre imprint and will thus be moving forward with the tyre, one increment at a time. The load must be applied to each meshing element with which the tyre makes contact at a given time. This is illustrated in Figure 19. Figure 18 shows the tyre footprint.

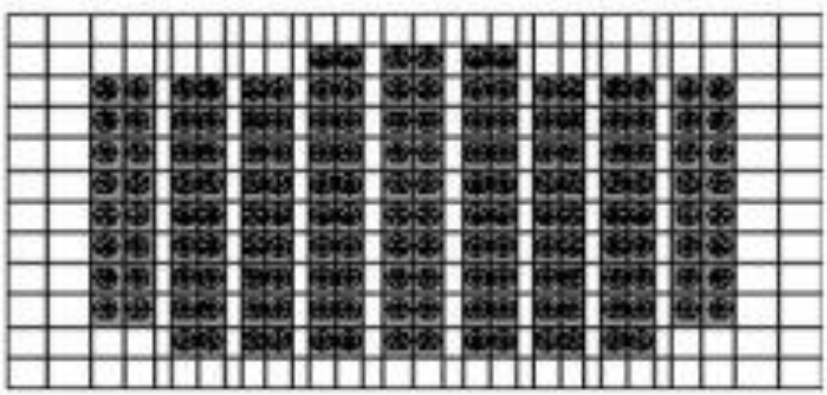

Figure 18: Tyre foot print[13]

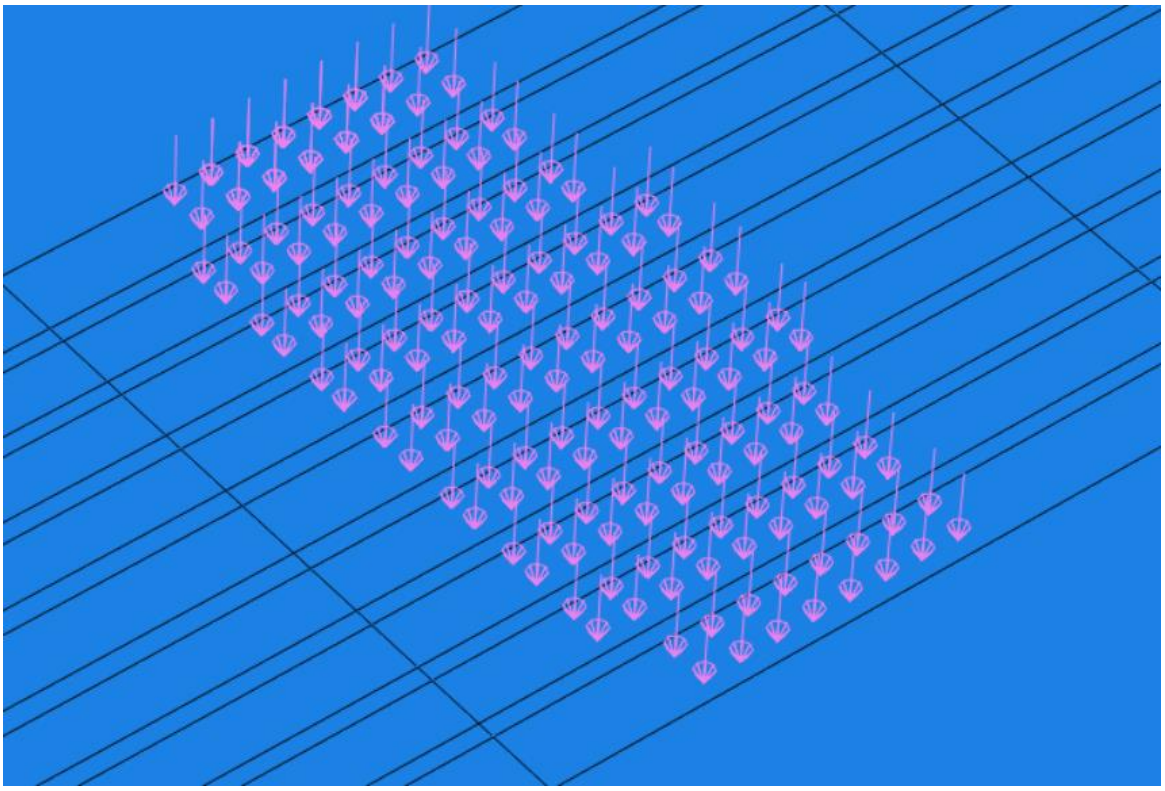

Figure 19: tyre load imprint in ABAQUS

3.7.2 Characterization of moving Wheel Load amplitude

In order to simulate the movement of a tire at a certain speed, the tire imprint area is gradually shifted over the loading area until a single wheel pass is completed. When a new piece of pavement comes into contact with a tyre, it will not experience the full load of the tyre (rib) immediately. Instead, during the time that the tyre is in contact with the piece of pavement, the load experienced by that piece of the pavement will rise from 0 to the maximum tyre rib load (load values given in the previous chapter) and then back to zero when the tyre loses contact with the piece of the pavement due to rolling further down the pavement. This variation in loading amplitude throughout a wheel pass will have to be modelled in ABAQUS as well.

To model this, two methods were proposed in the study by Yoo and Al-Qadi [13]; the trapezoidal impulsive loading amplitude and the continuous loading amplitude.

To simulate moving wheel loading in the FE model with a trapezoidal loading amplitude, the variation of the loading amplitude with time can be defined by the tabulated values and path as shown in Table 7 and Figure 20. Trapezoidal loading amplitude is characterised by the linear increase of load from zero to the maximum amplitude of the load in the first time step that a new set of loading area elements (the meshing blocks signifying the tyre ribs on the pavement) along the wheel path are loaded. Then the load amplitude stays maximum for the remaining steps that the loading area elements are loaded, except for during the final step when the elements are still loaded. During the final step, the load amplitude decreased linearly to 0 again.

Table 7: Tabulated data for the trapezoidal loading amplitude [13]

Time step	Amplitude
T_1	0
T_2	1
T_3	1
T_4	1
T_5	0

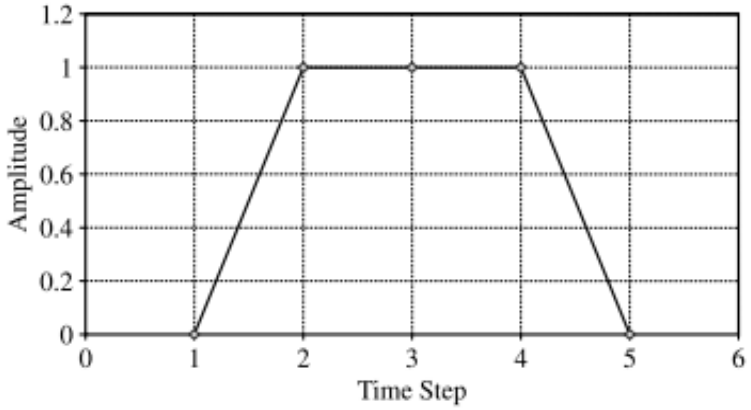

Figure 20: Definition of the trapezoidal loading amplitude

The second method, the continuous loading amplitude method, differs from the trapezoidal loading amplitude method in that the rise and fall of the loading amplitude no longer take place over the time of one step but instead now takes place over the time of multiple steps, as illustrated in Figure 20.

As the tyre approaches a given mesh element in the loading area, the element is loaded with the amplitude that simulates the increase in loading with time (Figure 21(a)). Similarly, as the tyre moves away from a given element, the loading amplitude that simulates the decrease in loading with time is used (Figure 21(b)). Also, important to note is that the entrance and the exit of the tyre are not symmetric and that the rate of increase or decrease of the loading amplitude depends on the speed of the vehicle (step time).

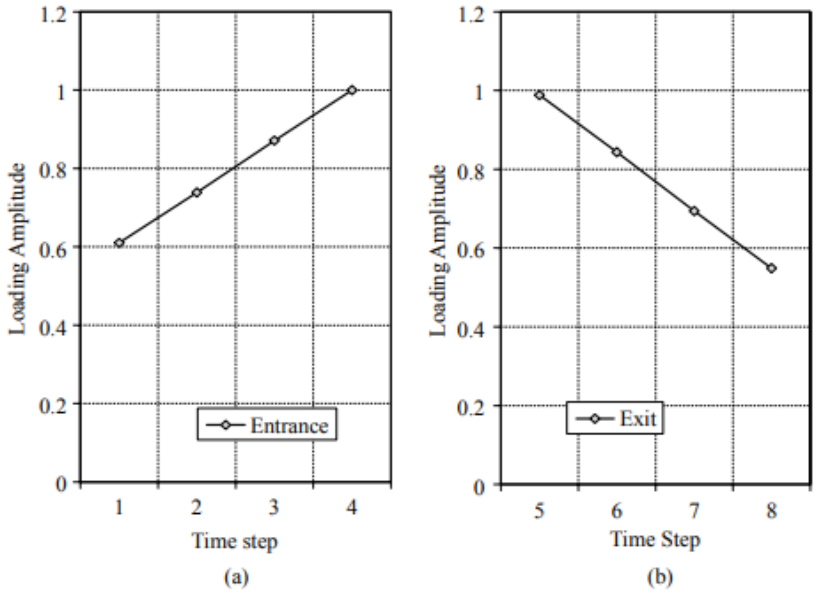

Figure 21: Continuous loading amplitude for (a) the entrance part of the tyre imprint elements and (b) the exit part of the tyre imprint elements [13]

The study by Yoo and Al-Qadi [13] concluded that the continuous loading amplitude is the most accurate method. However, this study uses the trapezoidal loading amplitude method to save computational time. The resultant loss of model accuracy was deemed acceptable. Using the trapezoidal method will result in slightly underestimated surface strains.

3.8 Infinite element

The infinite element layer at the bottom of the pavement block symbolises the “infinite” depth of the ground underneath the pavement. The infinite elements also help reduce the otherwise large number of far-field elements without significant loss of accuracy and create “silent” boundaries for the dynamic analysis. In the studies by Wang and Al-qadi [5], and Wang [4], the sides of the model were also considered infinite elements. In the paper used to base the majority of this model, only the bottom was an infinite element.

To implement a finite element in ABAQUS, it is suggested to read the ABAQUS user’s manual [15] and watch some videos online showing the technique. Figure 22 shows the finished ABAQUS model with an infinite layer.

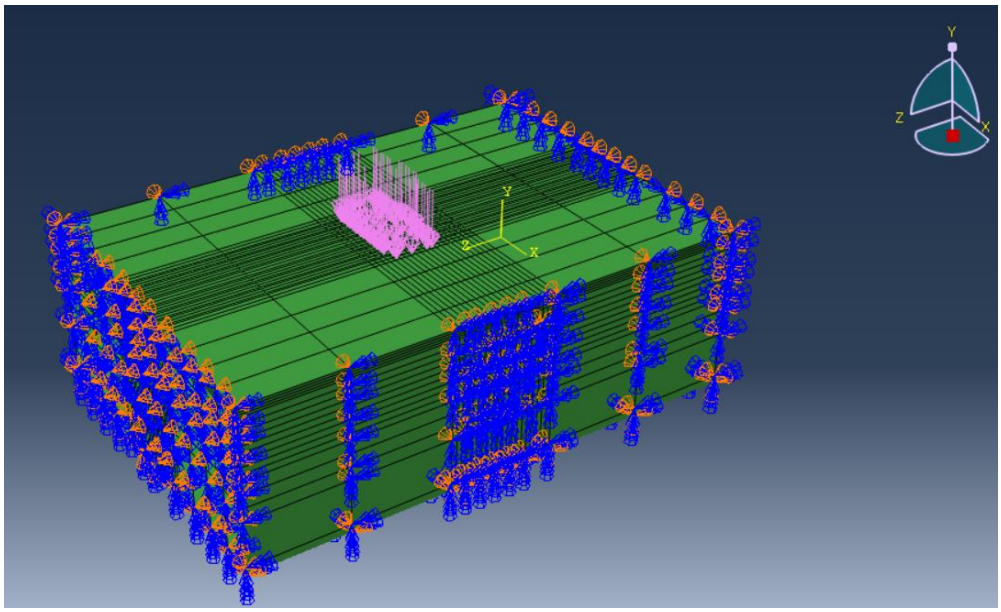

Figure 22: Finished model in ABAQUS

4 Model Validation

In this chapter, the 3D finite element model of the pavement will be validated. This is done to ensure that the model is reliable and that there have been no mistakes regarding its design. A certain load case selected from the literature will be reproduced in the project model to validate the model. The load case chosen for this validation is from the same study by Yoo and Al-Qadi [13] on which the model's design was based. Then a simulation will be run to compare the simulation results to those of the simulations in the literature. To validate the model, the simulation results and the results given in the study should be roughly the same.

4.1 Model Validation steps

In this chapter, the model produced in chapter 3 will be validated. This means checking whether the produced model is a good and truthful representation of reality or at least an accurate reproduction of a validated model of another study. To achieve this, the constructed model of this project is given the same Input parameters as the model from the paper on which the project model is based [13]. Then the results of the simulations are compared in order to check if they are somewhat similar. If the results seem to be somewhat equal, it can be concluded that the project model is an accurate reproduction of the model from the study and thus also an accurate enough representation of reality.

In this study, the validation is done by comparing with simulation results of the study by Yoo and Al-Qadi [13], the same study on which the design of the project model was based. The model's input parameters for the validation were a temperature of 25°C, a tyre load of 38 kN, tyre nominal pressure of 720 kPa, and a tyre speed of 72 km/h (20 m/s) and 8 km/h (2,2222 m/s). A wide base tyre was used. The parameters used in the papers vary. The pavement in the study [13] used for the comparison is based on pavement characteristics of the “Virginia smart road – section B” (the same road the pavement model used in this project was based on).

The validation will be subdivided into two parts. These parts will be vertical stress validation and longitudinal strain validation. The results from the simulation will be compared with the results from the simulations of the two studies mentioned above.

4.1.1 Vertical stress validation

In this chapter, vertical stress will be examined. The shape and maximum values obtained from the project model simulation should be as close as possible to the values obtained from the paper by Yoo and Al-Qadi [13] to ensure that the project model is accurate and truthful enough to reality.

First, the results for the project model simulation with tyre speed of 72 km/h will be examined. A simulation was run, and the vertical stress was measured for the centre tyre rib and the outer tyre rib. The measurements were taken at the bottom of the AC1 layer since the measurements in the study used for the comparison were also taken at this position in the pavement. The measurements were taken at the 10^{th} mesh line (the middle of the loading area length), using the centroid met

Figure 23 shows the project model results for the vertical stress measurements of the centre and outer tyre rib.

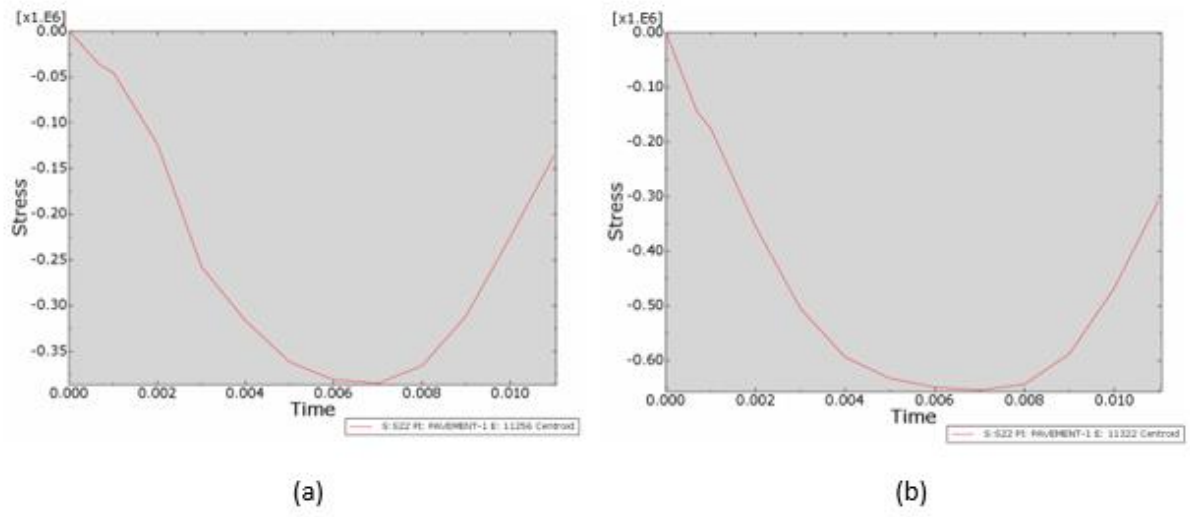

Figure 23:Vertical stress results for outer tyre rib (a) and centre tyre rib (b) at the bottom of the wearing surface (AC1: 0.58m) – speed: 72 km/h

To make a comparison the following graph (Figure 24) is available from the study by Yoo and Al-Qadi [13].

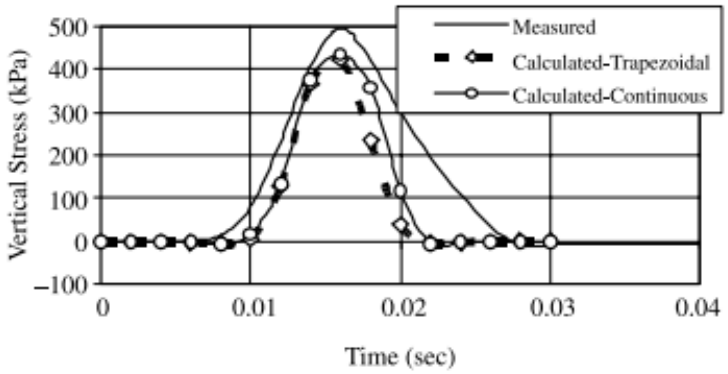

Figure 24: Vertical stress at the bottom of the wearing surface (AC1: 0.58m) at a speed of 72 km/h and 38 kN wheel load at 25°C [13]

For the above graph in Figure 24, there is no information about at which tyre rib the values were measured, and there is also no information about the type of tyre used (wide base or dual base). It seems to match the results from the vertical stress plot of the outer tyre rib (Figure 23a). The maximum vertical pressure for the project simulation (Figure 23a) of the outer tyre rib seems to be around 350-400 kPa, while the maximum vertical pressure of the comparison model (Figure 24) seems to be around 400-450 kPa. Also, the shape of the graphs from the project model seems somewhat similar to the shape of the graph from the comparison model.

4.1.2 Longitudinal strain validation

Now the longitudinal strain will be examined. The shape and maximum values obtained from the project model simulation should be as close as possible to the values obtained from the paper by Yoo and Al-Qadi [13] to ensure that the project model is accurate and truthful enough to reality.

The results for the project model simulation with tyre speed 8 km/h will be examined. A simulation was run, and the longitudinal strain was measured for the centre tyre rib and the outer tyre rib. The measurements were taken at the bottom of the AC2 layer since the measurements in the study, which will be used for the comparison, were also taken at this position in the pavement.

Figure 25 shows the project model results for the longitudinal strain measurements of the centre and outer tyre rib.

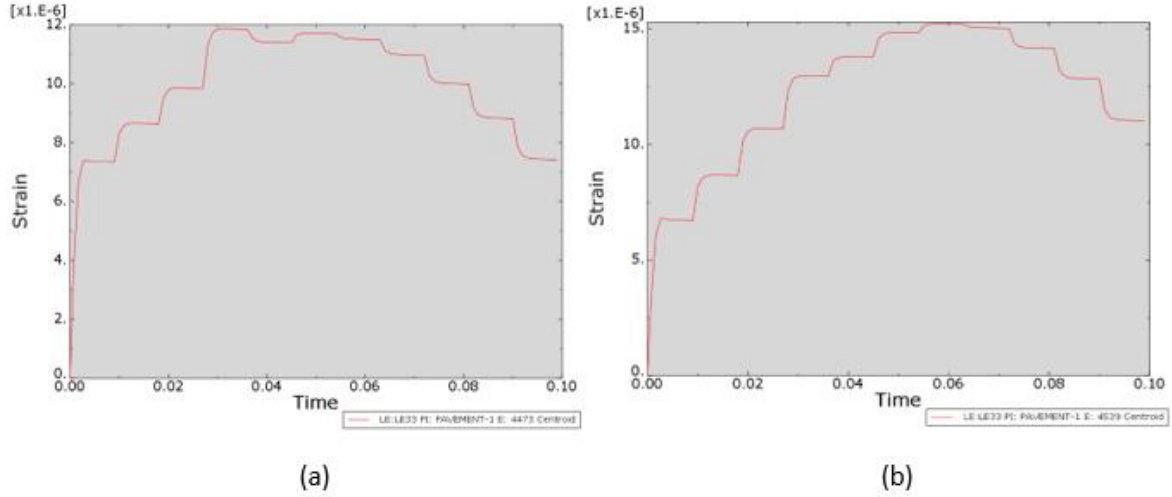

Figure 25: Longitudinal strain results for the outer rib (a) and centre rib (b) at the bottom of the BM-25.0 layer (AC2 layer – 0.43m) - speed: 8 km/h

To make a comparison, the following graph (Figure 26) is available from the study by Yoo and Al-Qadi [13].

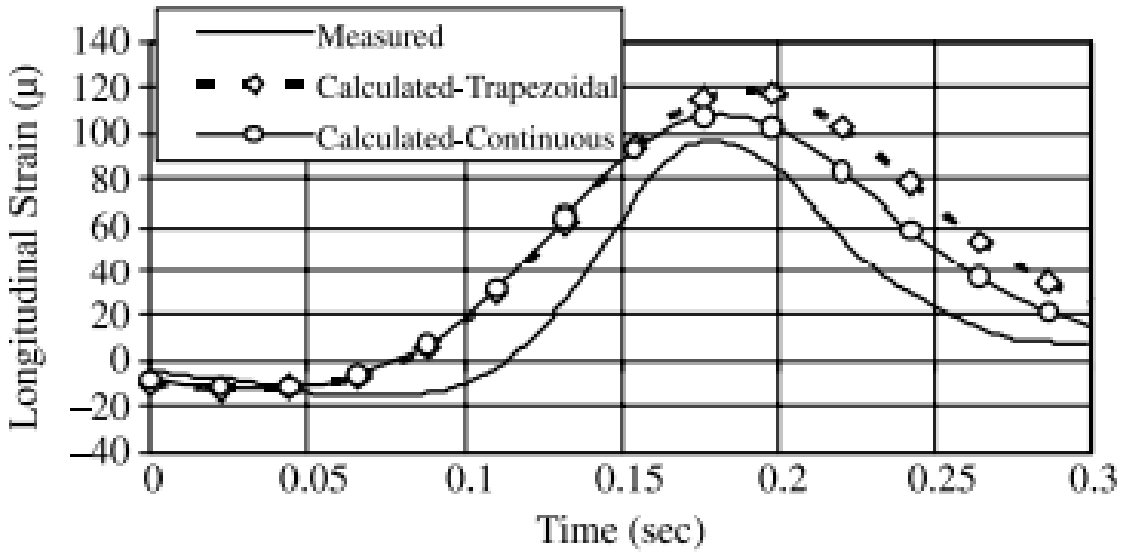

Figure 26: longitudinal strain at the bottom of the BM-25.0 layer (AC2 layer - 0.43 m) at a speed of 8 km/h and 38 kN wheel load at 25°C - wide base tyre [13]

In the measurements of Figure 26, a wide base tyre was used, the load was 38 kN, and the measurements were taken at the bottom of the AC2 layer. The only thing not known is at which tyre rib the measurement was taken. It seems likely, however, when examining the values in Figure 25a, that the tyre rib used in Figure 26 was the outer tyre rib (tyre rib 9). When observing the results from the project model simulation (Figure 25), the maximum value measured for the outer rib seems to be 10 times smaller than the maximum value from the graph in Figure 26.

The maximum strains from the simulation results of the paper by Yoo and Al-Qadi [13] are 100-120 μ, while the results of the project model are around 10-12 μ. This means that the longitudinal strain results for the project model are much smaller than they should be.

4.2 Model inaccuracies

Even though much effort was put into making the model resemble the original from the paper as closely as possible, there are still some inaccuracies in the model, which might explain some differences between the validation simulations of the project model and the results from the literature. These inaccuracies have arisen for several reasons. The first and most important reason is the lack of information in the literature regarding several parts of the model design. An example of this is the lack of transversal loading on the model. A transversal load was applied on the model in the literature, yet no values or positions of these loads were given. There was also no info in any of the references of the studied paper by Yoo and Al-Qadi [13] regarding this topic. Another reason for some inaccuracies is the amount of extra work required to implement certain features. Again, a lack of time and a more efficient way of implementing this feature caused the inaccuracies to be kept instead of resolved. In the chapter below, the currently know inaccuracies in the model are listed.

4.2.1 Current inaccuracies

1. Loading area length:

   The tyre imprint area is the surface over which the moving load of the tyre will move. It is the distance the moving load will travel. In this experiment, the tyre imprint area has a length of 400 mm divided into 20 parts of 20 mm in length. In the paper on which the model is based, the length of the loading area is not specified. In other literature, such as the study by Gungor et al. [7], this area is specified to be 1000mm, 2000mm, or even 10 000mm in length, with 1000 mm as sufficient. However, this means that the number of steps will be very high (one mesh element is 20 mm in length, so min 50 steps, which is too much). It was therefore decided to use a loading area with 400 mm length, which is 20 steps. This is much more manageable.

2. No transversal loading

   In the paper by Yoo and Al-Qadi [13], which was used for the design of the project model, transversal loads (loads perpendicular to the direction in which the wheel load moves) were included. However, no values can be found defining these in the paper of in the references, nor is there any explanation of how these loads were situated and implemented. Therefore this is left out of the model. The effect of the exclusion of these transversal loads on the other results is unknown.

3. Boundary Conditions

   In one examined study by Wang et al. [4], infinite element boundary conditions were used for the bottom and the sides of the pavement block in the model. The paper by Yoo and Al-Qadi [13] on which the model used in this project is based, does not specify if the sides are also infinite element blocks. Therefore it was chosen to make only the bottom of the pavement block as an infinite element block, as other examined studies by Gungor et al. [7] and Yoo and Al-Qadi [14] only specify the bottom of the model as being infinite in dimension.

4. Fully bonded layers

   Currently, the model makes use of fully bonded interaction between the layers of the pavement. This, however, is said to cause a gross underestimation of the strains and stresses in the pavement [13], particularily the strains. It can also predict compressive strain at some interfaces in which a tensile field may exist.

5. Minimum Step time size

   ABAQUS can only compute step time sizes of 9 digits after the comma. Anything smaller will be rounded of by ABAQUS automatically. The step times, calculated in the following chapter, will have 16 digits after the comma. This means that much info will disappear due to the rounding off, and this might result in almost no difference between the consecutive step times of the AV or non-AV model, or even worse, there being almost no difference between the step times of the AV and non-AV model. This could mean that there will be almost no difference in the AV's and non-AV's simulation results. The initial speed for the loads was already lowered from 20 m/s to 12 m/s in order to make the difference between the step times bigger, but that had only limited effect, and the difference between the AV and non-AV step times remains minimal. This might be a reason to bring the starting speed even down further. It was decided not to do this, however, for reasons of realism. Because the model used in this research has to be as real as possible, it would be strange to have an initial speed of, for example, 5 m/s (18 km/h). This speed would be too low to seem realistic. Remember that this project tries to simulate a car in a normal traffic situation, stopping for an object in front of it or approaching an intersection. Therefore, any speed below 12 m/s seems too low to be realistic and not fitting for the proposed deceleration behaviours.

4.3 Model validation conclusion

Concerning the vertical stress values, the project model seems to be reasonably accurate. The values for the outer tyre rib seem to be close enough to the results from the study by Yoo and Al-Qadi [13]. No information was available of results for the centre tyre rib, nor the longitudinal stress. It can be concluded that the project model seems to suffice in regards to the vertical stress. The longitudinal strain, however, poses a problem. Here the values from the project model seem to be ten times smaller than expected.

However, there are several things to take into account that could explain the difference in longitudinal strain. First, there are the inaccuracies that have already been mentioned. The problems concerning the fully bonded pavement layers seem to be the most likely to have caused the strange strain values. It is stated in the paper by Yoo and Al-Qadi [13] that using fully bonded layers grossly underestimates the strain. This can be an explanation for the low strain values of the model. In the same paper, it can be concluded that lateral loading only has a marginal effect on the longitudinal strain, so this inaccuracy has a relatively negligible effect on the strain values. Lastly, there is the loading area that is too short. However, since the loading area seems to be long enough to show a complete stress pulse from beginning to end, it can be concluded that this will also not affect the strain values. This leaves the inaccuracy of the fully bonded layers as the most plausible cause of the strange stain values.

Another thing to note is that the form of the longitudinal strain graphs of the project model and the papers seem roughly the same. This concludes that the pavement model behaves as expected, and the problem is more situated around the magnitude of the strain rather than the general pavement behaviour. The stress values, which seem correct compared to those from the papers, reinforce this statement.

In the end, it can be concluded that even though the strain values are wrong, the rest of the model seems to function correctly. The maximum stress values of the project model seem to be the same as those of the literature, and also, the shape of the stress graphs is roughly the same as in the literature. For the strain, the shape of the graphs is roughly the same as in the literature, and only the maximum values are smaller. On top of that, the rest of this study will mainly focus on comparing the project model with different parameters against itself. Therefore, there is more focus on the difference between two simulations with different parameters than the magnitude of stress-strain values. It can be concluded that having a model that underestimates the strain values does not affect the rest of the study. This means that the model can be considered validated and can be used for this study.

5 Simulation setup

This chapter will discuss the input parameters that have not yet been explained in detail in the methodology. This will include an explanation concerning the interpretation of the AV and non-AV deceleration behaviour and the determination of the formulas representing this behaviour, and the step time period calculation results. Other input parameters, such as the layer properties and the loads applied, have already been discussed in the methodology.

5.1 Deceleration behaviour

As mentioned in the literature review, there is a difference between the "normal" deceleration behaviour of automated vehicles (AVs) and non-automated vehicles (non-AVs). When a non-AV, driven by a person, approaches an obstacle on the road, its deceleration behaviour will be characterised by caution. The driver will decelerate firmly at the beginning of the deceleration sequence to not come close to the object at the end of the manoeuvre. This is done for two reasons: firstly, an ordinary person cannot perfectly calculate the distance between himself and an object in front of him. The second reason is that he cannot perfectly calculate which deceleration is required to stop in time. This all leads to a conservative approach when braking. In the beginning, a normal person brakes firmer to take an extra margin and not accidentally hit the object in front of him because of misjudging the distance. However, this type of braking is not as smooth. The sharp braking, in the beginning, is relatively inefficient and will probably cause higher stress in the pavement than necessary. The following formula represents the non-AV deceleration behaviour, found in a study by Deligianni et al. [10], and can be seen as parabolic deceleration behaviour.

$$a^2 = 2.96 * t \tag{16}$$

With
a the deceleration (m/s²)
t the time (s)

It is this caution and difference in efficiency that will distinguish AV deceleration behaviour from non-AV deceleration behaviour. An AV, driven by artificial intelligence, will not have the same issues with calculating its distance to the object on the road and applying a required deceleration. This is because AVs can use sensors to calculate the distance perfectly and then calculate and apply the desired deceleration rate in milliseconds. This means that an AV is not required to brake sharply in the beginning since it does not have to take an extra margin to account for inaccuracy in misjudging speed and distance. The only factors an AV has to consider are passenger comfort (i.e., acceleration limit and jerk limit), as mentioned in the literature study. Therefore, a more efficient braking behaviour can be defined. In the study by Deligianni et al. [10] a linear type of deceleration was proposed. This behaviour is typified by the lack of dips or sharp increases in deceleration magnitude (which is the case for the parabolic deceleration represented by formula 16). This means a much smoother gradual increase in deceleration and probably less stress than parabolic deceleration. The following formula represents the AV deceleration behaviour, found in the study by Deligianni et al. [10], and can be seen as linear deceleration behaviour.

$$a = -0.71 * t \tag{17}$$

With
a the deceleration (m/s²)
t the time (s)

The deceleration behaviour is represented by the graph below (Figure 27), clearly showing the parabolic and linear nature of the different types of deceleration behaviour.

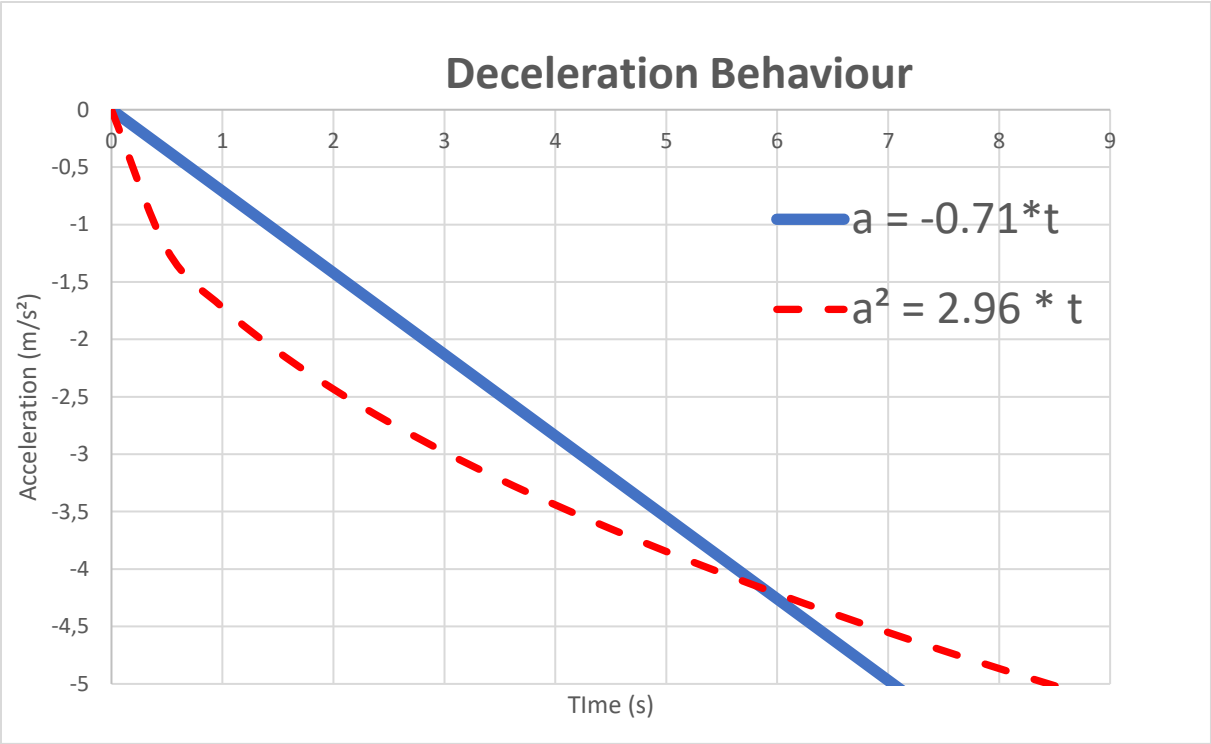

Figure 27: Functions for AV and non-AV deceleration behaviour [10]

5.2 Step time period calculation

In the program ABAQUS, there is no module to directly fill in the speed of our moving load. This is instead done through the step time period. Our tyre imprint will have to move 200 mm in total, and this movement is divided into smaller bits of 20 mm each. In total, ten steps will have to be taken by our tire to simulate its change in position, plus one step for the initial placement of the tyre imprint. So, in total, there will be eleven steps of each 20 mm in length. The distance calculates the time these steps will take our tyre will move divided by the speed by which it will be moving. This time, is the step time period, and it is the mechanism used to represent the tyre's speed.

With the deceleration formulas (16) and (17) we can define formula's for speed and distance. These will be used to calculate the step times. Since speed is the derived function of distance, and acceleration is the derived formula of speed, we can use integrals to calculate these formulas.

5.2.1 Determining of the speed and distance formulas

First the speed and distance equations for the non-AVs will be determined.

$$a(t) = -\left(\sqrt{2.96 * t}\right) \tag{18}$$

This formula is determined by writing formula (1) solely in function of the deceleration *a*. By integrating the function a(t) the function for speed of non-AVs can be determined.

$$v(t) = \int a(t)dt = \int (-(\sqrt{2.96 * t})\, dt \tag{19}$$

$$v(t) = -(1.14698 * t^{1,5}) + c_1 \tag{20}$$

With c_1 the integration constant representing the speed at t = 0 s. Now the speed formula (formula 20) must be integrated to become the distance formula x(t).

$$x(t) = \int v(t)dt = \int (-(1.14698 * t^{1,5}) + c_1)dt \tag{21}$$

$$x(t) = -(0.458791 * t^{2,5}) + c_1 * t + c_2 \tag{22}$$

With c_2 the integration constant for the distance at t = 0 s. The value of the integration constants will appear later in this chapter.

Now the same is done for calculating the distance and speed equations of AVs. First, the speed equation v(t):

$$a(t) = -0.71 * t \tag{23}$$

$$v(t) = \int a(t)dt = \int (-0{,}71 * t)dt \tag{24}$$

$$v(t) = -0{,}355 * t^2 + c_1 \tag{25}$$

And for the distance equation of AVs:

$$x(t) = \int v(t)dt = \int (0{,}355 * t^2 + c_1)dt \tag{26}$$

$$x(t) = -0.118333 * t^3 + c_1 * t + c_2 \tag{27}$$

5.2.2 Determining the integration constants

Now the integration constants c_1 and c_2 still need to be determined. c_2 marks the beginning distance of our moving load, and therefore it is 0 since we have not moved yet at $c_1$marks the beginning speed of the moving load, and by extension, the vehicle. This has been taken as 12 m/s.

Initially, it was decided to have the initial speed be 20 m/s. This, however, resulted in too small differences between the step times due to the high speed (the faster the load is moving, the faster it will cross 20 mm distance, the lower the step time is going to be). ABAQUS can only calculate step times with nine digits after the comma. With speeds above 12 m/s, the difference in step time becomes so small that ABAQUS can no longer discern the difference between the different step times.

So, with $c_1 = 12$ and $c_2 = 0$ the formulas for AVs and Non-AVs become :

- Formulas for Non-AVs:

$$a(t) = -\left(\sqrt{2.96 * t}\right) \quad (28)$$

$$v(t) = -(1.14698 * t^{1,5}) + 12 \quad (29)$$

$$x(t) = -(0.458791 * t^{2,5}) + 12 * t \quad (30)$$

- Formulas for AVs

$$a(t) = -0.71 * t \quad (31)$$

$$v(t) = -0{,}355 * t^2 + 12 \quad (32)$$

$$x(t) = -0.118333 * t^3 + 12 * t \quad (33)$$

With
a is deceleration (m/s²)
v is speed (m/s)
x is distance (m)
t is time (s)

5.2.3 Calculation of the step time

With the equations for the speed, distance and deceleration determined, it is now easy to calculate the step time for each step. With each step having a length of 20 mm and with the distance equation, the step time can be calculated.

Table 8; Step time of Non-Automated Vehicles (Non-AVs)

step	X(t)	t (s)	step time (s)	V(t) (m/s)	A(t)
0	0,00	0,0000000000000000	0,0000000000000000	12,0000000000	0,0000000000
1	0,02	0,0016666710023548	0,0016666710023548	11,9999219576	-0,0702377830
2	0,04	0,0033333578599811	0,0016666868576263	11,9997792612	-0,0993314616
3	0,06	0,0050000675885343	0,0016667097285532	11,9995944731	-0,1216560729
4	0,08	0,0066668054150053	0,0016667378264710	11,9993756437	-0,1404768452
5	0,10	0,0083335757217192	0,*0016667703067139*	11,9991274247	-0,1570585373
6	0,12	0,0100003823621150	0,0016668066403958	11,9988529542	-0,1720497945
7	0,14	0,0116672288172040	0,0016668464550890	11,9985545355	-0,1858359419
8	0,16	0,0133341182871410	0,0016668894699370	11,9982339528	-0,1986680400
9	0,18	0,0150010537504160	0,0016669354632750	11,9978926411	-0,2107204762
10	0,20	0,0166680380047810	0,0016669842543650	11,9975317874	-0,2221202208
11	0,22	0,0183350736969350	0,0016670356921540	11,9971523944	-0,2329631261

Table 9: Step time of Automated Vehicles (AVs)

step	X(t)	t	step time (s)	V(t)	A(t)
0	0,00	0,0000000000000000	0,0000000000000000	12,0000000000	0,0000000000
1	0,02	0,0016666667123199	0,0016666667123199	11,9999990139	-0,0011833334
2	0,04	0,0033333336985587	0,0016666669862388	11,9999960556	-0,0023666669
3	0,06	0,0050000012326364	0,0016666675340777	11,9999911250	-0,0035500009
4	0,08	0,0066666695884730	0,0016666683558366	11,9999842222	-0,0047333354
5	0,10	0,0083333390399903	0,0016666694515173	11,9999753472	-0,0059166707
6	0,12	0,0100000098611120	0,0016666708211217	11,9999644999	-0,0071000070
7	0,14	0,0116666823257650	0,0016666724646530	11,9999516804	-0,0082833445
8	0,16	0,0133333567078750	0,0016666743821100	11,9999368887	-0,0094666833
9	0,18	0,0150000332813780	0,0016666765735030	11,9999201246	-0,0106500236
10	0,20	0,0166667123202050	0,0016666790388270	11,9999013883	-0,0118333657
11	0,22	0,0183333940982970	0,0016666817780920	11,9998806798	-0,0130167098

Figure 28 shows a graph in which the change in step time for AVs and non-AVs is visualised. As the deceleration equations indicate, the step time for non-AVs will increase much more than for AVs during the moving of the load from 0 to 220 mm. This is caused by the harsher braking of Non-AVs at the beginning of their braking behaviour, and will result in a larger decrease of speed in the beginning. This can also be seen in Tables 8 and 9 when comparing the speeds.

The calculated step times were put into the model. In Figure 28 below, the step times can be seen, and the size they were limited to automatically by ABAQUS. Higher starting speeds, as mentioned before, would have the difference in step time too small for ABAQUS to process.

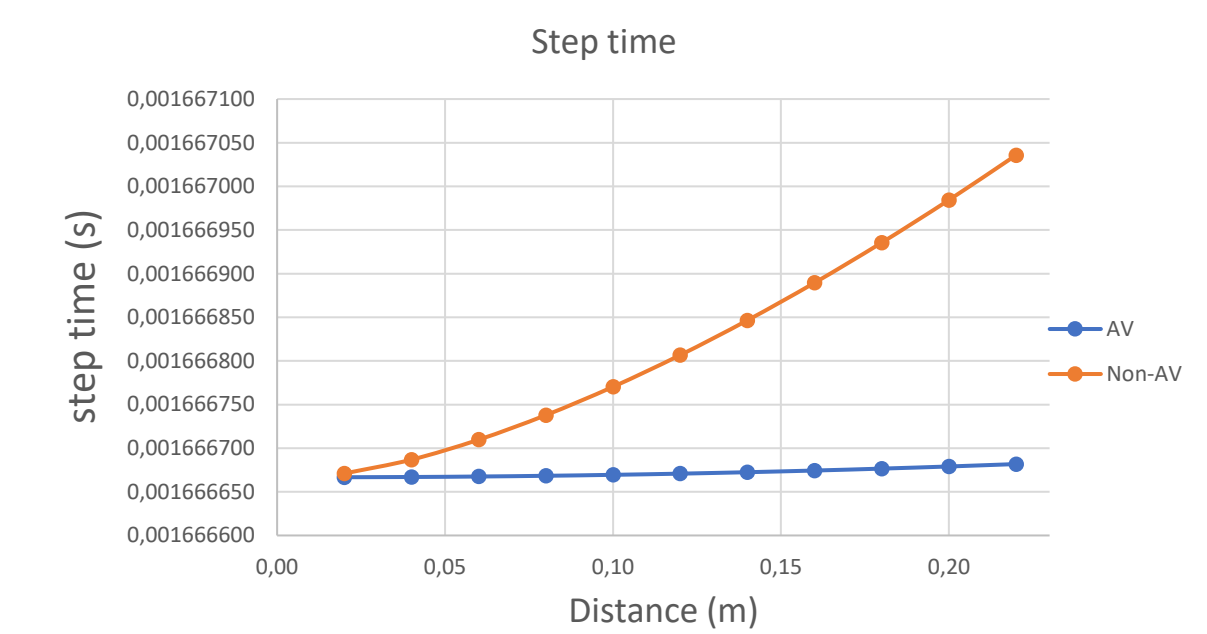

Figure 28: Change in step time due to deceleration in function of distance travelled

6 Simulation results

With all the parameters defined, the simulation can now be performed. This chapter will show the results of the simulations.

6.1 Vertical Stress

First, the vertical stress on the pavement will be measured. This will be done for both AV and the Non-AV model. First, the general situation is shown in Figure 29. The differing colours indicate the change in magnitude of vertical stress. The place where the tyre is positioned is clearly visible.

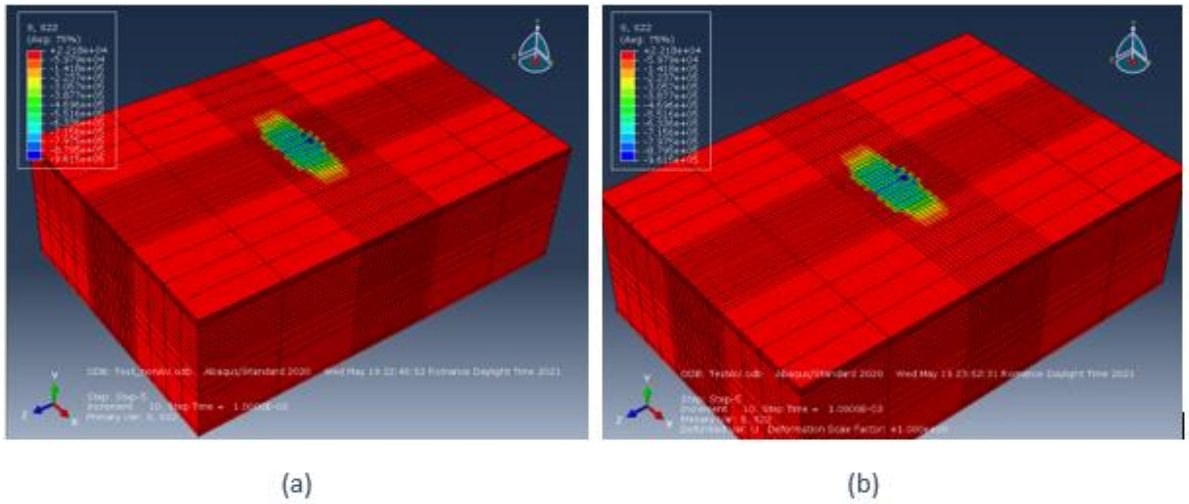

(a) (b)

Figure 29: Non-AVs' Vertical stress Situation (a), AVs' vertical stress situation (b)

The graphs below (Figures 30, 31, 32, and 33) show the change in vertical stress on the pavement surface during time progression for the AV and non-AV simulation. The measurements were taken in the middle of the tyre imprint area at the 10th mesh line (200 mm)and under tyre ribs 5 (centre rib) and tyre rib 9 (outer tyre rib) at the surface of the pavement. The units of the axis' are pascal (Pa) and seconds (s). First, the graphs for the vertical stress under the outer tyre rib are examined.

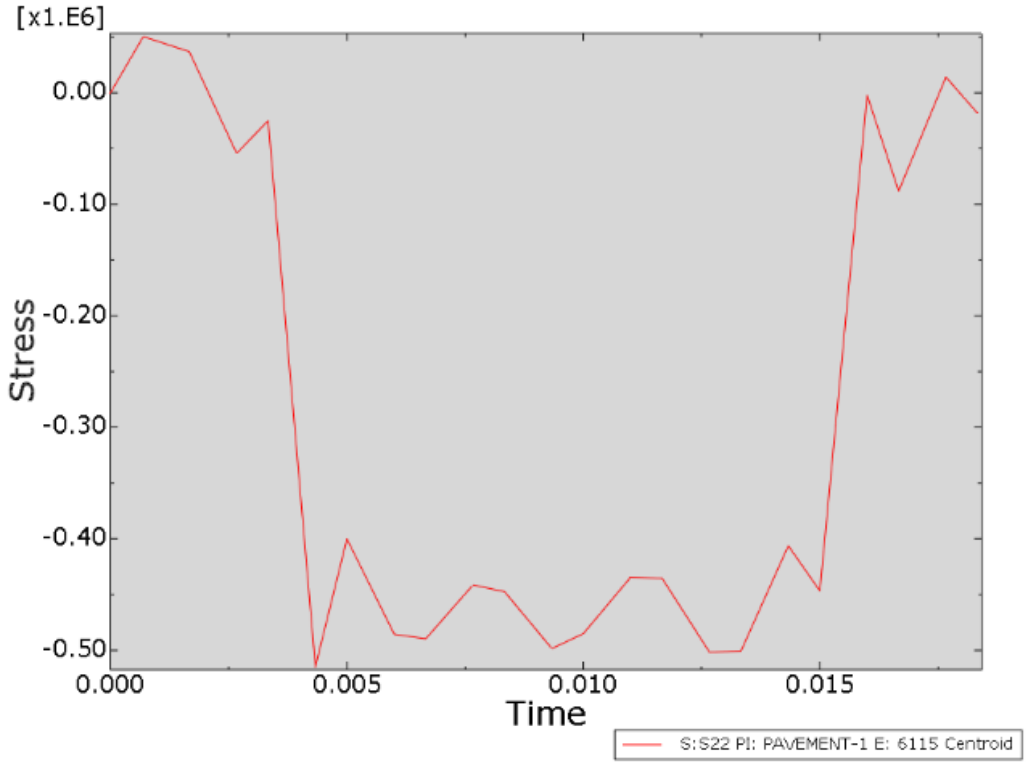

Figure 30: Non-AV vertical stress for outer tyre rib

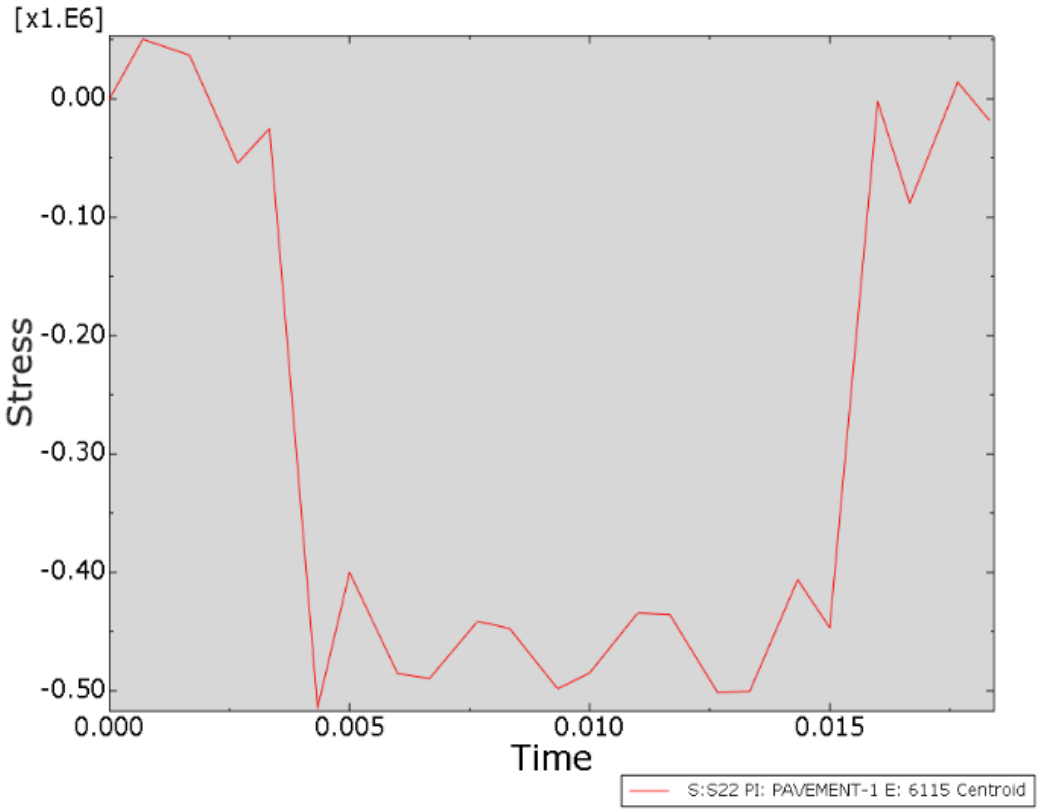

Figure 31: AV vertical stress for outer tyre rib

The maximum and mean values in the table were taken from the ABAQUS simulation dataset. For each graph plot in ABAQUS, the program also provides numerical data. From this dataset, the Maximum value and mean value of all data were calculated. Lastly, the difference between the values of the AV and non-AV is also given in a percentage, to better show the difference between the values. This goes for all other tables that will follow as well. In Table 10 below, the values are summarized for the vertical stress below the outer tyre rib.

Table 10: table with the maximum values, the mean values of vertical stress for the centre rib (rib 9)

Vertical Stress		Max Value (Pa)	Mean Value (Pa)	Diff. Max Value (%)
Non-AV	Outer rib	-514596	-298665,9909	0,000194327
AV		-514595	-298668,4436	

Next, the same procedure is repeated, but this time for the centre tyre rib (rib 5).

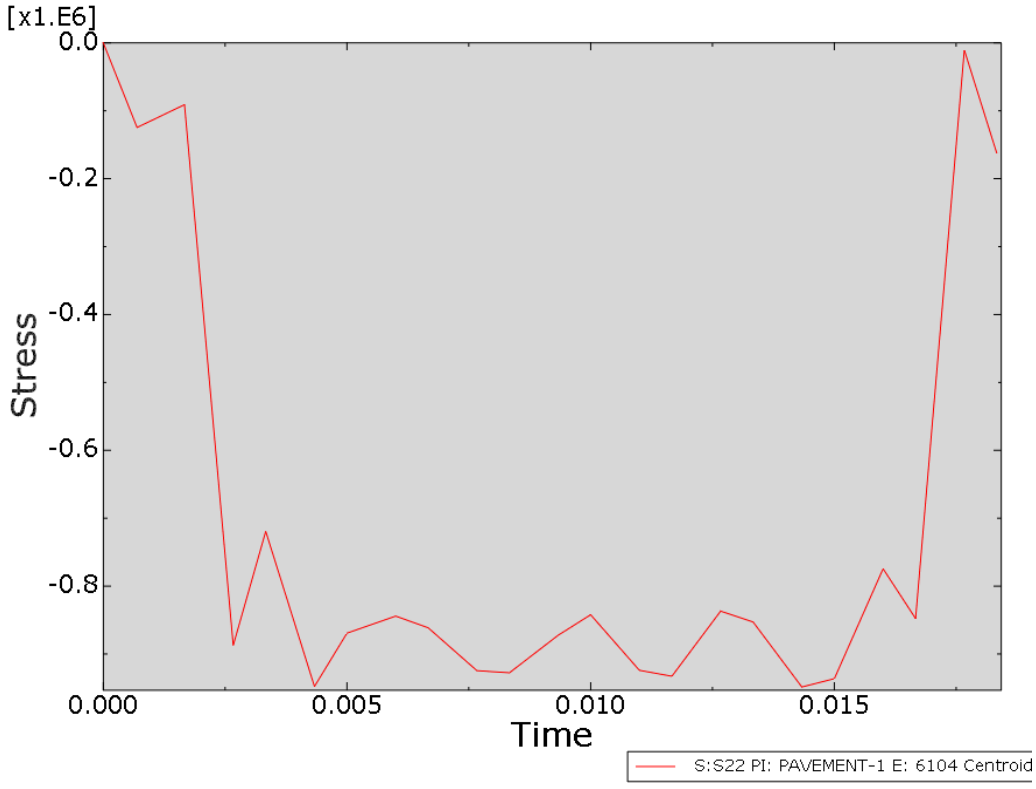

Figure 32: non-AV vertical stress for centre tyre rib

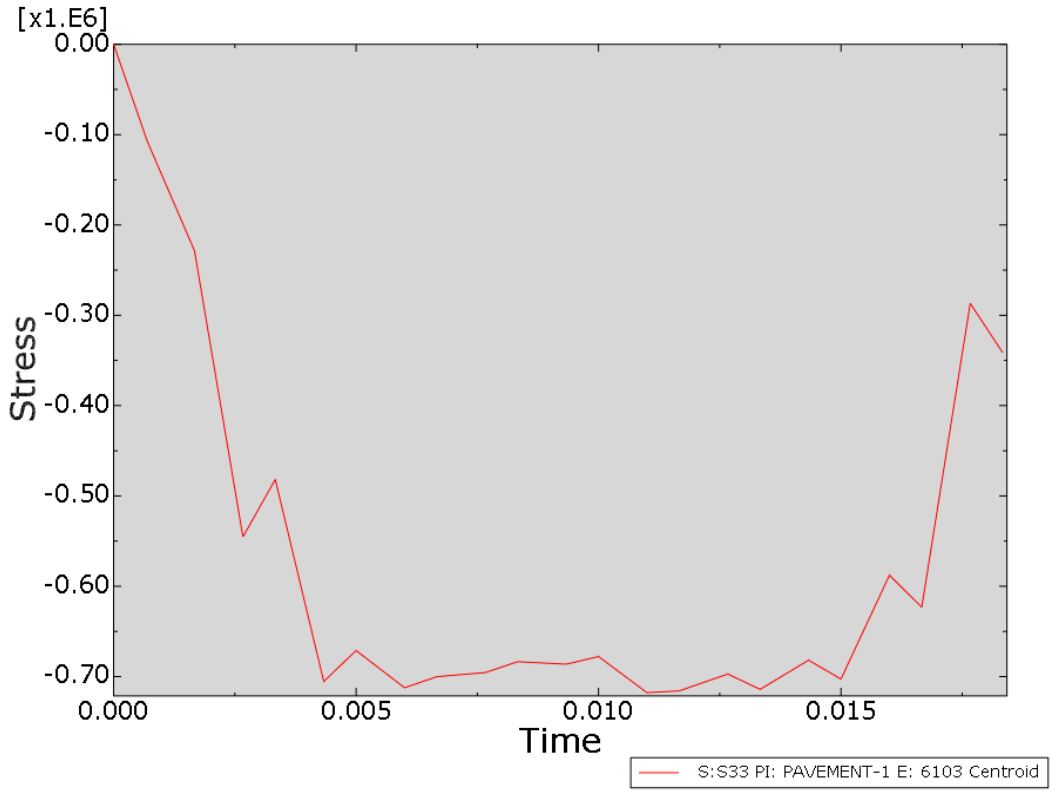

Figure 33: AV vertical stress for centre tyre rib

In Table 11 below the values are summarized for the vertical stress below the centre tyre rib.

Table 11: table with the maximum and mean values of vertical stress for the centre rib (rib 9)

Vertical Stress		Max Value (Pa)	Mean Value (Pa)	Diff Max Value (%)
Non-AV	Centre rib	-948571	-727840,3424	0,000316265
AV		-948574	-727845,8455	

6.2 Longitudinal Stress

Next, the longitudinal stress on the pavement has been calculated and measured. This will be done for both AV and the non-AV model. First, the general situation is shown again in Figure 34.

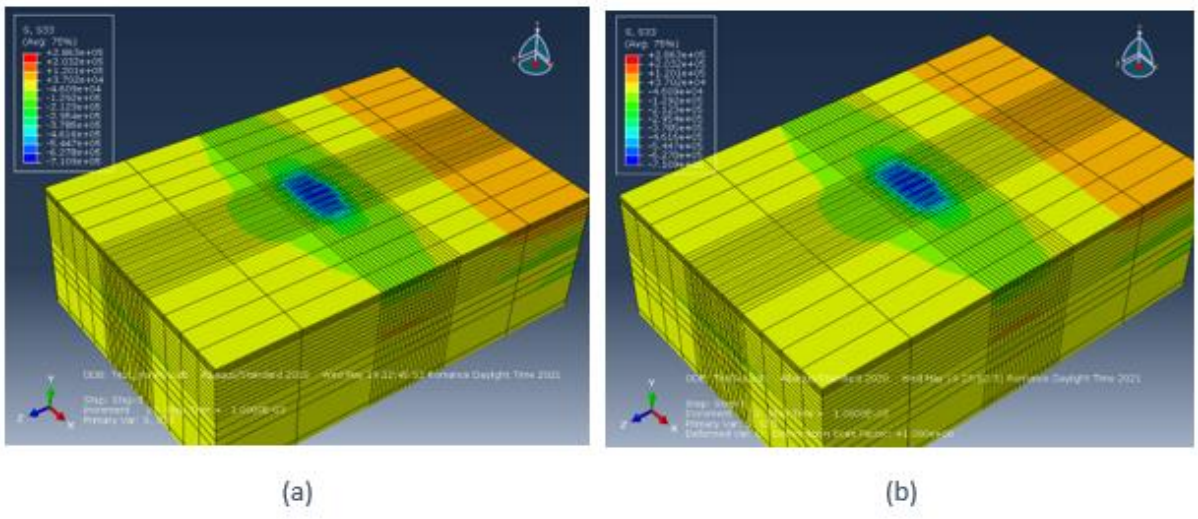

Figure 34: Non-AV longitudinal stress situation (a), AV Longitudinal Stress situation (b)

The graphs below (Figures 35, 36, 37, and 38) show the change in Longitudinal stress on the pavement surface during time progression for the AV and non-AV simulation. The measurements were taken in the middle of the tyre imprint area at the 10th mesh line (200 mm) , and under tyre ribs 5 (centre rib) and tyre rib 9 (outer tyre rib). The units of the axis' are pascal (Pa) and seconds (s). First, the graphs for the longitudinal stress under the centre tyre rib are examined (Figures 35 and 36).

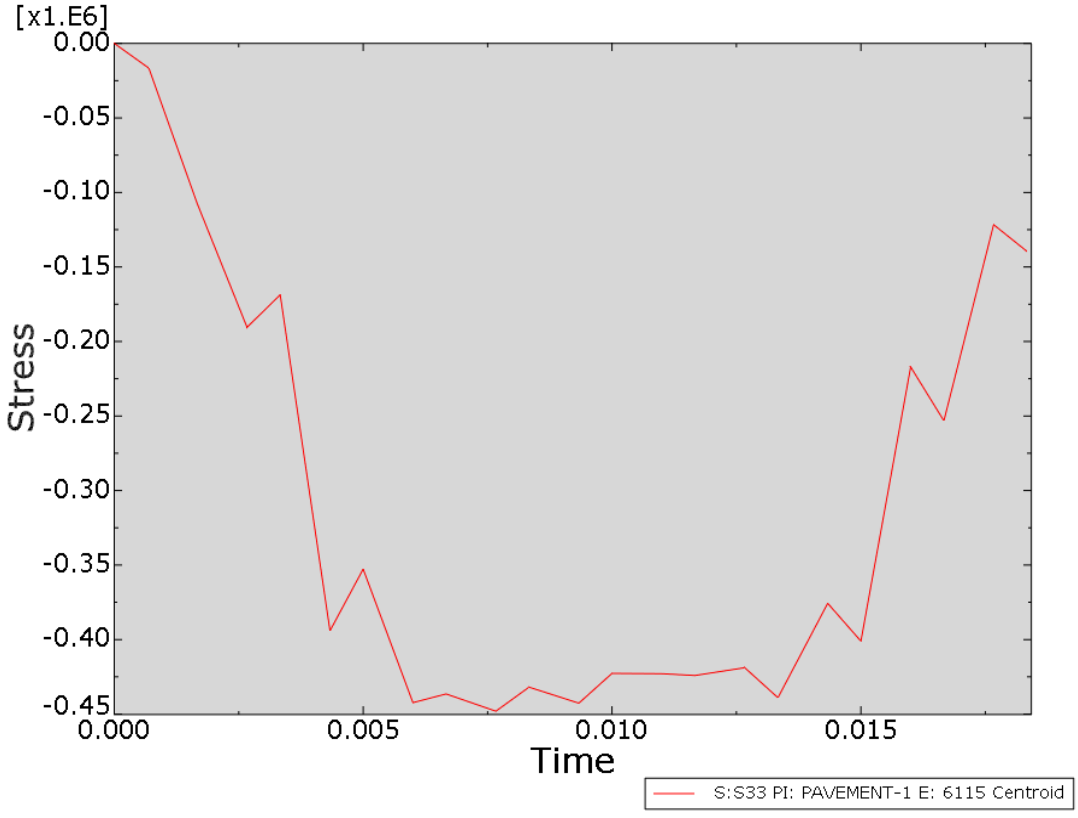

Figure 35: Non-AV longitudinal stress for outer tyre rib

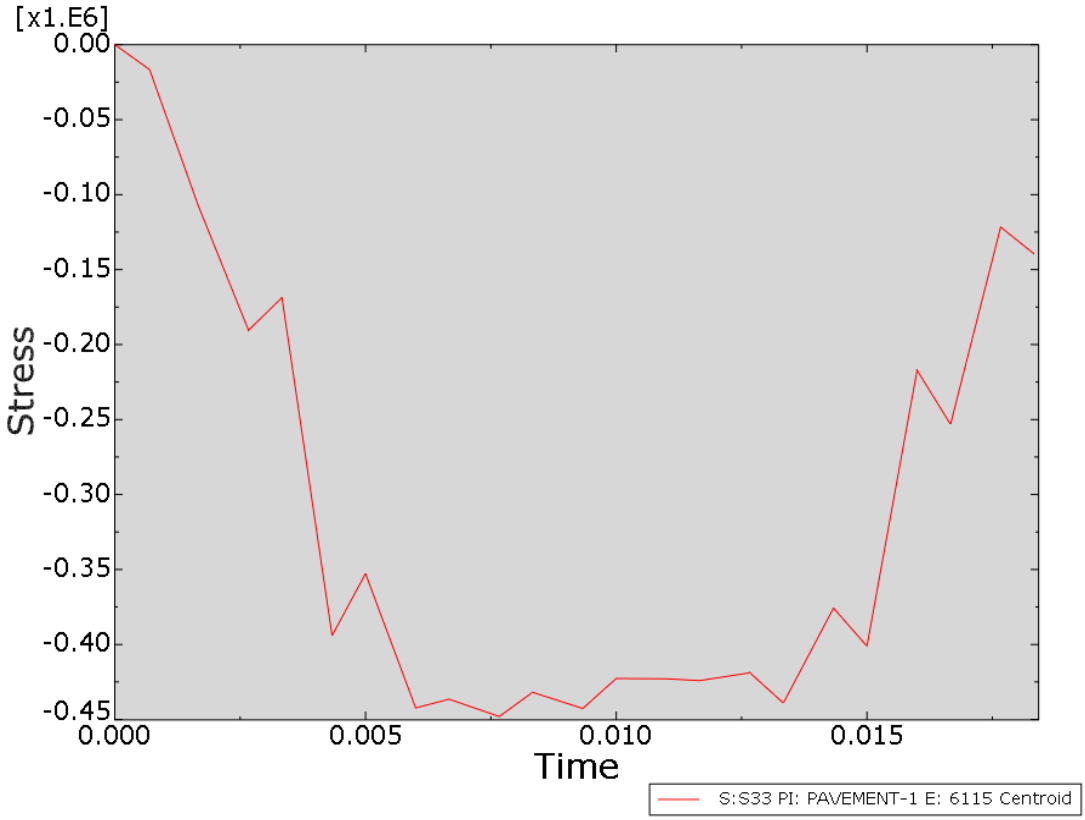

Figure 36: AV longitudinal stress for outer tyre rib

In Table 12 below, the values are summarized for the longitudinal stress below the outer tyre rib.

Table 12: table with the maximum and mean values of longitudinal stress for the outer tyre rib (rib 9)

Longitudinal Stress		Max Value (Pa)	Mean Value (Pa)	Diff Max Value (%)
Non-AV	Outer rib	-448065	-318333,4879	0,00111591
AV		-448060	-318336,3061	

Next, the same procedure is repeated for the centre tyre rib (rib 5).

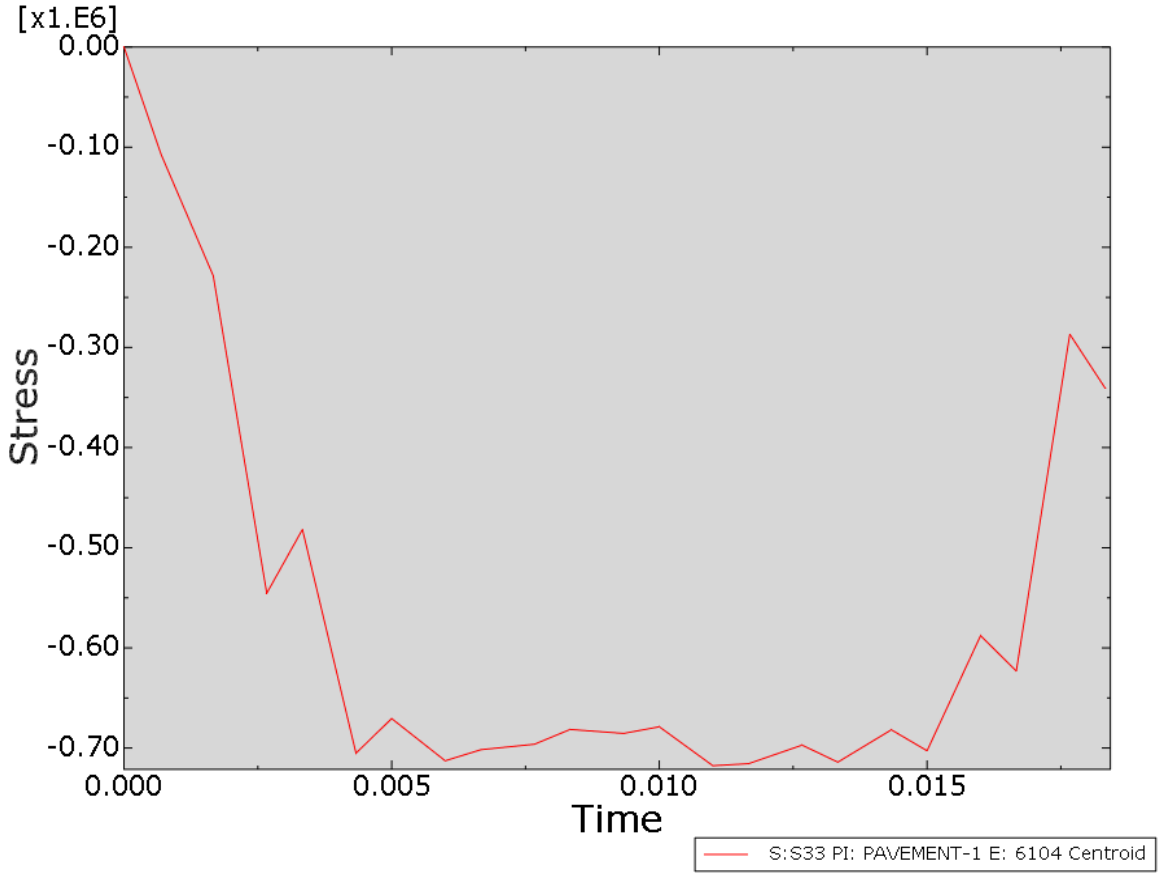

Figure 37:Non-AV longitudinal stress for centre tyre rib

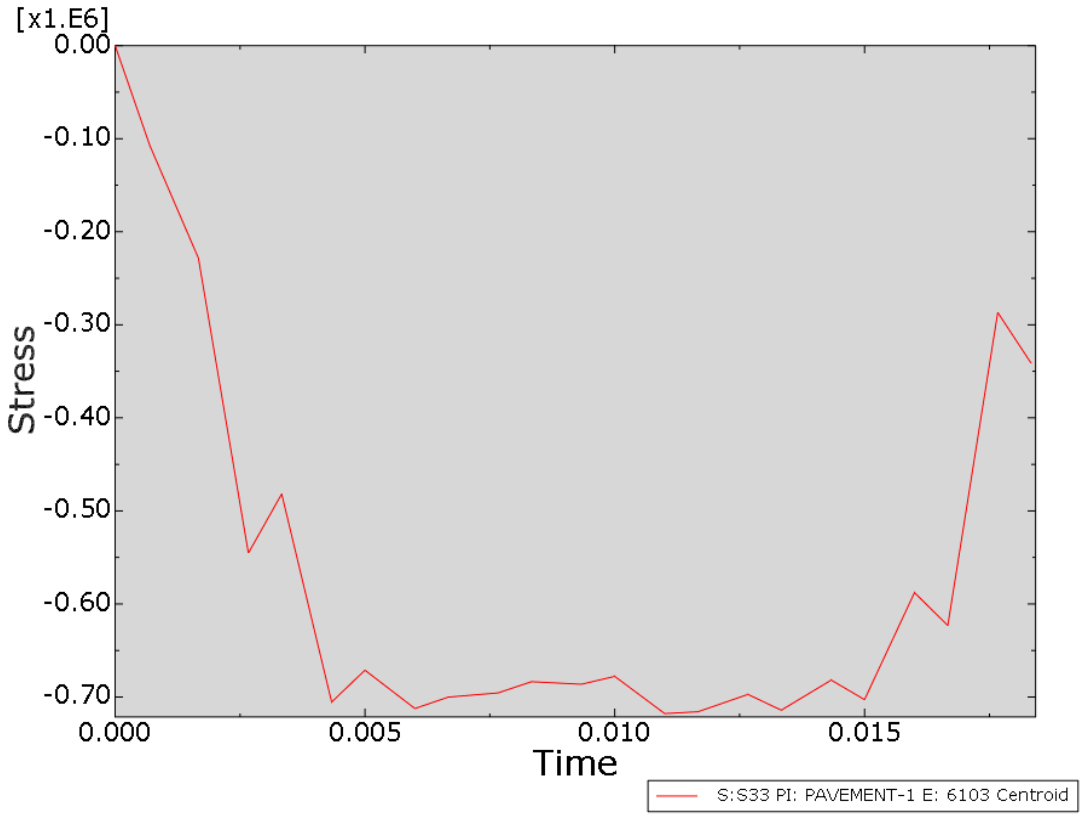

Figure 38: AV longitudinal stress for centre tyre rib

In Table 13 below, the values are summarized for the longitudinal stress below the centre tyre rib.

Table 13: table with the maximum and mean values of longitudinal stress for the centre tyre rib (rib 5)

Longitudinal Stress		Max Value (Pa)	Mean Value (Pa)	Diff Max Value (%)
Non-AV	Centre rib	-717690	-580642,6667	0,019089022
AV		-717827	-580692,5758	

6.3 Vertical Strain

Next, the vertical strain on the pavement will be measured. This will be done for both AV and the Non-AV model. First, the general situation is shown in Figure 39. The differing colours indicate the change in magnitude of vertical strain. The place where the tyre is positioned is clearly visible.

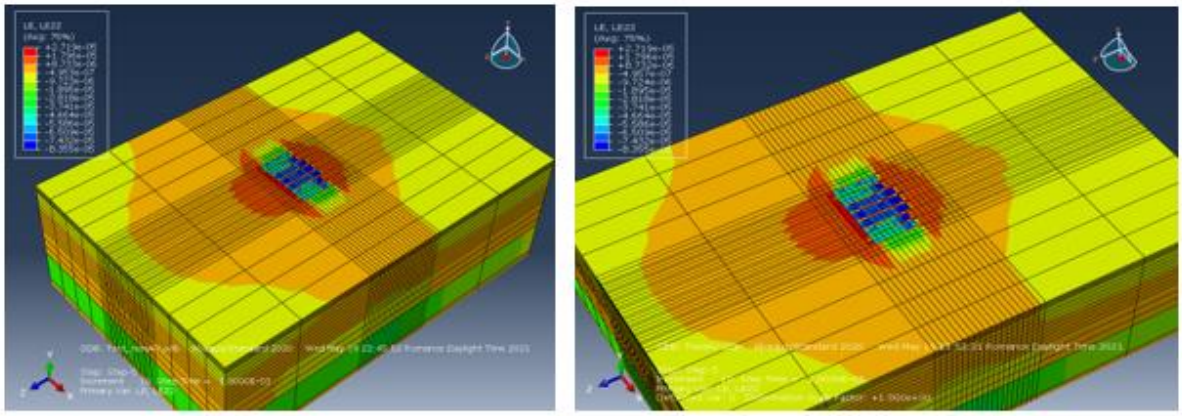

Figure 39: Non-AV Vertical strain situation (a), AV Vertical strain (b)

The graphs below (Figures 40, 41, 42, and 43) show the change in vertical strain on the pavement surface during time progression for the AV and non-AV simulation. The measurements were taken in the middle of the tyre imprint area at the ten mesh line (200 mm) and under tyre ribs 5 (centre rib) and tyre rib 9 (outer tyre rib). The units of the axis' are micro-strain (µm/m) and seconds (s).

First, the results for the outer rib (rib 9) are shown in Figures 40 and 41.

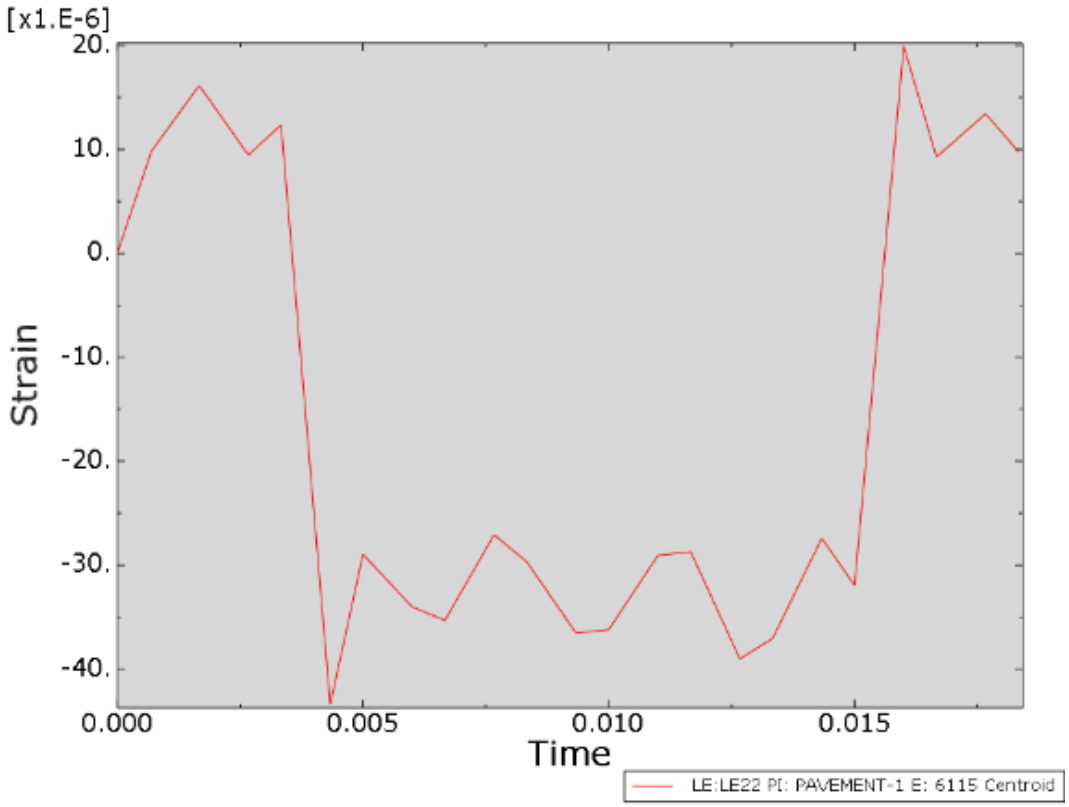

Figure 40: non-AV vertical strain for outer tyre rib

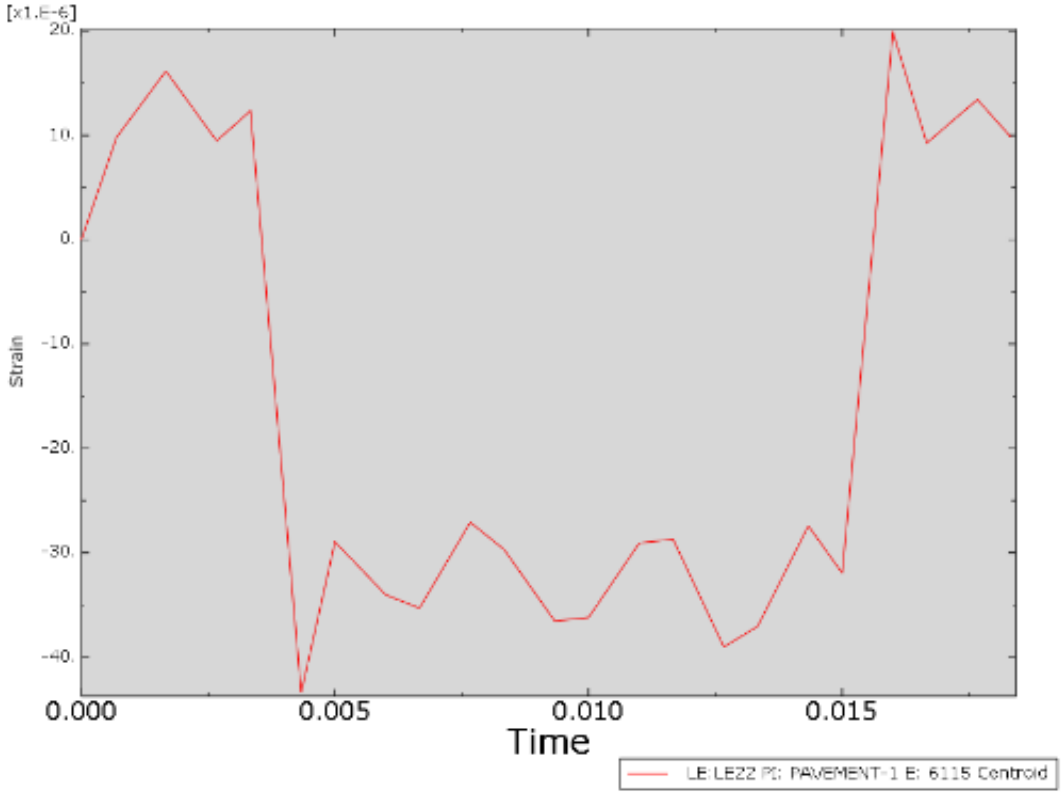

Figure 41: AV vertical strain for outer tyre rib

In Table 14 below, the values are summarized for the Vertical strain below the outer tyre rib.

Table 14: the maximum and mean values of vertical strain for the outer tyre rib (rib 9)

Vertical strain		Max Value (µm/m)	Mean Value (µm/m)	Diff Max Value (%)
Non-AV	Outer rib	-43,426	-16,7989597	0,000230277
AV		-43,4259	-16,79912182	

Next, the same procedure is repeated for the centre tyre rib (rib 5).

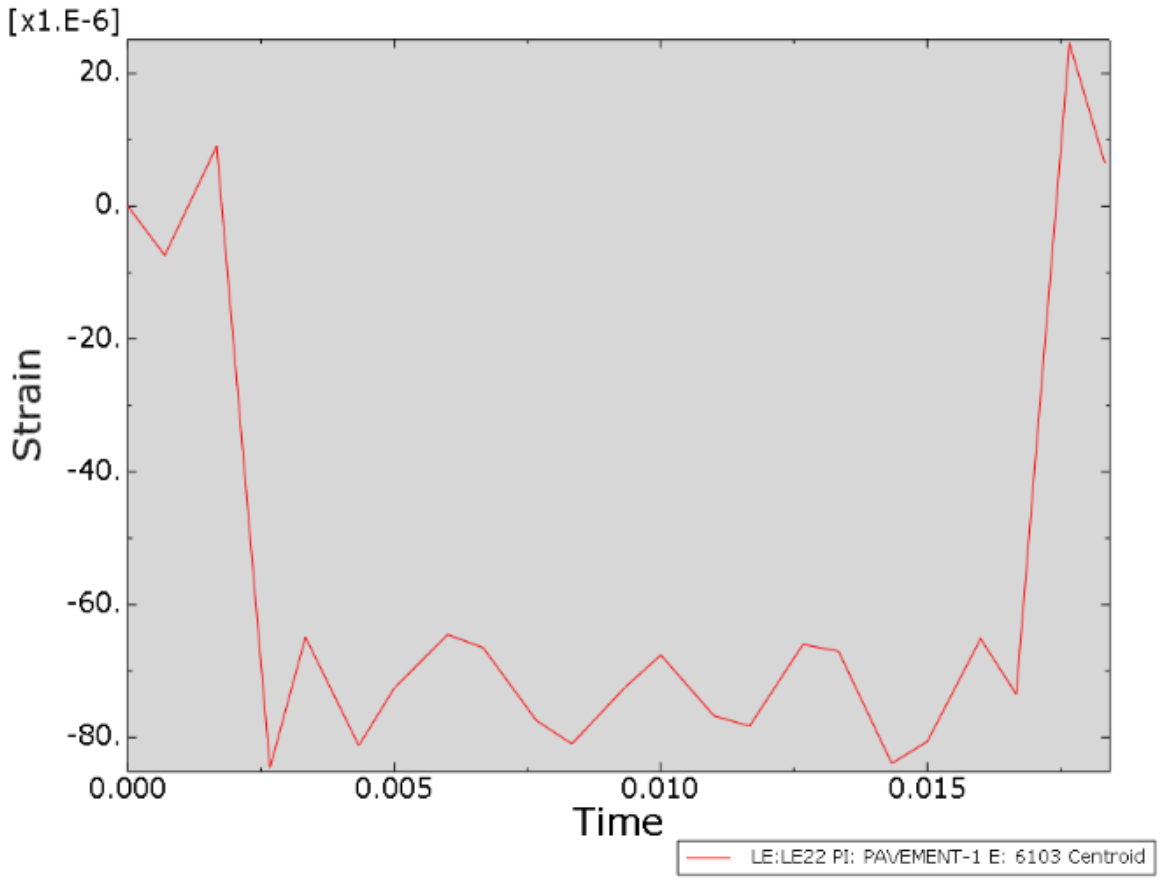

Figure 42: non-AV vertical strain for centre tyre rib

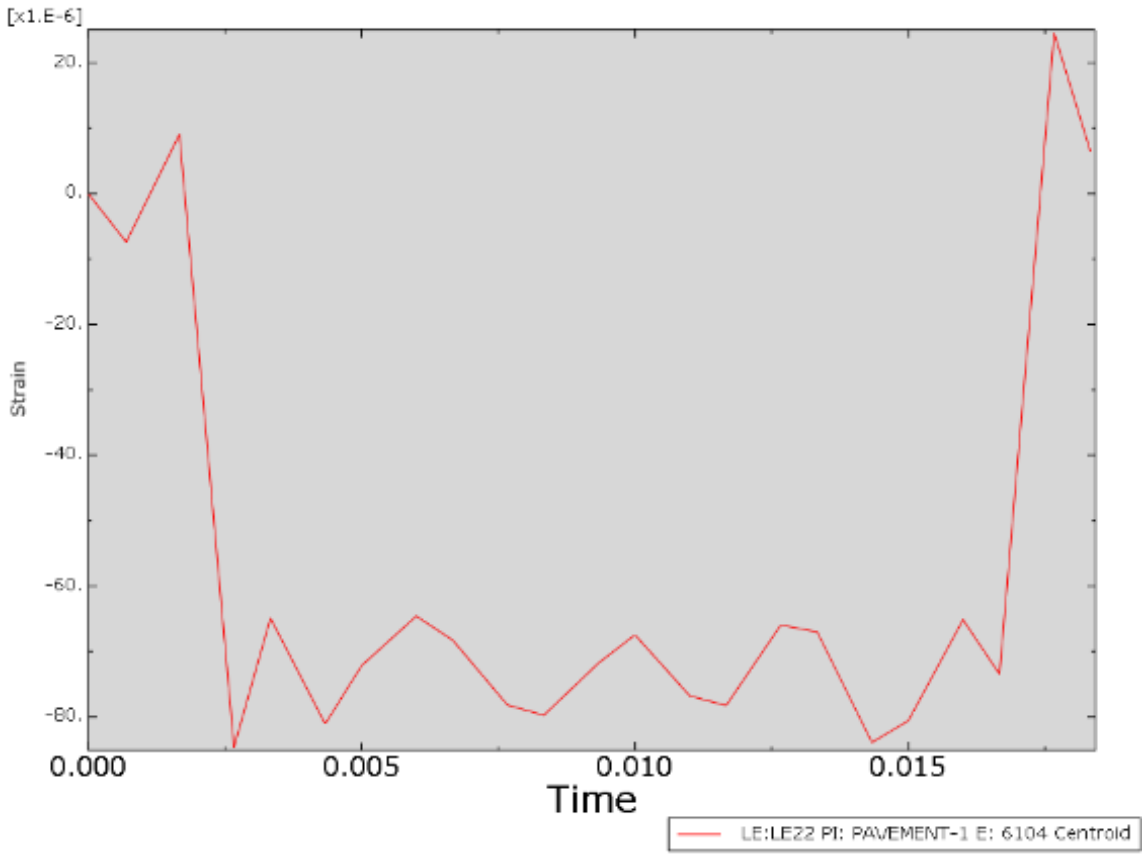

Figure 43: AV vertical strain for centre tyre rib

In Table 15 below, the values are summarized for the vertical strain below the centre tyre rib.

Table 15: maximum and mean values of vertical strain for the centre tyre rib (rib 5)

Vertical strain		Max Value (µm/m)	Mean Value (µm/m)	Diff Max Value (%)
Non-AV	Centre rib	-84,5803	-58,61285909	0
AV		-84,5803	-58,61383364	

6.4 Longitudinal Strain

Lastly, the longitudinal strain on the pavement will be measured. This, again, will be done for both AV and the Non-AV model. First, the general situation is shown in Figure 44. The differing colours indicate the change in magnitude of longitudinal strain. The place where the tyre is positioned is clearly visible.

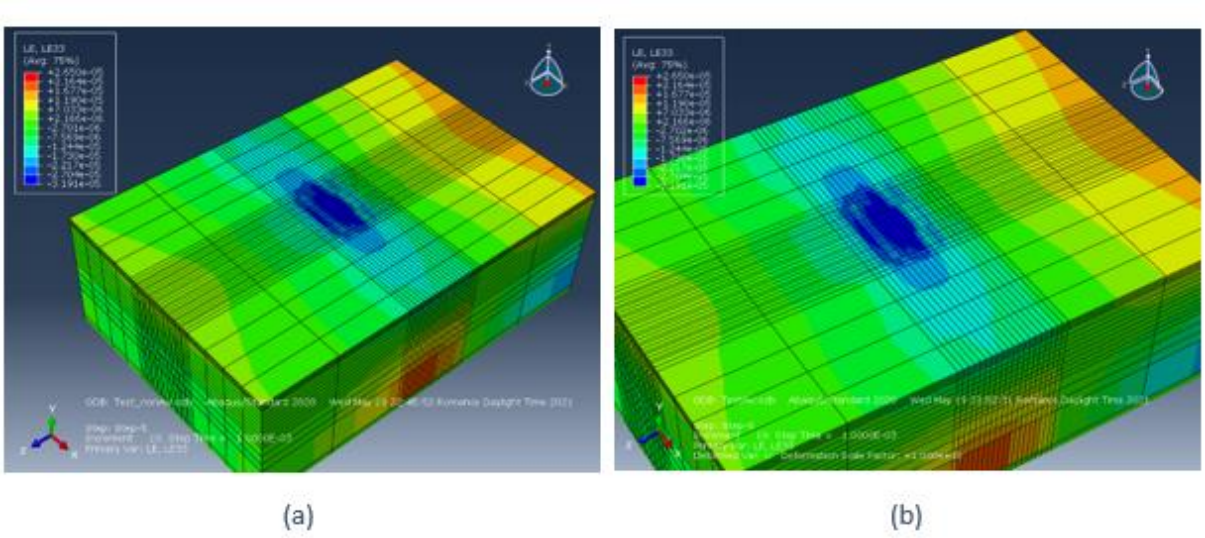

Figure 44: non-AV longitudinal strain situation (a), AV longitudinal strain situation (b)

The graphs below (Figures 45, 46, 47, and 48) show the change in longitudinal strain on the pavement surface during time progression for the AV and non-AV simulation. The measurements were taken in the middle of the tyre imprint area at the ten mesh line (200 mm) and under tyre ribs 5 (centre rib) and tyre rib 9 (outer tyre rib). The units of the axis' are micro-strain (µm/m) and seconds (s). First, the results for the outer tyre rib are given.

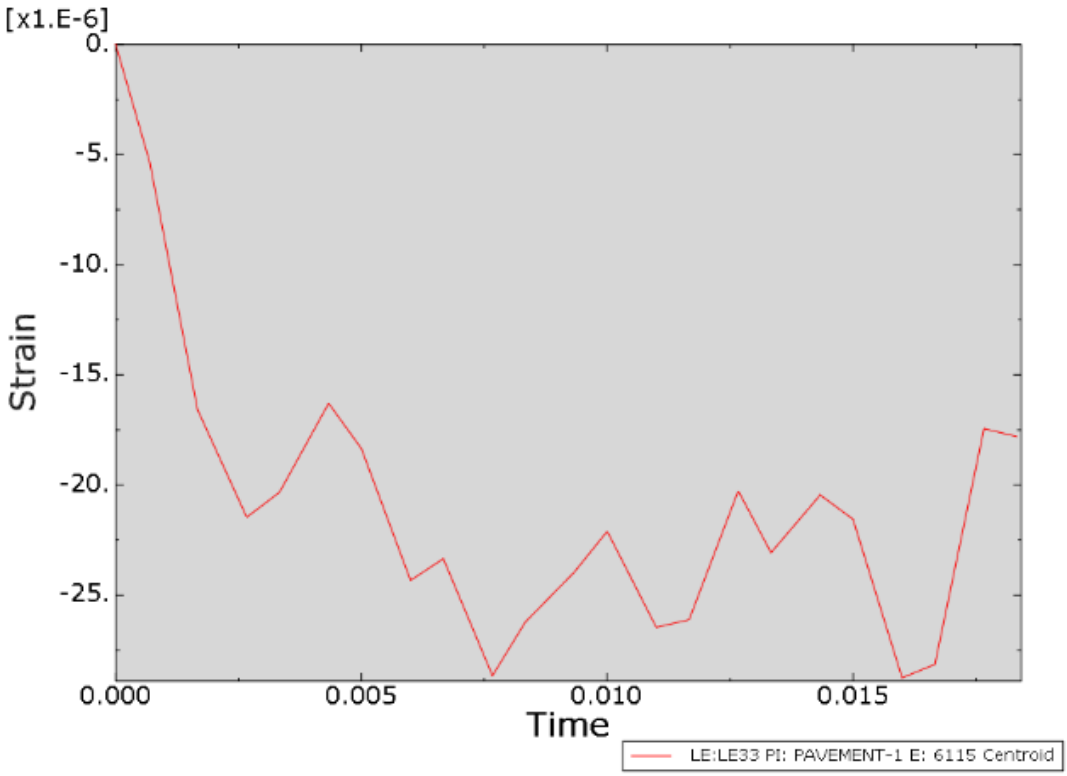

Figure 45: non-AV Longitudinal strain for outer tyre rib

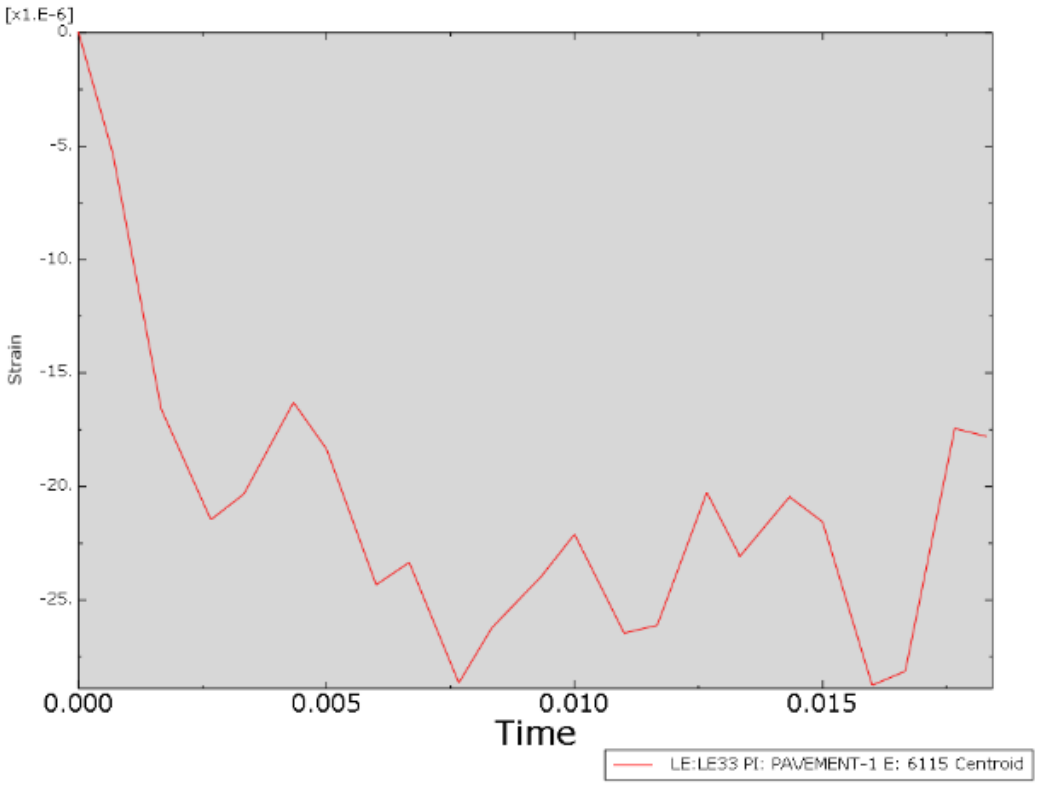

Figure 46: AV longitudinal strain for outer tyre rib

In Table 16 below the values are summarized for the longitudinal strain below the outer tyre rib.

Table 16: maximum and mean values of vertical strain for the outer tyre rib (rib 9)

longitudinal strain		Max Value (µm/m)	Mean Value (µm/m)	Diff Max Value (%)
Non-AV	Outer rib	-28,7574	-21,30083758	0,007302468
AV		-28,7595	-21,30107091	

Next the same procedure is repeated, this time for the centre tyre rib (rib 5).

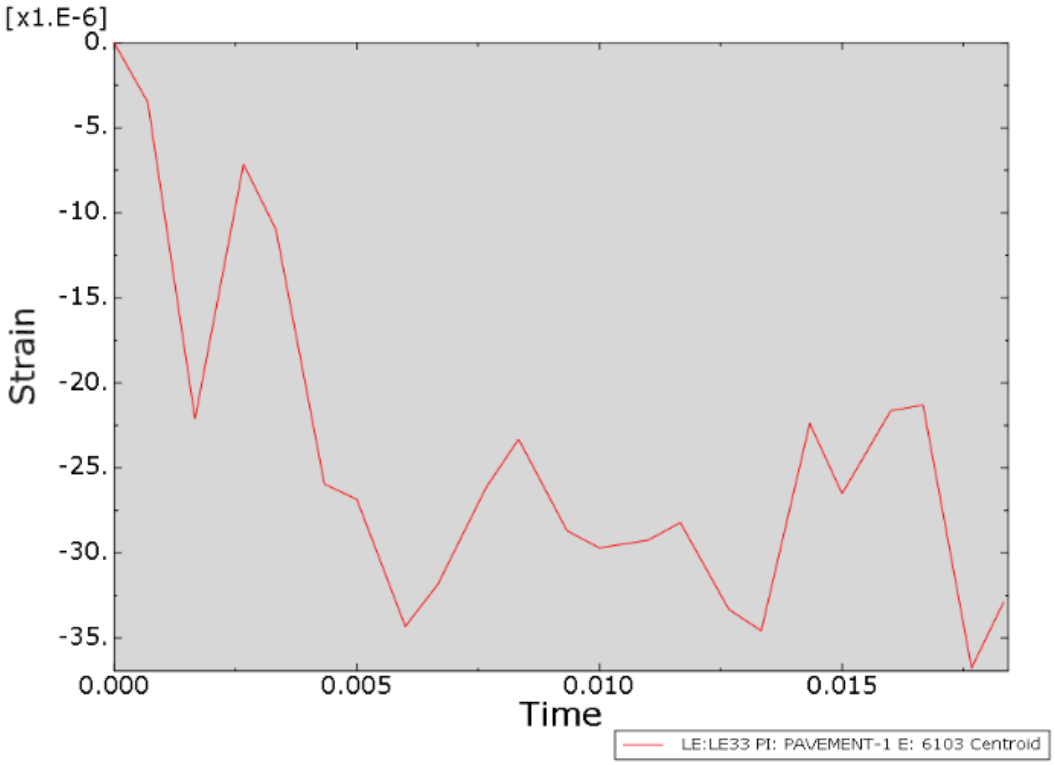

Figure 47: non-AV longitudinal strain for centre tyre rib

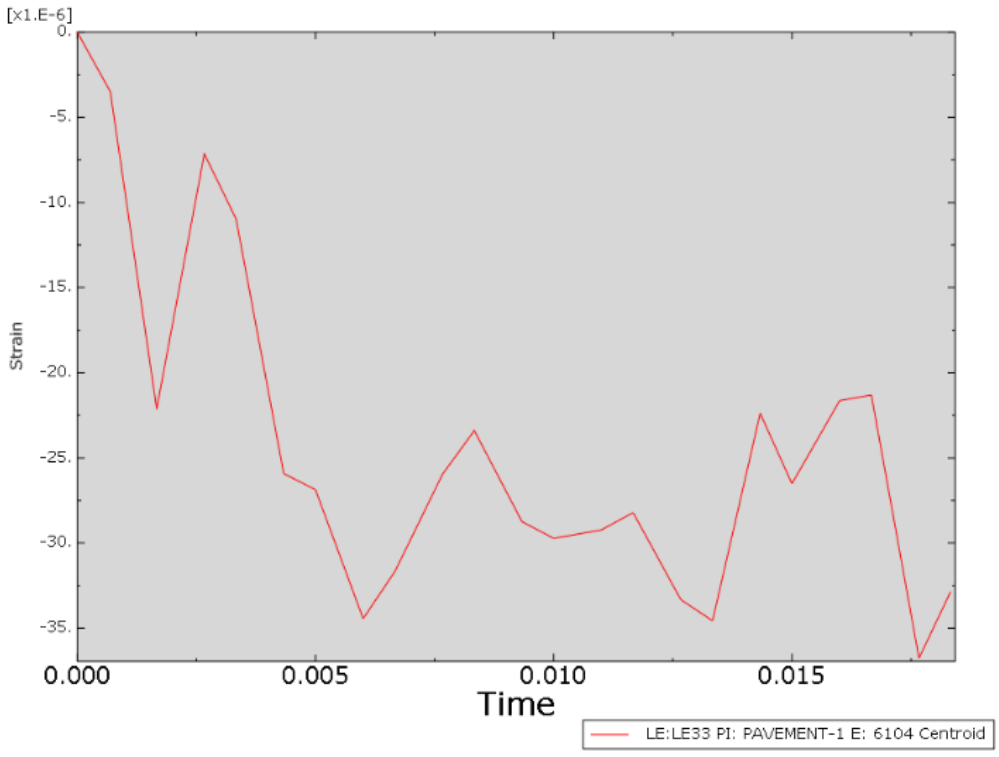

Figure 48: AV longitudinal strain for centre tyre rib

In Table 17 below the values are summarized for the longitudinal strain below the centre tyre rib.

Table 17: maximum and mean values of longitudinal strain for the centre tyre rib (rib 5)

longitudinal strain		Max Value (µm/m)	Mean Value (µm/m)	Diff Max Value (%)
Non-AV	Centre rib	-36,754	-24,62845333	0,02475921
AV		-36,7631	-24,62442848	

7 Discussion of results

The hypothesis for this project was that AVs, with their different deceleration behaviour, might positively impact the pavement stress-strain response. Due to AVs' less abrupt deceleration behaviour as opposed to non-AVs, it would seem logical that this would result in lower stress and strain, or surely at least in the longitudinal direction. This would reduce pavement damage potential and result in longer longevity of the asphalt layer on roads.

First, the vertical stress will be examined. The maximum and mean values of the datasets from the previous chapter are summarized in Table 18.

Table 18: Vertical stresses – summary

Vertical Stress		Max Value (Pa)	Mean Value (Pa)	Diff Max Value (%)
Non-AV	Outer rib	-514596	-298665,9909	0,000194327
AV		-514595	-298668,4436	
Non-AV	Centre rib	-948571	-727840,3424	0,000316265
AV		-948574	-727845,8455	

For the vertical stress, there is seemingly no discernible difference between the values attained for AVs and non-AVs. However, this might not be abnormal, as deceleration would not influence the vertical loads on the pavement, and the difference in loading time is sufficiently small and have no significant impact. The maximum value for the vertical stress is higher for the non-AV for the outer rib, and higher for the AV for the centre rib. The differences are, however, only 3 and 1 Pa, which does not seem very significant. The same goes for the mean values. There is again some difference, but no more than 5 Pa, which is not significant.

Next, the longitudinal stress results will be examined. The maximum and mean values are summarized in Table 19.

Table 19: longitudinal Stresses – summary

Longitudinal Stress		Max Value (Pa)	Mean Value (Pa)	Diff Max Value (%)
Non-AV	Outer rib	-448065	-318333,4879	0,00111591
AV		-448060	-318336,3061	
Non-AV	Centre rib	-717690	-580642,6667	0,019089022
AV		-717827	-580692,5758	

For the longitudinal stress there seems to be slight difference between the AV and non-AV, with the maximum values even being identical for the outer rib. This is perhaps harder to explain as it would be expected that hard braking would result in higher shear forces applied by the tyres on the pavement surface. However, another study by Wang et al. [4] indicates that this is not as abnormal as it would seem as the shear stress in this study also seems to remain somewhat the same under different tyre rolling conditions and braking. This could mean that the longitudinal stress is also unaffected by tyre braking. According to the study by Wang et al. [4], the real difference will be found in the horizontal strain.

The vertical and horizontal strains will be examined in the following section, beginning with the vertical strains. The maximum and mean values of the datasets from the previous chapter are summarized in Tables 20 and 21.

Table 20: Vertical strains – summary

Vertical strain		Max Value (µm/m)	Mean Value (µm/m)	Diff Max Value (%)
Non-AV	Outer rib	-43,426	-16,7989597	0,000230277
AV		-43,4259	-16,79912182	
Non-AV	Centre rib	-84,5803	-58,61285909	0
AV		-84,5803	-58,61383364	

Again, for the vertical strains as well, no discernible difference seems to be observable. The values seem more or less the same, indicating that there is perhaps no effect of different braking behaviour on the vertical strain. It also seems logical that different braking behaviour would not necessarily affect the pavement's vertical load effects and, therefore, will not affect the vertical strains.

Finally, the results for the measurements of the longitudinal strain will be examined. The maximum and mean values are summarized in Table 21.

Table 21: Longitudinal strains – summary

longitudinal strain		Max Value (µm/m)	Mean Value (µm/m)	Diff Max Value (%)
Non-AV	Outer rib	-28,7574	-21,30083758	0,007302468
AV		-28,7595	-21,30107091	
Non-AV	Centre rib	-36,754	-24,62845333	0,02475921
AV		-36,7631	-24,62442848	

When examining the values of the vertical strain, it must again be concluded that there is no significant difference between the values of the AV and non-AV. This means that the hypothesis is disproven. It seems that even though the braking behaviour is different, the stresses and strains remain the same. There are, however, some possible explanations for this.

The first explanation focuses on the speed difference between the AV and the non-AV at a given time, and also the loading time of each pavement element. Due to the harsher deceleration of the non-AV at the beginning of the braking manoeuvre, a difference in speed is created between the AV and non-AV. This can clearly be seen in the graph in Figure 49. As time progresses, this difference in speed will lessen again, as both vehicles will eventually come to a standstill. In the beginning, however, there is a difference in vehicle velocity, which causes longer step times for the non-AV. The step times indicate how long the tyre imprint takes to move forward one mesh element in ABAQUS. The higher the step time, the longer the currently loaded set of pavement elements remains loaded. The time a pavement experiences the tyre load is called the loading time of an element. In Figure 50, the tyre imprint can be seen. Each step, the tyre imprint moves one meshing element forward.

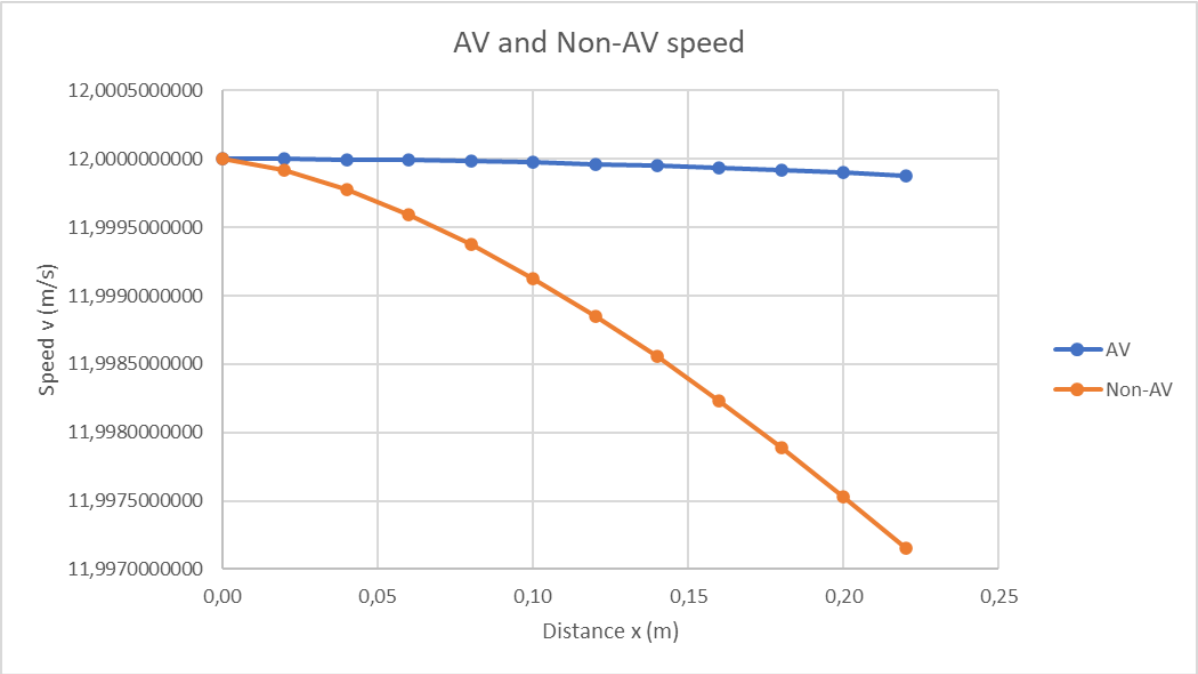

Figure 49: Evolution of the speed of AV and non-AV load caused by their different deceleration behaviours

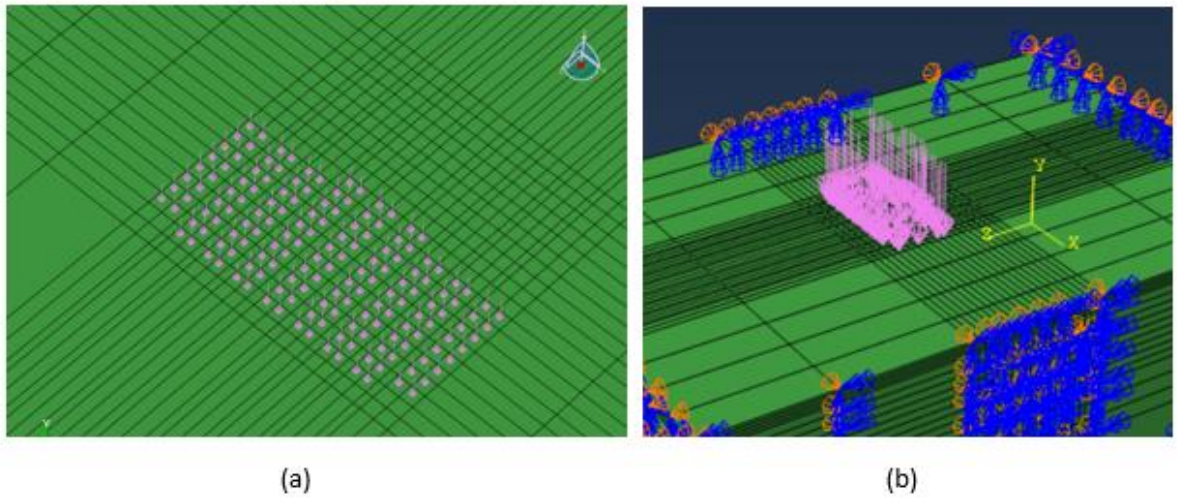

Figure 50: Closeup of tyre imprint and load position (a), model with the loads visible (b)

In the study by Wang et al. [4], it can clearly be seen that the speed of the moving load has a significant impact on the stress and strain results. The higher the speed of the vehicle, the lower the shear strain of the pavement. This means that a higher loading time (lower speed) causes higher shear strain in the pavement.

The lack of difference in the longitudinal strain results can thus be explained by a lack of difference in loading time between the AV and non-AV, a lack of difference in speed between the AV and non-AV. Figure 51 shows the evolution of the step times in time. It can clearly be seen that although the step times for the non-AV rise, it is only by a minimal amount (see vertical axis).

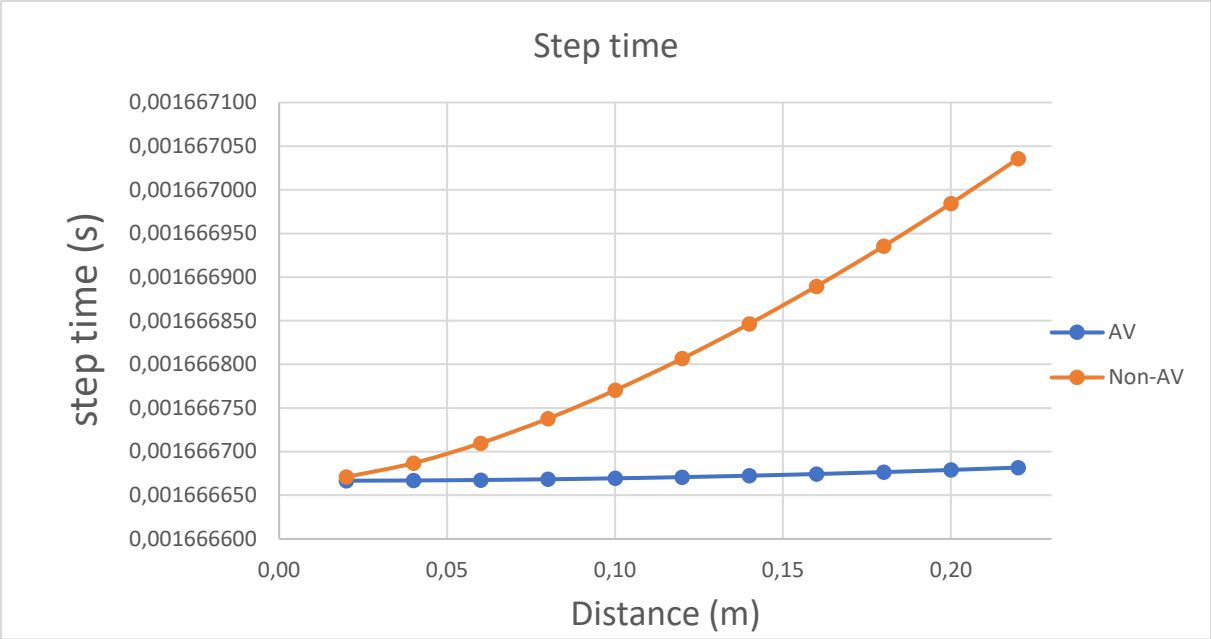

Figure 51: Step time (loading time) increase for both deceleration models

It must thus be concluded that the difference in loading time between the AV and non-AV model is too small to show a significant difference in results. Since the time window chosen for the simulation finds itself right at the beginning of the deceleration manoeuvre, it might be a solution to select a different time window, further on in time, halfway between the beginning of the deceleration and standstill of the vehicles. Here the difference in speed between the AV and non-AV might be more pronounced.

Another explanation for the lack of difference in the strain results is the lack of multiple vehicle passes. Right now, only one wheel pass is simulated. In reality, hundreds of cars will pass over a certain section of pavement every day. Due to simulating only one car pass, the size of the stress and strain might be underestimated. It is possible that with multiple wheel passes over time, a difference in stress and strain might become visible. Due to a high number of repeated passes, the difference in loading time, which is small when only one wheel pass is completed, might accumulate over consecutive wheel passes until it becomes significant enough to result in a difference in stress and strain results between AVs and non-AVs. However, no information has been found as of yet about a method to simulate multiple load passes in ABAQUS. Therefore, this hypothesis cannot be investigated further.

Finally, there is the issue regarding the simulation of deceleration and braking. In this project, vehicle braking/deceleration was simulated by changing the step times. Each step corresponds with a traversed distance of 20 mm. Deceleration was simulated by increasing the step times and making the load take longer and longer to traverse the same distance. This makes that the difference between the AV and non-AV is mainly down to loading time. There is no other mechanic implemented to simulate the braking behaviour of a moving load. In the study by Wang et al. [4] friction between tyre and pavement was mentioned, but no further information was given about this. There might be other methods to do this, but no information has been found in the literature regarding this.

Apart from the inaccuracies mentioned in chapter 4, this study has another limitation. This is about defining AV deceleration behaviour. No practical designs for this concept exist in the literature, so a

behaviour had to be defined based on expectations and assumptions of how AVs are thought to behave. The thought process for defining this behaviour is explained in more detail in chapters 3 and 5. This proposed deceleration behaviour is, however, not grounded in any real-life implementation. Thus, the feasibility of this method needs to be further researched in the future.

The results of this study bring with an important implication. Because little useful information is available about the deceleration behaviour of automated vehicles, a behaviour has been proposed for this project based on a study about the deceleration behaviour of non-AVs [10]. The linear deceleration pattern was chosen for the AVs because it seemed to hold a positive advantage over the parabolic non-AV deceleration behaviour. In hindsight, this proved not to be entirely true. This needs to be acknowledged by anyone trying to define AV deceleration behaviour regarding the pavement stress-strain response in the future. The lack of difference in the stress and strain results in this study might prove valuable information and might be a reason to try a different approach than the one used in this paper.

It would be recommended that more research be done on the topic of AV deceleration behaviour. Further study is required to design a more detailed AV deceleration behaviour. Also, creative ways need to be found for implementing braking in ABAQUS. Lastly, a method must be found to simulate multiple wheel passes in ABAQUS.

8 Conclusion

This thesis examined the effects of a decelerated moving load of automated vehicles on the pavement stress-strain responses using 3-D finite element modelling. The first research was conducted into pavement stress-strain responses due to moving loads in order to get an understanding of the physics. Then research was done into the deceleration behaviour of non-AVs and AVs. Since not a lot of practical information was available for AVs about this topic, it was decided to design a deceleration model for the AVs. A linear deceleration model was chosen for the AVs, while a parabolic deceleration model was chosen for the non-AVs.

After designing the deceleration models, a pavement model was constructed with the 3-D finite element modelling software ABAQUS. This pavement model was based on the "Virginia Smart Road – Section B" 's real-life pavement consisting of 5 layers and an infinite layer at the bottom. The layer interaction was defined as fully bonded. The asphalt layers were characterised as viscoelastic materials, and a Prony series represented the viscoelastic properties. A wide base tyre was used in the simulations. A loading area length of 400 mm was chosen, and the moving wheel load was characterized as trapezoidal impulsive loading. A load of 38 kN was applied. The hypothesis before the testing was that the AVs would cause less damage to pavements since they would produce lower peak stress and strain due to their smoother deceleration characteristics.

After the design of the pavement model and the loads, the model was validated by using simulation results from the study by Yoo and Al-Qadi. [13]. After validating the model, simulations of moving decelerating loads were run on this model with ABAQUS for both the AV and non-AV situations. This was done to achieve insight into the pavement stress-strain response and find out if there is a difference in its reaction to AVs compared to non-AVs.

These tests showed no difference in maximum and mean values for the vertical and longitudinal stress and strain. These results are, however, not wholly conclusive. There are several explanations for these results, which each might be investigated further.

Finally, it can be concluded that the results of this research, even though inconclusive, show some potential because of the possible further investigation. Further research, tests, and improvement of the used pavement model are required to come to a more conclusive result.

Bibliography

[1] T. Hilgert *et al.*, "ScienceDirect ScienceDirect Potentials of Autonomous Vehicles in a Changing Private Potentials of Autonomous Vehicles in a Changing Private Transportation System – a Case Study in the Stuttgart Region Transportation System – a Case Study in the Stuttgart ," *Transp. Res. Procedia*, vol. 26, no. 2016, pp. 13–21, 2017, doi: 10.1016/j.trpro.2017.07.004.

[2] X. Hu, A. N. M. Faruk, J. Zhang, M. I. Souliman, and L. F. Walubita, "ScienceDirect Effects of tire inclination (turning traffic) and dynamic loading on the pavement stress – strain responses using 3-D finite element modeling," *Int. J. Pavement Res. Technol.*, vol. 10, no. 4, pp. 304–314, 2017, doi: 10.1016/j.ijprt.2017.04.005.

[3] S. S. Adlinge and P. A. K. Gupta, "Pavement Deterioration and its Causes," pp. 9–15.

[4] H. Wang, I. L. Al-qadi, and H. W. I. L. Al-qadi, "Road Materials and Pavement Design Evaluation of Surface-Related Pavement Damage due to Tire Braking Evaluation of Surface-Related Pavement Damage due to Tire Braking," no. December 2012, pp. 37–41, 2010, doi: 10.3166/RMPD.11.101-121.

[5] H. Wang and I. L. Al-qadi, "Near-Surface Pavement Failure Under Multiaxial Stress State in Thick Asphalt Pavement," pp. 91–99, doi: 10.3141/2154-08.

[6] H. Wang, "Pavement Damage Due to Different Tire and Loading Configurations on Secondary Roads."

[7] O. E. Gungor, I. L. Al-qadi, and A. Gamez, "In-Situ Validation of Three-Dimensional Pavement Finite Element Models In-Situ Validation of Three-Dimensional Pavement Finite Element Models," no. September, 2016, doi: 10.1007/978-3-319-42797-3.

[8] Z. Binshuang, C. Jiaying, Z. Runmin, and H. Xiaoming, "Skid resistance demands of asphalt pavement during the braking process of autonomous vehicles," vol. 2, no. 201 9, pp. 1–7.

[9] I. Bae, J. Moon, and J. Seo, "Toward a comfortable driving experience for a self-driving shuttle bus," *Electron.*, vol. 8, no. 9, pp. 1–13, 2019, doi: 10.3390/electronics8090943.

[10] S. P. Deligianni, M. Quddus, A. Morris, A. Anvuur, and S. Reed, "Analyzing and Modeling Drivers ' Deceleration Behavior from Normal Driving," doi: 10.3141/2663-17.

[11] P. S. Bokare and A. K. Maurya, "Acceleration-Deceleration Behaviour of Various Vehicle Types," *Transp. Res. Procedia*, vol. 25, pp. 4733–4749, 2017, doi: 10.1016/j.trpro.2017.05.486.

[12] J. A. Matute, M. Marcano, A. Zubizarreta, and J. Perez, "Longitudinal Model Predictive Control with comfortable speed planner," *18th IEEE Int. Conf. Auton. Robot Syst. Compet. ICARSC 2018*, no. April, pp. 60–64, 2018, doi: 10.1109/ICARSC.2018.8374161.

[13] P. J. Yoo, I. L. Al-Qadi, M. A. Elseifi, and I. Janajreh, "Flexible pavement responses to different loading amplitudes considering layer interface condition and lateral shear forces," *Int. J. Pavement Eng.*, vol. 7, no. 1, pp. 73–86, 2006, doi: 10.1080/10298430500516074.

[14] P. J. Yoo and I. L. Al-Qadi, "The truth and myth of fatigue cracking potential in hot-mix asphaltf Numerical analysis and validation," *Asph. Paving Technol. Assoc. Asph. Paving Technol. Tech. Sess.*, vol. 77, pp. 549–590, 2008.

[15] C. A. E. User, "Abaqus 6.11."

Appendix

8.1 Numerical results of the simulations

Vertical Stress
Non AV
Rib 9

x	y
0	0
0,000693492	50337,5
0,00166667	36822
0,00166667	36822
0,00266667	-54379
0,00333336	-25078,8
0,00333336	-25078,8
0,00433336	-514596
0,00500007	-400110
0,00500007	-400110
0,00600007	-485561
0,00666681	-489659
0,00666681	-489659
0,00766681	-441363
0,00833358	-447420
0,00833358	-447420
0,00933358	-498420
0,0100004	-485048
0,0100004	-485048
0,0110004	-434431
0,0116672	-435544
0,0116672	-435544
0,0126672	-501659
0,0133341	-500603
0,0133341	-500603
0,0143341	-406204
0,0150011	-446715
0,0150011	-446715
0,0160011	-2186,7
0,016668	-88222,8
0,016668	-88222,8
0,017668	14052,5
0,0183351	-18410,8

Vertical Stress
AV
Rib 9

x	y
0	0
0,000693492	50337,5
0,00166667	36822
0,00166667	36822
0,00266667	-54379
0,00333334	-25076,8
0,00333334	-25076,8
0,00433334	-514595
0,00500001	-400110
0,00500001	-400110
0,00600001	-485568
0,00666668	-489649
0,00666668	-489649
0,00766668	-441361
0,00833335	-447410
0,00833335	-447410
0,00933335	-498409
0,01	-485033
0,01	-485033
0,011	-434417
0,0116667	-435540
0,0116667	-435540
0,0126667	-501650
0,0133334	-500622
0,0133334	-500622
0,0143334	-406244
0,015	-446752
0,015	-446752
0,016	-2192,94
0,0166667	-88230,7
0,0166667	-88230,7
0,0176667	14063,2
0,0183334	-18440,4

Vertical Stress

Non AV

Rib 5

x	y
0	0
0,000693492	-124592
0,00166667	-91000,9
0,00166667	-91000,9
0,00266667	-887248
0,00333336	-719389
0,00333336	-719389
0,00433336	-947767
0,00500007	-869295
0,00500007	-869295
0,00600007	-844157
0,00666681	-861356
0,00666681	-861356
0,00766681	-924477
0,00833358	-927658
0,00833358	-927658
0,00933358	-872374
0,0100004	-842157
0,0100004	-842157
0,0110004	-923967
0,0116672	-932718
0,0116672	-932718
0,0126672	-836861
0,0133341	-852846
0,0133341	-852846
0,0143341	-948571
0,0150011	-936298
0,0150011	-936298
0,0160011	-774407
0,016668	-847745
0,016668	-847745
0,017668	-10591,5
0,0183351	-162793

Vertical Stress

AV

Rib 5

x	y
0	0
0,000693492	-124592
0,00166667	-91000,9
0,00166667	-91000,9
0,00266667	-887248
0,00333334	-719388
0,00333334	-719388
0,00433334	-947769
0,00500001	-869288
0,00500001	-869288
0,00600001	-844156
0,00666668	-861346
0,00666668	-861346
0,00766668	-924477
0,00833335	-927632
0,00833335	-927632
0,00933335	-872365
0,01	-842142
0,01	-842142
0,011	-923961
0,0116667	-932716
0,0116667	-932716
0,0126667	-836869
0,0133334	-852881
0,0133334	-852881
0,0143334	-948574
0,015	-936319
0,015	-936319
0,016	-774444
0,0166667	-847796
0,0166667	-847796
0,0176667	-10599,1
0,0183334	-162841

Longitudinal Stress

Non AV

Rib 9

x	y
0	0
0,000693492	-16589,1
0,00166667	-107551
0,00166667	-107551
0,00266667	-190457
0,00333336	-168701
0,00333336	-168701
0,00433336	-394107
0,00500007	-352729
0,00500007	-352729
0,00600007	-442336
0,00666681	-436497
0,00666681	-436497
0,00766681	-448065
0,00833358	-431936
0,00833358	-431936
0,00933358	-442686
0,0100004	-422687
0,0100004	-422687
0,0110004	-422913
0,0116672	-424107
0,0116672	-424107
0,0126672	-418892
0,0133341	-439019
0,0133341	-439019
0,0143341	-375684
0,0150011	-401080
0,0150011	-401080
0,0160011	-217097
0,016668	-253226
0,016668	-253226
0,017668	-121626
0,0183351	-139487

Longitudinal Stress

AV

Rib 9

x	y
0	0
0,000693492	-16589,1
0,00166667	-107551
0,00166667	-107551
0,00266667	-190457
0,00333334	-168700
0,00333334	-168700
0,00433334	-394107
0,00500001	-352734
0,00500001	-352734
0,00600001	-442339
0,00666668	-436495
0,00666668	-436495
0,00766668	-448060
0,00833335	-431904
0,00833335	-431904
0,00933335	-442680
0,01	-422676
0,01	-422676
0,011	-422895
0,0116667	-424095
0,0116667	-424095
0,0126667	-418881
0,0133334	-439065
0,0133334	-439065
0,0143334	-375722
0,015	-401135
0,015	-401135
0,016	-217117
0,0166667	-253195
0,0166667	-253195
0,0176667	-121628
0,0183334	-139523

Longitudinal Stress

Non AV

Rib 5

x	y
0	0
0,000693492	-107322
0,00166667	-228404
0,00166667	-228404
0,00266667	-545423
0,00333336	-481739
0,00333336	-481739
0,00433336	-705141
0,00500007	-670586
0,00500007	-670586
0,00600007	-712739
0,00666681	-701674
0,00666681	-701674
0,00766681	-696226
0,00833358	-681457
0,00833358	-681457
0,00933358	-685400
0,0100004	-678799
0,0100004	-678799
0,0110004	-717690
0,0116672	-715618
0,0116672	-715618
0,0126672	-697104
0,0133341	-714111
0,0133341	-714111
0,0143341	-681804
0,0150011	-702741
0,0150011	-702741
0,0160011	-587803
0,016668	-623154
0,016668	-623154
0,017668	-286795
0,0183351	-341195

Longitudinal Stress

AV

Rib 5

x	y
0	0
0,000693492	-107322
0,00166667	-228404
0,00166667	-228404
0,00266667	-545423
0,00333334	-481743
0,00333334	-481743
0,00433334	-705451
0,00500001	-671188
0,00500001	-671188
0,00600001	-712379
0,00666668	-700148
0,00666668	-700148
0,00766668	-695569
0,00833335	-683529
0,00833335	-683529
0,00933335	-686316
0,01	-677841
0,01	-677841
0,011	-717827
0,0116667	-715837
0,0116667	-715837
0,0126667	-697215
0,0133334	-714154
0,0133334	-714154
0,0143334	-681833
0,015	-702829
0,015	-702829
0,016	-587839
0,0166667	-623178
0,0166667	-623178
0,0176667	-286789
0,0183334	-341190

Vertical Strain

Non AV

Rib 9

x	y
0	0
0,000693492	9,81E-06
0,00166667	1,62E-05
0,00166667	1,62E-05
0,00266667	9,47E-06
0,00333336	1,23E-05
0,00333336	1,23E-05
0,00433336	-4,34E-05
0,00500007	-2,90E-05
0,00500007	-2,90E-05
0,00600007	-3,40E-05
0,00666681	-3,53E-05
0,00666681	-3,53E-05
0,00766681	-2,71E-05
0,00833358	-2,97E-05
0,00833358	-2,97E-05
0,00933358	-3,65E-05
0,0100004	-3,62E-05
0,0100004	-3,62E-05
0,0110004	-2,91E-05
0,0116672	-2,87E-05
0,0116672	-2,87E-05
0,0126672	-3,90E-05
0,0133341	-3,71E-05
0,0133341	-3,71E-05
0,0143341	-2,74E-05
0,0150011	-3,19E-05
0,0150011	-3,19E-05
0,0160011	1,99E-05
0,016668	9,27E-06
0,016668	9,27E-06
0,017668	1,34E-05
0,0183351	9,80E-06

Vertical Strain

AV

Rib 9

x	y
0	0
0,000693492	9,81E-06
0,00166667	1,62E-05
0,00166667	1,62E-05
0,00266667	9,47E-06
0,00333334	1,23E-05
0,00333334	1,23E-05
0,00433334	-4,34E-05
0,00500001	-2,90E-05
0,00500001	-2,90E-05
0,00600001	-3,40E-05
0,00666668	-3,53E-05
0,00666668	-3,53E-05
0,00766668	-2,71E-05
0,00833335	-2,97E-05
0,00833335	-2,97E-05
0,00933335	-3,65E-05
0,01	-3,62E-05
0,01	-3,62E-05
0,011	-2,91E-05
0,0116667	-2,87E-05
0,0116667	-2,87E-05
0,0126667	-3,90E-05
0,0133334	-3,71E-05
0,0133334	-3,71E-05
0,0143334	-2,74E-05
0,015	-3,19E-05
0,015	-3,19E-05
0,016	1,99E-05
0,0166667	9,27E-06
0,0166667	9,27E-06
0,0176667	1,34E-05
0,0183334	9,80E-06

Vertical Strain

Non AV

Rib 5

x	y
0	0
0,000693492	-7,40E-06
0,00166667	9,03E-06
0,00166667	9,03E-06
0,00266667	-8,46E-05
0,00333336	-6,49E-05
0,00333336	-6,49E-05
0,00433336	-8,12E-05
0,00500007	-7,26E-05
0,00500007	-7,26E-05
0,00600007	-6,45E-05
0,00666681	-6,65E-05
0,00666681	-6,65E-05
0,00766681	-7,75E-05
0,00833358	-8,10E-05
0,00833358	-8,10E-05
0,00933358	-7,24E-05
0,0100004	-6,76E-05
0,0100004	-6,76E-05
0,0110004	-7,68E-05
0,0116672	-7,83E-05
0,0116672	-7,83E-05
0,0126672	-6,60E-05
0,0133341	-6,70E-05
0,0133341	-6,70E-05
0,0143341	-8,39E-05
0,0150011	-8,06E-05
0,0150011	-8,06E-05
0,0160011	-6,51E-05
0,016668	-7,35E-05
0,016668	-7,35E-05
0,017668	2,45E-05
0,0183351	6,37E-06

Vertical Strain

AV

Rib 5

x	y
0	0
0,000693492	-7,40E-06
0,00166667	9,03E-06
0,00166667	9,03E-06
0,00266667	-8,46E-05
0,00333334	-6,49E-05
0,00333334	-6,49E-05
0,00433334	-8,11E-05
0,00500001	-7,22E-05
0,00500001	-7,22E-05
0,00600001	-6,46E-05
0,00666668	-6,83E-05
0,00666668	-6,83E-05
0,00766668	-7,82E-05
0,00833335	-7,98E-05
0,00833335	-7,98E-05
0,00933335	-7,18E-05
0,01	-6,75E-05
0,01	-6,75E-05
0,011	-7,68E-05
0,0116667	-7,83E-05
0,0116667	-7,83E-05
0,0126667	-6,60E-05
0,0133334	-6,70E-05
0,0133334	-6,70E-05
0,0143334	-8,39E-05
0,015	-8,06E-05
0,015	-8,06E-05
0,016	-6,51E-05
0,0166667	-7,35E-05
0,0166667	-7,35E-05
0,0176667	2,45E-05
0,0183334	6,36E-06

Longitudinal Strain

Non AV

Rib 9

x	y
0	0
0,00069349	-5,35E-06
0,00166667	-1,66E-05
0,00166667	-1,66E-05
0,00266667	-2,15E-05
0,00333336	-2,03E-05
0,00333336	-2,03E-05
0,00433336	-1,63E-05
0,00500007	-1,84E-05
0,00500007	-1,84E-05
0,00600007	-2,43E-05
0,00666681	-2,33E-05
0,00666681	-2,33E-05
0,00766681	-2,87E-05
0,00833358	-2,62E-05
0,00833358	-2,62E-05
0,00933358	-2,40E-05
0,0100004	-2,21E-05
0,0100004	-2,21E-05
0,0110004	-2,65E-05
0,0116672	-2,61E-05
0,0116672	-2,61E-05
0,0126672	-2,03E-05
0,0133341	-2,31E-05
0,0133341	-2,31E-05
0,0143341	-2,05E-05
0,0150011	-2,16E-05
0,0150011	-2,16E-05
0,0160011	-2,88E-05
0,016668	-2,81E-05
0,016668	-2,81E-05
0,017668	-1,74E-05
0,0183351	-1,78E-05

Longitudinal Strain

AV

Rib 9

x	y
0	0
0,000693492	-5,35E-06
0,00166667	-1,66E-05
0,00166667	-1,66E-05
0,00266667	-2,15E-05
0,00333334	-2,03E-05
0,00333334	-2,03E-05
0,00433334	-1,63E-05
0,00500001	-1,84E-05
0,00500001	-1,84E-05
0,00600001	-2,43E-05
0,00666668	-2,33E-05
0,00666668	-2,33E-05
0,00766668	-2,87E-05
0,00833335	-2,62E-05
0,00833335	-2,62E-05
0,00933335	-2,40E-05
0,01	-2,21E-05
0,01	-2,21E-05
0,011	-2,65E-05
0,0116667	-2,61E-05
0,0116667	-2,61E-05
0,0126667	-2,03E-05
0,0133334	-2,31E-05
0,0133334	-2,31E-05
0,0143334	-2,05E-05
0,015	-2,16E-05
0,015	-2,16E-05
0,016	-2,88E-05
0,0166667	-2,81E-05
0,0166667	-2,81E-05
0,0176667	-1,74E-05
0,0183334	-1,78E-05

Longitudinal Strain
Non AV
Rib 5

x	y
0	0
0,00069349	-3,50E-06
0,00166667	-2,21E-05
0,00166667	-2,21E-05
0,00266667	-7,14E-06
0,00333336	-1,10E-05
0,00333336	-1,10E-05
0,00433336	-2,59E-05
0,00500007	-2,68E-05
0,00500007	-2,68E-05
0,00600007	-3,43E-05
0,00666681	-3,19E-05
0,00666681	-3,19E-05
0,00766681	-2,61E-05
0,00833358	-2,33E-05
0,00833358	-2,33E-05
0,00933358	-2,87E-05
0,0100004	-2,97E-05
0,0100004	-2,97E-05
0,0110004	-2,92E-05
0,0116672	-2,82E-05
0,0116672	-2,82E-05
0,0126672	-3,33E-05
0,0133341	-3,46E-05
0,0133341	-3,46E-05
0,0143341	-2,24E-05
0,0150011	-2,65E-05
0,0150011	-2,65E-05
0,0160011	-2,16E-05
0,016668	-2,13E-05
0,016668	-2,13E-05
0,017668	-3,68E-05
0,0183351	-3,29E-05

Longitudinal Strain
AV
Rib 5

x	y
0	0
0,000693492	-3,50E-06
0,00166667	-2,21E-05
0,00166667	-2,21E-05
0,00266667	-7,14E-06
0,00333334	-1,10E-05
0,00333334	-1,10E-05
0,00433334	-2,59E-05
0,00500001	-2,69E-05
0,00500001	-2,69E-05
0,00600001	-3,44E-05
0,00666668	-3,17E-05
0,00666668	-3,17E-05
0,00766668	-2,60E-05
0,00833335	-2,34E-05
0,00833335	-2,34E-05
0,00933335	-2,87E-05
0,01	-2,97E-05
0,01	-2,97E-05
0,011	-2,92E-05
0,0116667	-2,82E-05
0,0116667	-2,82E-05
0,0126667	-3,33E-05
0,0133334	-3,46E-05
0,0133334	-3,46E-05
0,0143334	-2,24E-05
0,015	-2,65E-05
0,015	-2,65E-05
0,016	-2,16E-05
0,0166667	-2,13E-05
0,0166667	-2,13E-05
0,0176667	-3,68E-05
0,0183334	-3,28E-05